SPATIAL AND TEMPORAL REGULATION OF EARLY FRUIT GROWTH IN APPLE

by

YANYU YAO

(Under the Direction of Anish Malladi)

ABSTRACT

Apple (*Malus × domestica*) is a flavorful, edible fruit with great commercial significance. The fruit consists of two fleshy tissues, pith and cortex, that display differential growth. Early growth of the fruit cortex involves intensive cell production, while later stages are mediated largely by cell expansion. In this work, the spatial and temporal regulation of fruit growth was evaluated particularly during early fruit development (EFD). Transcriptome analyses during EFD indicated that early de-repression of growth was associated with enhanced cell division related gene expression. Phytohormone profiling during this period indicated that ABA, ethylene and JAs together function as components of a growth-restricting module during bloom and shortly thereafter. The roles of two transcription factors in regulating EFD were evaluated. Spatio-temporal expression patterns of *MdTCP2b* (*TEOSINTE BRANCHED1; CYCLOIDEA; PROLIFERATING CELL FACTOR*) were consistent with negative regulation of cell production, and determination of the timing of exit from cell production to cell expansion-mediated growth during EFD. *MdTCP2b* was post-transcriptionally regulated spatially and temporally by miR319. Heterologous expression of *MdTCP2b* in *Arabidopsis thaliana* promoted flowering, reduced leaf size and promoted positive curvature of the leaves, consistent with a role as a negative regulator of organ growth. MdTCP2b binds to the promoter of a cell cycle inhibitor, *KIP RELATED PROTEIN, MdKRP4,* and promotes its expression, thereby regulating cell production. GROWTH

REGULATING FACTORs (GRFs) are positive regulators of cell production and growth. Transcript abundance of *MdGRF11* and a *GRF INTERACTING FACTOR*, *MdGIF3,* are consistent with positive regulation of cell production during EFD. *MdGRF11* is post-transcriptionally regulated by miR396. MdGIF3, which functions as a transcriptional co-activator, was identified as a partner protein of MdGRF11 through yeast two-hybrid assays (Y2H), suggesting that this complex functions to promote cell production during EFD.

INDEX WORDS: Cell division, Cell differentiation, TCP, GRF, RLM-RACE, GIF, Y2H

SPATIAL AND TEMPORAL REGULATION OF EARLY FRUIT GROWTH IN APPLE

by

YANYU YAO

B.S., Shanxi Agricultural University, China, 2016

M.S., Purdue University, United States of America, 2018

A Dissertation Submitted to the Graduate Faculty of The University of Georgia in Partial Fulfillment of the Requirements for the Degree

DOCTOR OF PHILOSOPHY

ATHENS, GEORGIA

2023

SPATIAL AND TEMPORAL REGULATION OF EARLY FRUIT GROWTH IN APPLE

by

YANYU YAO

Major Professor: Anish Malladi

Committee: Chang Hyun Khang

Wolfgang Lukowitz

Savithri Nambeesan

Dayton Wilde

Electronic Version Approved:

Ron Walcott
Vice Provost for Graduate Education and Dean of the Graduate School
The University of Georgia
August 2023

ACKNOWLEDGEMENTS

The five years of study at the University of Georgia were the most important period in my life. Therefore, I would like to express my sincere thanks to my major advisor, Dr. Anish Malladi, for giving me this valuable opportunity to study at the University of Georgia and continuously support and guide me throughout the project and enhance my critical thinking skills. I would also like to express my gratitude to my committee members, Dr. Chang Hyun Khang, Dr. Wolfgang Lukowitz, Dr. Savithri Nambeesan and Dr. Dayton Wilde, for their valuable time and energy in participating in the discussion of my research and their help in improving the research projects.

I am also very appreciative of the excellent previous work of Dr. Shan Jing, and the generous help of our former lab technician, Mr. John Doyle. I want to thank other lab members, Ms. Bayleigh Roussel, Ms. Priyanka Dahiya, Mr. Tej Acharya, Mr. Mark Whatley, Mr. Ranveer Pratap Singh and Ms. Ashley Rae Sorrow.

Last, but not the least, I want to express my deepest thanks to my parents, relatives and friends. Without you, I would not have been able to finish this dissertation. Thank you for your support and for encouraging me to overcome difficulties.

TABLE OF CONTENTS

Page

ACKNOWLEDGEMENTS iv

LIST OF TABLES vii

LIST OF FIGURES viii

CHAPTER

1 INTRODUCTION AND LITERATURE REVIEW 1

Fruit growth 3

Regulation of fruit growth 4

Perspective 13

References 14

2 INTERPLAY AMONG GROWTH-PROMOTING AND GROWTH-RESTRICTING PHYTOHORMONE MODULES REGULATES EARLY FRUIT DEVELOPMENT IN APPLE 22

Abstract 23

Introduction 24

Materials and methods 27

Results 29

Discussion 36

References 43

3 THE TCP MODULE AND REGULATION OF EARLY FRUIT GROWTH 59

Abstract 60

Introduction 61
Materials and methods 64
Results 69
Discussion 75
Conclusion 81
References 82
4 THE GRF/GIF MODULE AND REGULATION OF EARLY FRUIT GROWTH ... 97
Abstract 98
Introduction 99
Materials and methods 101
Results 105
Discussion 109
References 114
APPENDICES

LIST OF TABLES

Table 3.1 Probe sequence for electrophoretic mobility shift assay 87

Table 4.1 Number of cloned MdGRF11 transcripts displaying the ‘T and ‘C’ alleles during apple early fruit development 120

Table S2.1 Mapping statistics of the RNA-seq dataset..... 128

Table S2.2 The concentration of phytohormones in the ‘Empire’ apple fruit cortex 129

Table S4.1 List of 56 genotypes used for double-mismatch allele-specific (DMAS) qPCR . 131

LIST OF FIGURES

Figure 2.1 Fruit growth in ‘Empire’. Fruit diameter, length, and volume were measured from 6 d after full bloom 49

Figure 2.2 Identification of genes involved in early fruit development in ‘Empire’ apple 50

Figure 2.3 Gene ontology (GO) categorization of differentially expressed genes (DEGs) grouped into cluster 3..... 51

Figure 2.4 Differentially expressed genes (DEGs) in the apple cortex across different stages of early fruit development..... 53

Figure 2.5 The concentration of phytohormones in the ‘Empire’ apple cortex during early fruit development. 55

Figure 2.6 Transcript abundance of genes involved in abscisic acid (ABA) metabolism and signaling in the apple cortex during early fruit development 57

Figure 2.7 Transcript abundance of genes involved in jasmonic acid (JA) metabolism and signaling in the ‘Empire’ apple cortex during early fruit development. 58

Figure 3.1 Transcript abundance of *MdTCP2b* in ‘Golden Delicious Smoothee’ and ‘Empire’ fruit cortex and pith..... 88

Figure 3.2 Post-transcriptional regulation of *MdTCP2b* transcript by *miR319*. 89

Figure 3.3 Interaction of MdTCP2b with *MdKRP4* and *MdKRP5* promoters..... 90

Figure 3.4 Heterologous overexpression of *MdTCP2b* in Arabidopsis..... 92

Figure 3.5 Heterologous expression of *MdTCP2b* promotes flowering time and reduced leaf size in Arabidopsis 94

Figure 3.6 Heterologous expression of *MdTCP2b* promotes positive leaf curvature in Arabidopsis 95

Figure 4.1 Transcript abundance of *MdGRF11* and *MdGIF3* in 'Empire' fruit cortex and pith 121

Figure 4.2 Transcript abundance of *miR396* in 'Golden Delicious Smoothee' fruit cortex and pith 122

Figure 4.3 Post-transcriptional regulation of *MdGRF11* transcript by *miR396*..... 123

Figure 4.4 Genotyping of the MdGRF11 single nucleotide polymorphisms across 56 apple genotypes 124

Figure 4.5 Protein-protein interaction between MdGRF11 and MdGIF3 125

Figure S2.1 Multidimensional scaling (MDS) plot of the RNA-seq data..... 133

Figure S2.2 A heatmap of transcript abundance of identified genes involved in ethylene metabolism and signaling 134

Figure S2.3 Gene ontology (GO) enrichment analysis of differentially expressed genes (DEGs) in clusters 4 and 6 135

Figure S3.1 Transcript abundance of *miR319b* in 'Golden Delicious Smoothee' and 'Empire' fruit cortex and pith..... 137

Figure S3.2 SDS-PAGE gel for TCP-GST fusion protein and GST protein 138

Figure S3.3 Calculation of curvature index (CI) 139

CHAPTER 1

INTRODUCTION AND LITERATURE REVIEW

Apple (*Malus* × *domestica*) is a flavorful, edible fruit, which is cultivated worldwide. Fruit size is an important commercial trait in many crops including apple. Understanding growth and development of the fruit is not only of biological significance but also presents considerable economic worth. However, unlike other model fleshy fruit species, the fleshy part of the apple fruit is largely derived from non-ovarian tissue. Regulation of apple fruit growth is therefore significantly different from those model fleshy fruit species. Overall, apple fruit growth is an integration of multiple processes, including genotypic characteristics, phytohormone-dependent regulation, environmental regulation, and availability of metabolic resources (Malladi, 2020). These factors are likely to differentially regulate growth across multiple stages of fruit development, and across different fruit tissues.

Generally, fruits are considered as enlarged organs surrounding the seeds, or as the ripened ovary originating from the flower along with accessory parts. The apple fruit is a "pome" fruit which belongs to Rosaceae family. Such fruits typically consist of fleshy exocarp and mesocarp tissue and a cartilaginous endocarp surrounding the seeds, which together are referred to as the core or pith, and constitute a smaller part of the fruit volume (Malladi et al., 2020). Hence, this region is largely of ovarian origin. One fruit usually contains five carpels and each carpel can possess up to four ovules (Esau, 1977). The vascular traces of five sepals and five petals that surround the core together form the core-line. The tissue outside of core-line is referred to as the cortex or hypanthium (floral cup). It typically constitutes over 80% of the fruit volume at maturity

and is the economically important part of the apple fruit (Tukey and Young 1942; Goffinet et al. 1995; Malladi et al., 2020).

Despite the economic significance of the cortex tissue, the origin of the cortex is not completely clear. The receptacular and the appendicular hypotheses have been proposed to describe the origin of the pith and cortex (MacDaniels 1940). The receptacular hypothesis proposes that the major part of fruit is originated from axial tissue extending from the stem (pedicel). The cortex tissue is the extension of the cortical region, while the pith is the extension of internal parenchymatous cells. As per this theory, the ovarian tissue is restricted to a few cell layers immediately surrounding the seeds. The appendicular hypothesis, supported by data from cytochimeras and comparative vascular anatomy of the Rosaceae family fruits, has gained greater acceptance (Pratt 1988; Malladi 2020). This theory suggests that the core-line is the fusion line between the floral tube (hypanthium) and the ovary. The peripheral tissue of core-line accounts for the largest portion of the fruit. Further, this tissue is proposed to be derived from the fused bases of the sepals, petals, and stamens (MacDaniels 1940). The fleshy tissue inside core-line surrounding seed locules is considered to originate from the ovary (MacDaniels 1940; Pratt 1988). Kotoda et al. (2000) and Yao et al. (1999) used MADS-box genes as markers and found that the cortex tissue was likely derived at least from sepal tissues. Facultatively parthenocarpic spontaneous mutants of apple suggested that petal and stamen tissues are unlikely to contribute significantly to the development of the cortex/floral tube region (Yao et al. 2001, 2018). Overall, these studies support the appendicular hypothesis indicating that the basal part of floral organs, particularly the sepals, contribute to development of fleshy tissue of the apple fruit.

Fruit growth

Apple fruit growth and development is a complex process beginning from fruit formation to ripening and can be separated into four stages: bloom and fruit set, early fruit development, mid fruit development, and ripening (late fruit development). Apple fruit development is a temporally long activity that requires around 150 d to produce a mature apple fruit. A brief timeline of apple fruit growth and development are summarized below. It should be noted that fruit growth and development differ based on the environmental conditions and genetic differences and hence, these timelines are generalized. The example below is from the cultivar, Royal Gala (Denne, 1960; 1963). Flower buds initiate in the previous season and progress through eight stages of morphological development before winter dormancy. Following bud-break, substantial growth mediated by cell production and expansion is noted (Foster et al., 2003; Malladi and Johnson 2011). Around a week before full bloom, growth of the hypanthium/cortex tissue ceases temporarily with an associated cessation of cell production and expansion (Smith, 1950; Malladi and Johnson, 2011). This cessation may prevent growth of the organ prior to pollination and fertilization. This period of quiescence continues until around 3-11 d after full bloom (DAFB). After full bloom, fruit undergoes an intensive period of cell division that is typically sustained until 35 days after full bloom (DAFB). By 35 DAFB cell division largely ceases, and fruit growth is mediated mostly by cell expansion, coincident with the start of starch accumulation (Jing and Malladi, 2020). Cell expansion reaches peak with greatest starch accumulation around 60 DAFB. At 90 DAFB, cell expansion activity decreases but continues until fruit maturity. Concomitantly starch levels start declining. Ripening time is highly variable but usually occurs over 30 ds, involving high metabolic activity that increases soluble sugar levels. At 150 DAFB, fruits are considered “tree ripe” with fully developed flavor and skin color that can be considered as fully ripened (Janssen, et al., 2008).

The apple fruit growth model has been argued for several decades. It was first described as sigmoid growth pattern by Pratt (1988). Several studies that monitored individual fruit growth proposed a double-sigmoid growth model. An expolinear model of growth of apple fruit was proposed by Lakso et al. (1995), and it fits measured fruit growth, especially under resource non-limiting conditions. In the expolinear model, early fruit growth is greatly contributed by intensive cell production; and extends from around 8 DAFB to 30 DAFB, but it may last until 49 DAFB, which depends on genotypic differences, environmental conditions, and availability of resources. Then it is followed by a linear phase of fruit growth associated with cell expansion, during which fruit size could increase by over 1000-fold (Bain and Robertson, 1951; Jing and Malladi, 2020). During this period, fruit growth and development is mostly limited by the supply of carbon (C) nitrogen (N) and other resources (Lakso et al., 1995). The final stage of fruit development is climacteric ripening. During this period, a series of changes in fruit color, soluble sugar content, fruit texture and acidity mark the end of fruit maturation and the beginning of fruit senescence. Fruit may continue growth through cell expansion at this stage (Lakso and Goffinet, 2017).

Regulation of fruit growth

Flowering before full bloom

Although flowering time is not accounted as part of the period of fruit development, flowering and pollination/fertilization are critical for fruit development. The flower buds are initiated one season before. After a vegetative-to-flower phase transition, production of 16 to 21 appendages such as bracts, true leaves, transition leaves and bud scales within flower buds can occur in the axils of the true leaves. The flower-bud primordia formation reaches a peak around 53 DAFB and is followed by the appearance of calyx lobes. Anthers develop around 90 DAFB, and pistil development occurs 30 d later. Cavities of ovaries appear around 135 DAFB, but ovules do not develop until the end

of winter dormancy (~280 DAFB) (Childers, 1961). Flower differentiation is completed shortly before the flower blossom/opening (Pratt 1988).

Carbon-nitrogen (C-N) relationship has been reported to be key in regulating flower bud formation. Carbohydrates provide energy and C backbones for flower bud formation; thus, factors that affect photosynthesis near spurs can alter formation of flower buds. Moderate application of N fertilizer can increase number of flower buds, while excessive application of N extends the vegetative growth period leading to reduction of flowering (Childers, 1961). Furthermore, there is evidence that phytohormones regulate flower bud formation. Gibberellins (GA) influence flower bud induction in pome fruits. GA_7 which is rich in apple seeds strongly suppresses flowering in apple. GA movement in phloem from spurs bearing fruits is higher than that without fruits (Marino and Greene, 1981). Exogenous application of cytokinin can relieve the suppression of GA in flower bud induction.

Early fruit development (EFD)

There are three major factors that regulate organ growth: cell production, cell expansion, and void space development. Although cell production and cell expansion are highly interrelated processes that significantly influence fruit size, cell number is often correlated with the final size of apple fruit (Harada et al., 2005; Malladi and Hirst, 2010). And during early fruit development (EFD), cell production is the major factor mediating fruit growth. Cell production refers to new cells produced through the process of cell division (Malladi 2020). The rate of cell production and the duration of this period within specific fruit tissues are the two factors that together determine final cell number.

Cortex and pith tissues originate differently and they display different growth patterns during fruit development. Cortex and pith tissue display similar sizes at the beginning of fruit

growth, but the cortex accounts for more than 80% of the fruit volume at maturity (Bain and Robertson, 1951; Jing and Malladi, 2020). Differential rates of tissue growth were noted between the pith and the cortex during early fruit development, with the cortex displaying greater relative tissue growth rate (RTGR) during this period (< 30 DAFB; Jing and Malladi, 2020). The higher growth in cortex than pith during early fruit development indicates that differential growth is established during that period. Differential metabolism between these tissues is an important component of the differential growth programs across these tissues. Intensive cell production requires carbohydrates and other nutrients as cell growth that precedes cell division requires synthesis of additional cell wall components, organelles, cytoplasmic material, and membranes. Concomitantly, higher availability of energy is required to sustain the synthesis of these components. Together, these processes require high metabolic activity (Beshir, et al., 2017). Jing and Malladi (2020) found that the cortex tissue displayed higher imported C and N resource metabolism during EFD. Potentially, such a metabolic program provides the energy, proteins, C backbones and osmolytes to support its higher growth. In contrast, the metabolic program within the pith displayed limited allocation of C and N to growth, but more to storage. Cell division requires great amount of energy and carbon skeletons derived from carbohydrate metabolism (Nguyen-Quoc and Foyer, 2001). Sucrose (Suc) and sorbitol (Sor) are the major C sources transported into the sink cell and are converted to fructose (Fru), glucose (Glc) and UDP-Glc. Fru is mainly phosphorylated to participate in the TCA (tricarboxylic acid cycle) cycle that provides energy and C intermediates, while phosphorylated Glc and UDP-Glc may be used for respiration, cell wall polysaccharide synthesis, and starch formation (Rolland, et al., 2006). Additionally, Suc, Fru and Glc may also be transported and stored in the vacuole (Rolland, et al., 2006). During EFD, imported Sor and Suc are rapidly utilized for cell division under the high activities of the enzymes

(Jing and Malladi, 2020). Concomitantly, extra soluble sugars and organic acids are stored in the vacuole.

There are four phases for the cell division cycle: 1. G1 phase – first growth phase or a gap phase occurs immediately after the generation of a new cell. 2. S phase – DNA replication phase results in doubling of the nuclear genome. 3. G2 phase – a gap between DNA synthesis and mitosis, involving cell growth. 4. M phase – cell growth ceases, and mitosis occurs. G1 to S phase, and G2 to M phase are two important transitions during the cell cycle (Francis, 2007; Inze and De Veylder, 2006). Many genes are identified as being directly associated with the cell cycle; the key classes of regulatory units in cell division are *CYCLINs (CYC)* and *CYCLIN DEPENDENT KINASES (CDKs)*. The CDKA/CYCD complex facilitates the G1 to S transition by dissociating the E2F/DP complex from RBR (retinoblastoma-related protein). The E2F/DP complex subsequently triggers the transcription of genes for DNA duplication (Inze and De Veylder, 2006). CDKA/B and CYCA/B/D control G2 to M transition by promoting the binding of MYB repeat transcription factors to M phase Specific Activators (MSA), elements that promote the expression of M phase specific genes (Berckmans and De Veylder, 2009). The *CYCLIN-DEPENDENT KINASE INHIBITOR 1 (ICK1)/ KIP-RELATED PROTEINs (KRPs)* are direct inhibitors of CDK activity that inhibit the complex of CDKA/CYCD to negatively regulate progression of the cell cycle. In apple, two *KRPs* (*MdKRP4* and *MdKRP5*) were identified to be negatively associated with cell production during fruit growth. These KRPs present complementary transcript abundance patterns to those of positive regulators such as the *CYCs* and *CDKBs* (Malladi and Johnson, 2011). The transcript abundance of *MdKRP4* and *MdKRP5* decreased during early fruit development and increased during the transition from cell production to expansion (Malladi and Johnson, 2011). CDKB1;1 has been identified as positive cell cycle indicator in Arabidopsis leaf development. A

microarray-based analysis indicated that two homologs of *CDKB1;1* in apples also showed high expression level during EFD, and then decreased with the cessation of apple cell division (Janssen et al., 2008). Moreover, many *CDKBs* and several positive cell cycle indicators showed increased expression level during the fruit set period (Malladi and Johnson, 2011).

Cell cycle activity is strongly influenced by many phytohormones at different stages, including auxin, cytokinin (CK), GA, brassinosteroid (BR), abscisic acid (ABA) and methyl jasmonate (MeJA). Among them, auxin, CK, GA, and BR are generally considered to function as positive regulators that promote the cell cycle, while ABA and MeJA are negative regulators (Achard et al., 2009; Castellano Mdel et al., 2004; Magyar et al., 2005; Noir et al., 2013). Auxins (*e.g.* indole-3-acetic acid; IAA) are a class of plant hormones that regulate organ growth by promoting cell wall loosening and stimulating cell expansion. Injection of IAA into the fruit of 30 DAFB significantly promotes apple fruit growth, resulting in larger fruit (Devoghalaere, et al., 2012). Endogenous auxin can regulate fruit growth as well as fruit displaying larger size had higher free IAA content (Bu, et al., 2020). Cytokinin is a well-known plant hormone with established roles in promotion cell production. The application of plant growth regulator, 6-benzyl adenine (6-BA), can result in a reduction in fruit load that indirectly increases the fruit size of the remaining fruit in apple (Stern et al., 2003). In contrast, ABA was reported to negatively regulate the cell cycle by activating the expression of *KRPs* in Arabidopsis (Wang, et al., 1998).

The core cell cycle machinery promotes cell production to facilitate fruit growth, while there are many other genes that appear to coordinate regulation of organ size. Many organ size related genes have been identified in model plants such as *Arabidopsis* and tomato (*Solanum lycopersicum*). For example, the *FRUIT WEIGHT 2.2 (FW2.2)/ CELL NUMBER REGULATOR (CNR)* gene identified initially in tomato functions as a fruit weight related gene (Frary, et al.,

2000). It has been identified that it negatively regulates fruit growth in tomato. Large-fruited cultivars of tomato transformed with the *fw2.2* allele produced reduced size fruit (Frary, et al., 2000). *FW2.2* is responsible for up to 30% of the variation in fruit size between large and domesticated tomatoes (Nesbitt and Tanksley, 2001). Several putative *CNR* homologs were found in other Rosaceae family members (peach and cherry) and two of them co-localized to cherry fruit size QTLs (De Franceschi et al., 2013). Jing and Malladi (2022) identified multiple *CNR* genes in apple. They reported the identification of *CNR20a* and *CNR20b* as genes potentially associated with negative temporal regulation of cell production during fruit growth in apple. Interestingly, these two genes are similar to one of the genes from peach and cherry that co-localized to a cherry fruit size QTL (De Franceschi et al., 2013). Many other potential organ size regulators such as GROWTH REGULATING FACTORs (GRFs), GRF-INTERACTING FACTORs (GIFs), and AUXIN REGULATED GENE INVOLVED IN ORGAN SIZE (ARGOS) were also found to be associated with regulation of fruit growth, primarily during EFD (Jing and Malladi, 2022).

Mid fruit development (MFD)

Subsequent to cell division, the main factor that regulates fruit growth is cell expansion, which can increase cell volume up to 1500-fold. During the mid-development stage, most cell division has ceased and growth is largely mediated by cell expansion, thus it is also referred to as post-mitotic cell expansion. The increase of cell size may not be uniform or constant as the initial relative cell expansion rate (RCER), following the transitions from cell production to expansion, is relatively high, until around 40 DAFB (Dash and Malladi, 2012). Then, RCER seems to decrease significantly, and slightly increase later at late stages of fruit development (Dash and Malladi, 2012; Jing and Malladi, 2020).

Cell expansion is a combination of multiple steps, including cell wall loosening, cell wall extension, and vacuolar expansion, and relaxation of stress. The basis of post-mitotic cell expansion is turgor-driven vacuolar enlargement. Therefore, cell wall loosening is critical to accommodate the cell capacity as the vacuole expands. Cell wall loosening requires the coordination of multiple proteins such as the expansin family proteins (EXP), and xyloglucan endotransglucosylase/hydrolases (XTHs). The hemicellulose dynamics model proposed by Dyson et al. (2012) explains the collaboration of XTH and EXP family enzymes in expanding the cell wall. Furthermore, the activities of those enzymes are facilitated by the acidification of apoplast (Barbez, et al., 2017; Rose, et al., 2002; Wolf, et al., 2012). Auxin and brassinosteroid (BR) were reported to promote the activity of P-type plasma membrane proton ATPases that results in apoplast acidification (Caesar, et al., 2011; Kalve, et al., 2014; Yokoyama and Nishitani, 2001). It has been reported that free auxin concentration increases in the cortex tissue during mid-development stage, during the period when fruit cells display post-mitotic cell expansion (Devoghalaere, et al., 2012).

Several potential cell wall modifying protein-encoding genes have also been identified in regulating fruit growth in apple. *COBRA (COB*) gene family proteins are cell wall modifying proteins associated with oriented cell expansion in *Arabidopsis* (Schindelman, et al., 2001). *MdCOB1* was identified in apple and its transcript abundance rapidly increased by four-fold during transitions from cell production to cell expansion-mediated growth, which also overlaps with the period of highest cell expansion rate in apple (Dash, et al., 2013). Furthermore, its transcript abundance was significantly reduced by severe shading treatment that results in a decrease in cell production and expansion (Dash, et al., 2012).

Another feature in mid-development stage is the accumulation of starch concomitant with the high cell expansion activity. As most cells transition from cell division to cell expansion, requirement of C skeletons may decrease, as expansion involves a substantial extent of volume increase due to water intake. Up-regulated starch synthesis is noted during this period to store the extra C in insoluble form in plastids (Janssen, et al., 2008; Jing and Malladi, 2020).

It has been reported the enzymes activities involved in Suc-Suc cycle, such as sorbitol dehydrogenase (SDH), cell wall invertase (CWINV), neutral invertase (NINV), vacuolar acid invertase (vAINV), fructokinase (FK), hexokinase (HK) and sucrose-phosphate synthase (SPS) were high at early stages of fruit development, and decreased at the mid-development stage (Li et al., 2012). Among those enzymes, the activities of SDH and vAINV decreased from 40 DAFB to 108 DAFB; NINV, FK and HK decreased with the fruit development; and SPS decreased from 40 DAFB to 108 DAFB, and increased at fruit maturity. The transcript abundance with corresponding genes showed a similar pattern, except for *MdSDH2-9* (Li, et al., 2012). Further, Jing and Malladi (2020) found that the transcript abundance of *MdCWINV*, *MdNINV4* and *MdvAINV* decreased from the early fruit development stage and remained at low level in cortex during MFD.

Late fruit development (LFD)

Cell expansion is the primary mechanism mediating growth from the end of EFD and continues until the end of fruit development around 150 DAFB (Janssen, et al., 2008). However, fruit development still proceeds through several stages of metabolism to reach the fully ripened fruit. This, includes a decrease in starch content, increase in soluble sugars content, changes in volatile aroma compounds, change in fruit pigmentation, and reduction in fruit firmness (Janssen, et al., 2008; Li, et al., 2012; Jing and Malladi, 2020).

During the ripening stage, starch breaks down and sucrose accumulates with increased SPS activity (Dai, et al., 2011; Li, et al., 2012). Fru accumulates from MFD and attains a high concentration at fruit maturity. Glc also increases at late development stage, but remains lower compared to the Fru concentration. It has been noted that two special tonoplast monosaccharide transporters (TMTs) for Fru and Suc encoded by *MdTMT1* and *MdTMT2* are highly expressed at the ripening stage, indicating a role for them in accumulating Fru and Suc in apple fruit (Li, et al., 2012).

From an evolutionary perspective, the great flavor fruits attain by accumulating soluble sugars and by synthesizing various volatiles attract animals and humans which is beneficial for seed spreading. There are over 300 aroma compounds that have been identified in apple, with the major compounds being aldehydes, alcohols and esters produced by fatty acids and amino acids precursors (Dimick and Hoskin, 1983; Espino-Diaz, et al., 2016; Forney, 2009). Aldehydes appear at the early ripening stage, but their content reduces as fruit mature. Then the content of alcohols increases by the degradation of corresponding aldehydes mediated by alcohol dehydrogenase (ADH) activity. Alcohols account for 6-16% of the total volatiles in ripe apple fruit, while esters can constitute from 80-98% of total volatiles (Altisent, et al., 2011). Hence, the esters are the main volatile aroma components as apple matures and are synthesized through the activity of alcohol acyltransferase (AAT) enzymes.

The phytohormone ethylene is critical for apple fruit ripening as it regulates the climacteric respiration burst, fruit softening, and biosynthesis of volatile aroma compounds (Espino-Diaz et al., 2016; Lay-Yee et al., 1990; Li, et al., 2006). Ethylene has been reported to increase the content of esters by up-regulating the transcript abundance of *MdATT* genes (Defilippi, et al., 2005; Defilippi, et al., 2005; Yang, et al., 2016). Furthermore, ethylene treatment altered the transcript

abundance of several *LOX* genes, which suggests cross-talk between ethylene and jasmonates (JAs). It has been reported that JAs increase ATT activity to promote the synthesis of esters, indicating JAs also participate in the regulation of fruit ripening (Li, et al., 2006).

Perspective

In past few decades, considerable progress has been made in studying the molecular mechanisms related to apple fruit growth and development. Approaches including transcriptome analysis, and proteome analysis help us understand the molecular mechanisms and relationships in fruit development (Daccord, et al., 2017; Janssen, et al., 2008; Xu, et al., 2020; Li et al., 2022). For instance, Xu et al. (2020) revealed metabolic divergence during apple fruit development by transcriptome analysis. Another RNA-seq study identified the molecular mechanisms of early apple fruit ripening (Nawaz, et al., 2021). However, the major stage that regulates fruit cell number, EFD, has not been intensively investigated. The roles of phytohormones, and genes associated with growth and developmental control in contributing to the regulation of EFD in apple is the main focus of this dissertation research.

References

Achard, P., Gusti, A., Cheminant, S., Alioua, M., Dhondt, S., Coppens, F., Beemster, G. T., and Genschik, P. (2009). Gibberellin signaling controls cell proliferation rate in Arabidopsis. *Curr Biol* **19**, 1188-93.

Altisent, R.*, et al.* Increased straight-chain esters content after ultra low oxygen storage and its relation to the lipoxygenase system in 'Golden Reinders (R)' apples. *Eur Food Res Technol* 2011;232(1):51-61.

Bain, J.M. and Robertson, R.N. The physiology of growth in apple fruits. I. Cell size, cell number, and fruit development. *Aust J Sci Res B* 1951;4(2):75-107.

Barbez, E.*, et al.* Auxin steers root cell expansion via apoplastic pH regulation in Arabidopsis thaliana. *Proc Natl Acad Sci U S A* 2017;114(24):E4884-E4893.

Berckmans, B. and De Veylder, L. Transcriptional control of the cell cycle. *Curr Opin Plant Biol* 2009;12(5):599-605.

Beshir, W.F.*, et al.* Dynamic Labeling Reveals Temporal Changes in Carbon Re-Allocation within the Central Metabolism of Developing Apple Fruit. *Front Plant Sci* 2017;8:1785.

Bu, H.*, et al.* Endogenous Auxin Content Contributes to Larger Size of Apple Fruit. *Front Plant Sci* 2020;11:592540.

Caesar, K.*, et al.* A fast brassinolide-regulated response pathway in the plasma membrane of Arabidopsis thaliana. *Plant J* 2011;66(3):528-540.

Castellano Mdel, M., Boniotti, M. B., Caro, E., Schnittger, A., and Gutierrez, C. (2004). DNA replication licensing affects cell proliferation or endoreplication in a cell type-specific manner. *Plant Cell* **16**, 2380-93.

Childers, N.F. Modern fruit science; orchard and small fruit culture. New Brunswick, N.J.: Horticultural Publications, Rutgers University; 1961.

Daccord, N.*, et al.* High-quality de novo assembly of the apple genome and methylome dynamics of early fruit development. *Nat Genet* 2017;49(7):1099-1106.

Dai, N.*, et al.* Metabolism of soluble sugars in developing melon fruit: a global transcriptional view of the metabolic transition to sucrose accumulation. *Plant Mol Biol* 2011;76(1-2):1-18.

Dash, M., Johnson, L.K. and Malladi, A. Severe Shading Reduces Early Fruit Growth in Apple by Decreasing Cell Production and Expansion. *J Am Soc Hortic Sci* 2012;137(5):275-282.

Dash, M., Johnson, L.K. and Malladi, A. Reduction of Fruit Load Affects Early Fruit Growth in Apple by Enhancing Carbohydrate Availability, Altering the Expression of Cell Production-related Genes, and Increasing Cell Production. *J Am Soc Hortic Sci* 2013;138(4):253-262.

Dash, M. and Malladi, A. The AINTEGUMENTA genes, MdANT1 and MdANT2, are associated with the regulation of cell production during fruit growth in apple (Malus x domestica Borkh.). *BMC Plant Biol* 2012;12:98.

De Franceschi, P.*, et al.* Cell number regulator genes in Prunus provide candidate genes for the control of fruit size in sweet and sour cherry. *Mol Breed* 2013;32:311-326.

Defilippi, B.G., Dandekar, A.M. and Kader, A.A. Relationship of ethylene biosynthesis to volatile production, related enzymes, and precursor availability in apple peel and flesh tissues. *J Agr Food Chem* 2005;53(8):3133-3141.

Defilippi, B.G., Kader, A.A. and Dandekar, A.M. Apple aroma: alcohol acyltransferase, a rate limiting step for ester biosynthesis, is regulated by ethylene. *Plant Sci* 2005;168(5):1199-1210.

Denne, M.P. The Growth of Apple Fruitlets, and the Effect of Early Thinning on Fruit Development. *Annals of Botany* 1960;24(95):397-406.

Devoghalaere, F*., et al.* A genomics approach to understanding the role of auxin in apple (Malus x domestica) fruit size control. *BMC Plant Biol* 2012;12:7.

Dimick, P.S. and Hoskin, J.C. Review of Apple Flavor - State of the Art. *Crc Cr Rev Food Sci* 1983;18(4):387-409.

Dyson, R.J., Band, L.R. and Jensen, O.E. A model of crosslink kinetics in the expanding plant cell wall: Yield stress and enzyme action. *J Theor Biol* 2012;307:125-136.

Esau, K. Anatomy of seed plants. New York: Wiley; 1977.

Espino-Diaz, M*., et al.* Biochemistry of Apple Aroma: A Review. *Food Technol Biotechnol* 2016;54(4):375-397.

Forney, C.F. Postharvest Issues in Blueberry and Cranberry and Methods to Improve Market-Life. *Acta Hortic* 2009;810:785-798.

Foster, T., Johnston, R., and Seleznyova, A. (2003). A morphological and quantitative characterization of early floral development in apple (Malus x domestica Borkh.). Ann Bot 92, 199-206.

Francis, D. The plant cell cycle--15 years on. *New Phytol* 2007;174(2):261-278.

Frary, A*., et al.* fw2.2: a quantitative trait locus key to the evolution of tomato fruit size. *Science* 2000;289(5476):85-88.

Goffinet, M.C., T.L. Robinson, and A.N. Lakso. 1995. A comparison of 'Empire' apple fruit size and anatomy in unthinned and hand-thinned trees. J. Hortic. Sci. 70:375–387.

Harada, T., W. Kurahashi, M. Yanai, Y. Wakasa, and T. Satoh. 2005. Involvement of cell proliferation and cell enlargement in increasing the fruit size of Malus species. Scientia Hortic. 105:447–456.

Inze, D. and De Veylder, L. Cell cycle regulation in plant development. *Annu Rev Genet* 2006;40:77-105.

Janssen, B.J.*, et al.* Global gene expression analysis of apple fruit development from the floral bud to ripe fruit. *BMC Plant Biol* 2008;8:16.

Jing, S. and Malladi, A. Higher growth of the apple (Malus x domestica Borkh.) fruit cortex is supported by resource intensive metabolism during early development. *BMC Plant Biol* 2020;20(1):75.

Kalve, S., De Vos, D. and Beemster, G.T. Leaf development: a cellular perspective. *Front Plant Sci* 2014;5:362.

Kotoda, N., M. Wada, S. Komori, S. Kidou, K. Abe, T. Msuda, and J. Soejima. 2000. Expression pattern of homologues of floral meristem identity genes LFY and AP1 during flower development in apple. J. Am. Soc. Hortic. Sci. 125:398–403.

Lakso, A.N., L.C. Grappadelli, J. Barnard, and M.C. Goffinet. 1995. An expolinear model of the growth pattern of the apple fruit. J. Hortic. Sci. 70:389–394.

Lakso AN, Goffinet MC. In 'Advances in understanding apple fruit development'. In: Achieving sustainable cultivation of apples. Cambridge: Burleigh Dodds Science Publishing; 2017. p. 104–33.

Lay-Yee, M., Dellapenna, D., and Ross, G. S. (1990). Changes in mRNA and Protein during Ripening in Apple Fruit (Malus domestica Borkh. cv Golden Delicious). *Plant Physiol* **94**, 850-3.

Li, D.P.*, et al.* Salicylic acid, ethephon, and methyl jasmonate enhance ester regeneration in 1-MCP-treated apple fruit after long-term cold storage. *J Agric Food Chem* 2006;54(11):3887-3895.

Li, D.P.*, et al.* Molecular cloning and expression of a gene encoding alcohol acyltransferase (MdAAT2) from apple.(cv. Golden Delicious). *Phytochemistry* 2006;67(7):658-667.

Li, M., Feng, F. and Cheng, L. Expression patterns of genes involved in sugar metabolism and accumulation during apple fruit development. *PLoS One* 2012;7(3):e33055.

MacDaniels, L.H. 1940. The morphology of the apple and other pome fruit. New York (Cornell University) Agr. Expt. Sta. Mem. 230:3–30.

Magyar, Z., De Veylder, L., Atanassova, A., Bako, L., Inze, D., and Bogre, L. (2005). The role of the Arabidopsis E2FB transcription factor in regulating auxin-dependent cell division. *Plant Cell* **17**, 2527-41.

Malladi, A. (2020). "Molecular physiology of fruit growth in apple," in *Horticultural reviews*. Ed. Warrington, I. (Hoboken, New Jersey: Wiley), 1–42.

Malladi, A. and Hirst, P.M. Increase in fruit size of a spontaneous mutant of 'Gala' apple (Malus x domestica Borkh.) is facilitated by altered cell production and enhanced cell size. *J Exp Bot* 2010;61(11):3003-3013.

Malladi, A. and Johnson, L.K. Expression profiling of cell cycle genes reveals key facilitators of cell production during carpel development, fruit set, and fruit growth in apple (Malusxdomestica Borkh.). *J Exp Bot* 2011;62(1):205-219.

Marino, F. and Greene, D.W. Involvement of Gibberellins in the Biennial Bearing of Early Mcintosh Apples. *J Am Soc Hortic Sci* 1981;106(5):593-596.

Nawaz, I.*, et al.* RNA-Seq profiling reveals the plant hormones and molecular mechanisms stimulating the early ripening in apple. *Genomics* 2021;113(1 Pt 2):493-502.

Nesbitt, T.C. and Tanksley, S.D. fw2.2 directly affects the size of developing tomato fruit, with secondary effects on fruit number and photosynthate distribution. *Plant Physiol* 2001;127(2):575-583.

Nguyen-Quoc, B. and Foyer, C.H. A role for 'futile cycles' involving invertase and sucrose synthase in sucrose metabolism of tomato fruit. *J Exp Bot* 2001;52(358):881-889.

Noir, S., Bomer, M., Takahashi, N., Ishida, T., Tsui, T. L., Balbi, V., Shanahan, H., Sugimoto, K., and Devoto, A. (2013). Jasmonate controls leaf growth by repressing cell proliferation and the onset of endoreduplication while maintaining a potential stand-by mode. Plant Physiol 161, 1930-51.

Patricia Denne, M. Fruit development and some tree factors affecting it. *New Zealand Journal of Botany* 1963;1(3):265-294.

Pratt, C. 1988. Apple flower and fruit: morphology and anatomy. Hortic. Rev. 10:273–308.

Rolland, F., Baena-Gonzalez, E. and Sheen, J. Sugar sensing and signaling in plants: conserved and novel mechanisms. *Annu Rev Plant Biol* 2006;57:675-709.

Rose, J.K.*, et al.* The XTH family of enzymes involved in xyloglucan endotransglucosylation and endohydrolysis: current perspectives and a new unifying nomenclature. *Plant Cell Physiol* 2002;43(12):1421-1435.

Schindelman, G.*, et al.* COBRA encodes a putative GPI-anchored protein, which is polarly localized and necessary for oriented cell expansion in Arabidopsis. *Genes Dev* 2001;15(9):1115-1127.

Stern, R.A., R. Ben-Arie, O. Neria, and M. Flaishman. 2003. CPPU and BA increase fruit size of 'Royal Gala' (Malus domestica) apple in a warm climate. J. Hort. Sci. Biotech. 78:297–302.

Tukey, H.B. and J.O. Young. 1942. Gross morphology and histology of developing fruit of the apple. Bot. Gaz. 104:3–25.

Wang, H.*, et al.* ICK1, a cyclin-dependent protein kinase inhibitor from Arabidopsis thaliana interacts with both Cdc2a and CycD3, and its expression is induced by abscisic acid. *Plant J* 1998;15(4):501-510.

Wolf, S., Hematy, K. and Hofte, H. Growth control and cell wall signaling in plants. *Annu Rev Plant Biol* 2012;63:381-407.

Xu, J.*, et al.* Integrative Analyses of Widely Targeted Metabolic Profiling and Transcriptome Data Reveals Molecular Insight into Metabolomic Variations during Apple (Malus domestica) Fruit Development and Ripening. *Int J Mol Sci* 2020;21(13).

Yang, X.T.*, et al.* Ethylene and 1-MCP regulate major volatile biosynthetic pathways in apple fruit. *Food Chem* 2016;194:325-336.

Yao, J.-L., J. Xu, S. Tomes, W. Cui, Z. Luo, C. Deng, H.S. Ireland, R.J. Schaffer, and A.P. Gleave. 2018. Ectopic expression of the PISTILLATA homologous MdPI inhibits fruit tissue growth and changes fruit shape in apple. Plant Direct. 2:e00051.

Yao, J.-L., Y.-H. Dong, and B.A.M. Morris. 2001. Parthenocarpic apple fruit production conferred by transposon insertion mutations in a MADS-box transcription factor. Proc. Natl. Acad. Sci. USA. 98:1306–1311.

Yao, J.L., Y.H. Dong, A. Kvarnheden, and B. Morris. 1999. Seven MADS-box genes in apple are expressed in different parts of the fruit. J. Am. Soc. Hortic. Sci. 124:8–13.

Yokoyama, R. and Nishitani, K. A comprehensive expression analysis of all members of a gene family encoding cell-wall enzymes allowed us to predict cis-regulatory regions involved in cell-wall construction in specific organs of Arabidopsis. *Plant Cell Physiol* 2001;42(10):1025-1033.

CHAPTER 2

INTERPLAY AMONG GROWTH-PROMOTING AND GROWTH-RESTRICTING PHYTOHORMONE MODULES REGULATES EARLY FRUIT DEVELOPMENT IN APPLE

Abstract

The growth of major fleshy tissue of apple fruit is spatially-temporaly different. These tissues are spatially separated into cortex and pith. Cortex is the major fleshy region of the mature fruit which can be > 5-fold greater than pith during early fruit development. Early fruit growth is exponential and primarily associated with cell production, then the fruit growth exhibited a linear model and is more related to the cell expansion. However, the transcriptome of early fruit development remains poorly characterized. Using the apple cultivar 'Empire', we analyzed the transcriptome of the cortex tissue harvested at four different stages of early development. Our results indicate that different expressed genes related to microtubule movement, the cell cycle, and cell cycle core component protein activity were up-regulated between 6 and 10 DAFB and down-regulated between 18 and 26 DAFB, suggesting that apple fruit undergoes a high level of cell division during EFD and then transits to cell differentiation at later stage. The genes specifically expressed in cluster 6 are involved in microtubule function, cell wall biogenesis and organization, tissue development, and cell maturation, indicating the genes in cluster 6 were responsible for cell expansion and cell differentiation. Genes associated with photosynthesis partially provided the energy for intense cell division; however, the majority were supported by C metabolism in cluster 6, included carbohydrate metabolic process and glycosyl compound metabolic process. Our study provides a broader catalog of transcriptional changes associated with cell division and cell expansion and strength the comprehensive molecular system model that regulate early fruit growth and development.

Introduction

Apple fruit *(Malus × domestica)* is a sweet edible tree fruit that is cultivated worldwide. The apple fruit consists of two fleshy tissues of diverse origins. The central part of an apple fruit contains five locules derived from the carpels. The carpels also develop fleshy exocarp and mesocarp tissues and a cartilaginous endocarp. Together, these tissues may form the core of the fruit. Alternatively, the carpel derived tissues form a limited fleshy tissue surrounded by a fleshy pith tissue (MacDaniels 1940; Pratt 1988; Malladi, 2020). The majority of the fleshy fruit tissue of economic significance is comprised of accessory tissue, of non-ovarian origin, and generally termed as the cortex (Pratt 1988). The cortex and pith tissues display differential growth supported by differential metabolism during fruit development (Jing and Malladi, 2020). The cortex displays higher growth rate (> 5-fold) than the pith during early fruit development (EFD), which allows for this region to generally constitute over 80% of the fruit volume at maturity (Malladi et al., 2020).

Apple flower growth after bud-break and before bloom involves intensive cell production and cell expansion (Malladi and Johnson, 2011). Growth within the region of the flower corresponding to the fruit cortex ceases around one week before bloom (Smith, 1950; Malladi and Johnson, 2011). Cessation of growth before bloom is mediated by a dramatic decrease in cell production and cell expansion resulting in a period of quiescence prior to re-activation following fruit set. Quiescence in cell production is associated with reduction in transcript abundance of multiple cell cycle genes that promote progression of the cell cycle, and up-regulation of genes associated with negative regulation of the cell cycle (Malladi and Johnson, 2011). Resumption of growth following pollination and fertilization is typically observed 3-11 DAFB (Malladi and Johnson, 2011). Impairment of pollination and fertilization during this period results in a lack of growth resumption and subsequent abscission of the flower (Malladi and Johnson, 2011).

Resumption of growth during this period follows fruit set and marks the beginning of fruit growth. Apple fruit growth is mediated by intensive cell production during the initial growth period and cell expansion throughout fruit development. A rapid increase in the size of organ is observed immediately after fruit set. The exponential increase in fruit size during EFD is primarily associated with increased cell production and lasts usually around 3-5 weeks after full bloom (WAFB) but may continue for longer in some cultivars (Lakso et al., 1995; Malladi, 2020). Intensive cell production has been noted during EFD, from around 8 to 30 days after full bloom (DAFB) (Malladi and Johnson, 2011; Dash and Malladi, 2012; Malladi and Hirst, 2010). Fruit growth subsequently exhibits a linear pattern and is mostly driven by cell expansion.

Final size of the fruit is largely determined by the number of cells, which in turn is greatly dependent on cell production during EFD (Zhang et al., 2016). Cell proliferation, a process which includes cell growth, increase in volume and subsequent division of cells, during EFD requires inputs of energy and provision of carbon (C) backbones. Consistently, this period of fruit development involves high rates of respiration and consumption of C and N in the cortex (Beshir et al., 2017; Jing and Malladi, 2020). Therefore, EFD is not only crucial for fruit formation but is also a key period determining final fruit size.

Fruit growth regulation is a complex process that requires the coordination of multiple factors. Phytohormones are one such factor that regulate early growth and development of the fruit (Srivastava and Handa, 2005). Auxins regulate fruit set, growth, development and final fruit size in multiple fruits. In apple, exogenous indole-3-acetic acid (IAA) treatment to fruit during early stages of cell expansion increase cell size and fruit size (Devoghalaere et al., 2012). Free IAA concentration in the cortex is highest following the post-mitotic stage, indicating a role of auxin in cell expansion (Devoghalaere et al., 2012). Apple cultivars with greater fruit size also display

higher endogenous auxin concentration (Bu et al., 2020). Cytokinins are thought to promote cell division (Kieber and Schaller, 2014) and can therefore influence the rate and extent of cell production during EFD. Gibberillins (GAs) are thought to be involved in the regulation of fruit set in multiple fruits such as tomato, potentially by altering central C metabolism (Shinozaki et al., 2021). Abscisic acid (ABA) and ethylene may counter the roles of IAA and GAs in regulating fruit set (Vriezen et al., 2007). Jasmonic acid and its derivates called jasmonates (JAs) are another prominent class of phytohormones that are involved in the regulation of stress responses and various plant developmental processes such as senescence (Wasternack and Song, 2017). JAs may also be important for fruit growth and development. For example, the concentrations of JAs in strawberry and grapefruit are high at the immature fruit stages, and gradually decrease as fruit develop (Garrido-Bigotes et al., 2018; Liu et al., 2018).

A few previous studies have tried to address the regulation of fruit development through transcriptomic analyses in apple. However, these studies often focused on the whole process of fruit development, with limited emphasis on EFD (Janssen et al., 2008; Xu et al., 2020). A recent study performed comparative transcriptome analysis intensively during EFD across apple and peach (*Prunus persica* Batsch.) with the objective of identifying molecular components associated with fleshy fruit development across two distinct fruit types (pome and drupe, respectively) within the Rosaceae family (Li et al., 2022). In this study, expression of several MADS-box genes such as *PI* (*PISTILLATA*) and *TM6* was found to be negatively associated, while that of *FBP9* genes was positively associated, with fleshy fruit development. Further, this study suggested that auxin and GA biosynthesis could be directly induced by pollination within the apple hypanthium and together these phytohormones may regulate EFD. However, most of the previous studies in apple have not evaluated changes in phytohormone concentrations during EFD. Particularly, such

changes have not been explored in relation to changes in the transcriptome during EFD. In this study, the transcriptome of the apple fruit cortex was evaluated at multiple stages during EFD. Further, profiling of a broad range of phytohormones was also performed at the same stages to better understand the role of these regulators of growth and development.

Materials and methods

Plant material

Mature apple trees of the cultivar 'Empire' grown at the Mountain Research and Education Center, Blairsville, GA were used in this study. Flowers were manually thinned to the central (king) flower per cluster at 6 DAFB. Fruit diameter (d) and length (l) were measured by calipers, and the volume was calculated from the measured diameter and length ($\prod d^2 l/6$). The relative growth rates (RGR) of diameter, length, and volume were determined as: $[Ln(A_2) - Ln(A_1)] / [T_2 - T_1]$, where A_1 and A_2 are diameter/length/volume at two time points, T_1 and T_2, respectively. Four fruits were sampled at multiple stages. Cortex and pith tissues were separated manually, frozen in liquid nitrogen and stored at -80 °C until further use.

RNA extraction and sequencing

Total RNA was extracted using the CTAB method, as described previously (Vashisth et al., 2011). The RNA was treated with RNase-free DNase to reduce genomic DNA contamination. Three replicates of the cortex tissue at each stage (6, 10, 18 and 26 DAFB) were used in this study for transcriptome sequencing. cDNA library preparation was performed using the KAPA stranded mRNA-seq kit. The quality of the libraries was assessed using a Bio-Analyzer. The libraries were sequenced on the Illumina NexSeq500 platform using paired-end 75 bp read sequencing at the Georgia Genomics and Bioinformatics Core, University of Georgia.

RNA-seq Data analysis

Clean reads of sequences were retrieved by trimming the low-quality reads and adaptors from raw reads through Trimmomatic (Bolger et al., 2014). Reference genome of *Malus x domestica* Genome (GDDH13 v1.1) was generated by Bowtie2 (https://www.rosaceae.org). Trimmed paired-end reads were aligned to the reference genome using Tophat2 (Kim et al., 2013). FeatureCounts was employed to count the number of reads that mapped to genomic features (Liao et al., 2014). Expression level of transcripts per million (TPM) were calculated from counts generated from FeaureCounts, using edgeR. Scaled TPM were calculated in R to generate the heatmap through heatmap2 in R (R Core Team, 2020), RStudio (Rstudio Team, 2020). Linear modeling was used to compare the gene expression differences between any two stages: 6 DAFB versus (vs.) 10 DAFB, 6 DAFB vs. 18 DAFB, 6 DAFB vs. 26 DAFB, 10 DAFB vs. 18 DAFB, 10 DAFB vs. 26 DAFB, and 18 DAFB vs. 26 DAFB. Comparison of gene expression differences among four stages were also conducted by the ANOVA-like test. The average TPM of the differentially expressed genes (DEGs) derived from ANOVA analysis were used to generate gene clusters by R (R Core Team, 2020), and RStudio (Rstudio Team, 2020). Gene ontology (GO) enrichment analyses were performed within each cluster, and using DEGs across different stages using AgriGo (agriGO v2.0; http://systemsbiology.cau.edu.cn/agriGOv2/).

Phytohormone quantification

Quantification of phytohormones was performed at Metware Biotechnology Co. Ltd. (www.metwarebio.com). Fruit cortex tissue from 6, 10, 18 and 26 DAFB were used for these analyses. At each stage, four biological replicates were used for the analysis, except at 6 DAFB where limited tissue availability allowed only for quantification from three replicates. Extraction of phytohormones was performed using methanol:water:formic acid (15:4:1). After addition of an

internal standard mix, the extractants were centrifuged, evaporated to dryness and re-dissolved in 80% methanol. Quantification of metabolites was performed using an UPLC-ESI-MS/MS system (UPLC: ExionLC AD; MS: Applied Biosystems 6500 Triple Quadrupole). A Waters ACQUITY UPLC HSS T3 C18 column was used with the UPLC (100 mm × 2.1 mm i.d; 1.8 µm). The solvent system consisted of water (0.04% acetic acid): acetonitrile (0.04% acetic acid). The gradient program consisted of 95:5 V/V at 1 min, 5:95 V/V at 8 min, hold for 1 min, 95:5 V/V at 9 min; hold for 3 min. The flow rate was 0.35 mL/min; temperature was 40 °C and the injection volume was 2 µL. For the MS/MS, linear ion-trap and triple quadrupole scans were obtained on a QTRAP mass spectrometer with ESI operating in positive and negative ion modes. Data was acquired using Analyst 1.6.3 software (Sciex) and metabolites were quantified using Multiquant 3.0.3 software.

Results

Fruit growth

Fruit diameter increased by over 6-fold between 6 and 26 DAFB and continued to increase until 63 DAFB (Figure 2.1). Fruit length showed a similar trend with a 3.5-fold increase between 6 and 26 DAFB (Figure 2.1). Fruit volume increase until 63 DAFB could be well explained with a sigmoidal equation (Figure 2.1; R^2 = 0.996, P < 0.0001). The relative growth rate (RGR) of diameter, length and volume was high at the beginning of EFD, specifically at 10 and 18 DAFB and declined greatly thereafter, particularly between 18 and 26 DAFB. Subsequently, it remained low during the rest of measured fruit development (Figure 2.1).

Differentially expressed genes across developmental stages

Quality clean reads ranging from 8,423,712 to 20,664,355 were extracted by Trimmomatic after sequencing through Illumina NexSeq500 platform with paired-end reads. More than 89.1% reads could be mapped to the *Malus* × *domestica* reference genome (GDDH13 v1.1) (Table S2.1). The

concordant pair alignment rate ranged from 83.6% to 87.1%; and anything not within the concordant pairs was not selected for downstream analysis (Table S2.1). The gene expression level was normalized to gene length first and subsequently normalized to sequencing depth to calculate the transcripts per million (TPM).

Multidimensional scaling (MDS) analysis was performed to test similarity of the dataset. The MDS plot indicated that the three replicates of four different samples were clearly divided across two dimensions, especially for the samples of 18 and 26 DAFB, which clearly grouped into two tight clusters (Figure S2.1). Further, the four stages were clearly separable from each other. The three replicates at 10 DAFB displayed greater scatter, potentially owing to the inherent variability associated with fruit set at this developmental stage. One of the three replicates at 6 DAFB did not cluster with the remaining two replicates, but this stage was still clearly separable from the remaining stages of development. A heatmap generated from the identified genes during EFD further indicates the temporal differences in gene expression patterns during this period (Figure 2.2A). ANOVA indicated that there were 4873 genes that were differentially expressed across 6, 10, 18 and 26 DAFB with FDR (False discovery rate) < 0.001. Those DEGs were further analyzed with Mfuzz clustering analysis. The 4873 DEGs were separable into six clusters with distinct expression patterns. Around 1022 genes were assigned to cluster 1 which displayed a pattern of a dramatic decrease in abundance at the start of EFD (between 6 and 10 DAFB) and continued low abundance throughout this period (Figure 2.2B). 972 genes were grouped into cluster 2 which showed a decline in transcript abundance between 10 and 18 DAFB. The expression level of 544 genes grouped within cluster 3 increased between 6 and 10 DAFB, and later decreased between 18 and 26 DAFB 576 genes were grouped into cluster 4 which also displayed a decreasing pattern of expression between 18 and 26 DAFB, but this followed a trend of steady increase in expression

between 6 and 18 DAFB (Figure 2.1B). The 893 genes in cluster 5 displayed an increase in transcript abundance between 18 and 26 DAFB, while the 972 genes in cluster 6 showed a pattern of steady increase in expression during EFD.

To explore the significant changes of genes among different stages during EFD, linear modeling was performed to compare the pairwise gene expression differences among different stages. The number of DEGs within each pairwise comparison and a breakdown of these into up- and down-regulated genes is presented in Figure 2.4.

GO enrichment analysis of DEGs

To understand overall mechanisms represented by DEGs in different clusters and across pairwise development stage comparisons, GO enrichment analysis was used. Previous studies indicated that the cell proliferation is arrested around bloom and is re-initiated following pollination/fertilization (Smith, 1950; Malladi and Johnson, 2011; Liu et al., 2022). Further, cell proliferation-mediated growth continues in apple fruit until around 3-5 WAFB, after which growth is primarily mediated by cell expansion (Malladi, 2020). Hence, DEGs from the pairwise developmental stage comparisons: 6 vs. 10 DAFB, and 18 vs. 26 DAFB, were further investigated. GO terms enriched among up-regulated DEGs in 6 vs. 10 DAFB included microtubule-based process (GO:0007017) and microtubule-based movement (GO:0007018), suggesting that microtubule associated proteins are over-represented among genes up-regulated during this period when cell production is re-initiated (Figure 2.4B and Figure 2.4D). These GO terms were also enriched within down-regulated DEGs between 18 vs. 26 DAFB. The GO term, cell cycle (GO:0007049), was enriched among down-regulated DEGs in 18 vs. 26 DAFB. This included regulation of cell cycle (GO:0051726), cell cycle process (GO:0022402), mitotic cell cycle process (GO:1903047), mitotic nuclear division (GO:0007067), and regulation of cyclin-dependent protein kinase activity

(GO:1904029) (Figures 2.4C and 2.4E). Altogether, these results suggested that genes associated with microtubule movement and the cell cycle were co-regulated during early fruit development. In addition, photosynthesis related genes were observed in 18 vs. 26 DAFB down-regulated genes (GO:0015979).

The expression pattern of genes upregulated between 6 and 10 DAFB, and down-regulated between 18 and 26 DAFB are similar to the expression pattern of genes grouped in cluster 3. Therefore, GO enrichment classes of cluster 3 were further evaluated. The GO enrichment analysis results shows that genes associated with cell division are enriched in cluster 3, including microtubule-based movement (GO:0007018), spindle assembly (GO:0051225), regulation of cyclin-dependent protein kinase activity (GO:1904029), regulation of G2/M transition of mitotic cell cycle (GO:0010389), and cytokinetic process (GO:1902410) (Figures 2.3A and 2.3C). Furthermore, DNA replication is one of the major components in cell division. GO terms DNA replication (GO:0006260) and DNA replication initiation (GO:0006270) were identified within this cluster. Several GO terms associated with chromatin modifications that potentially alter DNA replication were also identified in cluster 3. These included DNA methylation (GO:0006306), histone lysine methylation (GO:0034968), and chromatin silencing by small RNA (GO:0031048). In addition, photosynthesis related GO terms were also identified in cluster 3. These GO terms included photosynthesis, light reaction (GO:0019684), photosynthetic electron transport chain (GO:0009767), and photosystem II assembly (GO:0010207), suggesting that photosynthetic activity, particularly that associated with the light reactions is down-regulated during later stages of EFD (Figure 2.3A).

GO terms enriched in cluster 4 included cell wall organization or biogenesis (GO:0071554), cell wall macromolecule biosynthetic process (GO:0044038), cell wall

polysaccharide biosynthetic process (GO:0070592), microtubule-based movement (GO:0007018), and microtubule cytoskeleton organization (GO:0000226) (Figure S2.3). Microtubules not only function in cell division, but also play an important role in cell expansion. Microtubules act as cytoskeleton to maintain cell shape and help cells resist compression force (Marchant and Hines, 1979). Previous studies also suggested that microtubules are important for cell wall by guiding the deposition of cellulose microfibrils (Giourieva and Panteris, 2021). Together, genes associated with cell expansion are enriched in cluster 4.

Genes associated with microtubule and cell wall biogenesis and organization were also enriched in cluster 6 indicating that these genes participate in cell expansion. Besides, presence of water transport (GO:0006833) and auxin transport (GO:0060918)-related genes further supports this possibility (Figure S2.3). The GO terms of developmental growth (GO:0048589), tissue development (GO:0009888), cell maturation (GO: 0021700), cell differentiation (GO:0030154), and trichoblast differentiation (GO:0010054) were enriched in cluster 6, indicating that the steady increase in transcript abundance of genes in cluster 6 also contributes to cell differentiation (Figure S2.3). GO terms enriched in cluster 6 also included stimulus response terms, such as response to nematode (GO:0009624), response to salt stress (GO:00009651), response to carbohydrate (GO:0009743), and response to UV-B (GO:000769) (Figure S2.3). The genes specifically expressed in cluster 6 were also assigned to GO terms including carbohydrate metabolic process (GO:0005975), flavonoid metabolic process (GO:0009812), phenylpropanoid metabolic process (GO:0009698), glycosyl compound metabolic process (GO:1901657), and glycolytic process (GO:0006096) (Figure S2.3). Overall, the GO enrichment analysis results show that genes associated with cell expansion, cell differentiation, and metabolism are enriched in cluster 6.

Phytohormone analysis during EFD

A heatmap of phytohormone concentrations in the apple fruit cortex tissue during EFD is presented in Figure 2.5A. Several phytohormones displayed high concentrations during early stages of EFD and a subsequent decline at later stages. ANOVA revealed that ABA and ABA-glucosyl ester (ABA-GE) displayed their highest concentration at 6 DAFB, which declined at 10 DAFB by around 4-fold and 2-fold, respectively (Figure 2.5B). These concentrations further declined by over 7- and 4-fold, respectively, between 10 and 18 DAFB. The concentration of the ethylene precursor, 1-aminocyclopropane carboxylate (ACC) was highest at 6 DAFB and declined by around 4-fold between 10 and 18 DAFB. IAA displayed the highest concentration at 6 DAFB and was not detectable at later stages of EFD. Among the GAs analyzed, GA_1 was the most abundant active GA. It displayed high concentrations during early stages of EFD and declined to largely undetectable levels by 18 DAFB. Among active cytokinins, *trans*-zeatin abundance in the fruit cortex was high at early stages but declined greatly at later stages of EFD (between 10 and 18 DAFB). Additionally, six of nine JA class hormones that were quantified displayed their highest concentrations at 6 and 10 DAFB, and decreased by 18 DAFB. Particularly, jasmonoyl-L-isoleucine (JA-ILE) and JA (jasmonic acid), concentrations remained high at 6 and 10 DAFB and declined by over 20-fold between 10 and 18 DAFB. Although, there was no significant differences in concentration of N-[(-)-jasmonoyl]-(l)-phenalanine (JA-Phe) and methyl jasmonate (MEJA) at four stages, they showed similar tendency (Figure 2.5D).

Considering the high abundance of ABA and its conjugate at 6 DAFB and their subsequent decline, genes associated with ABA metabolism and signaling were further evaluated using the transcriptome dataset. A heatmap of the transcript abundance patterns of identified metabolism and signaling genes indicates greater abundance of multiple ABA biosynthesis genes during early

stages of EFD (Figure 2.6A and Figure 2.6B). *NINE-CIS-EPOXYCAROTENOID DIOXYGENASE (NCED)* gene codes for a rate-limiting enzyme in ABA biosynthesis. Of 11 *NCED* genes identified from the dataset, seven displayed a reduction in transcript abundance during EFD. Two *NCED3* genes displayed their highest TPM abundance at 6 DAFB, after which it declined by over 3-fold. The transcript abundance of two *NCED5* genes displayed highest abundance at 6 and 10 DAFB and declined by over 4-fold subsequently (Figure 2.6C). The TPM of *REGULATORY COMPONENT OF ABA RECEPTOR 1 (PYL1)* was high at 6 DAFB and decreased to around 25% at later stages (Figure 2.6D). The TPM of *ABA INSENSITIVE 2 (ABI2)* and *HIGHLY ABA-INDUCED PP2C GENE 3 (PP2C 3)* was high at 6 DAFB, declined at 10 DAFB and remained extremely low at 18 and 26 DAFB. The TPM of *SNF1-RELATED KINASE 2B (SnRK)* remained high during EFD most of EFD.

As multiple JAs displayed high abundance during early stages of EFD and coordinately declined sharply thereafter, its metabolism and signaling-related genes were further evaluated. Most JA metabolism genes were abundant at 6 and 10 DAFB, and subsequently declined at 18 and 26 DAFB (Figure 2.7A). For example, the transcript abundance of *LIPOXYGENASE 2 (LOX2)*, an *ALLENE OXIDE CYCLASE 4 (AOC4),* and *OPR2* genes was high at EFD and subsequently declined at 18 and 26 DAFB by 3- to 6-fold (Figure 2.7C). The JA signaling genes showed similar expression patterns to that of JA metabolism. Genes coding for the JA-zim-domain protein (JAZ), novel interactor of JAZ (NINJA), and TOPLESS-related proteins (TPL) displayed high transcript abundance during early stages of EFD and decreased greatly between 10 and 18 DAFB. (Figure 2.7B and 2.7D). For instance, the transcript abundance of *JAZ1* declined around 4-fold from 1163 to 312 TPM between 10 and 18 DAFB (Figure 2.7D).

Discussion

Phytohormone regulation of growth around the bloom interval

Fruit set is preceded by development of flower development leading to full bloom. In apple, growth during this period is mediated by cell production and expansion (Malladi and Johnson, 2011). At later stages of this period, approaching bloom, cessation of growth associated with a decline in cell production and expansion are noted indicating a period of quiescence. Fruit growth resumes after pollination and fertilization, which together are completed between 3-12 DAFB (Malladi and Johnson, 2011; Li et al., 2012). The earliest stage sampled in this study at 6 DAFB likely represents a stage of quiescence. Growth was likely re-initiated between 6 and 10 DAFB, considering that 10 DAFB was when RGR was generally high. This is further supported by the increase in transcript abundance of multiple genes associated with cell division between 6 and 10 DAFB.

Regulation of growth cessation around the period of bloom remains poorly understood. In the current study, the concentrations of multiple phytohormones peaked around 6 and 10 DAFB and declined dramatically thereafter. While some of these phytohormones such as auxins, gibberillins and cytokinins are known to promote growth, others such as ABA and ethylene repress it. Hence, it is proposed that an interplay between the growth-promoting and growth-repressing activities of multiple phytohormones tilts the balance toward growth cessation during the period.

Auxins are key regulators of fruit set and may play an important role in promoting EFD in apple as expression of an auxin biosynthesis gene (*YUCCA6a*) increased upon pollination in the cortex and pith tissues (Serrani et al., 2007; De Jong et al., 2009; Galimba et al., 2019; Li et al., 2022). In the current study, indole-acetic acid (IAA) was detectable only at 6 DAFB. Conversely, 2-oxindole-3-acetic acid (oxIAA), an inactive auxin generated as an IAA degradation product displayed highest abundance at 10 DAFB. These data suggest that IAA is actively degraded during

early stages of EFD. Other detectable auxins also displayed their highest abundance at 6 DAFB and declined to low or undetectable levels at later stages. Gibberellins typically promote growth of plant organs and are known to induce parthenocarpy in a range of fruit crops including apple (Bukovac, 1963; Bukovac and Nakagawa, 1967; Galimba et al., 2009). Among the GAs analyzed, the biologically active GA_1 and its precursor GA_{19} displayed overall greater abundance while GA_3 and the GA_4 precursor, GA_9, were also detectable during EFD. These GAs displayed higher abundance at 6 and 10 DAFB and declined substantially by 18 DAFB. Among the active cytokinins analyzed, *trans*-zeatin (*t*Z), displayed high concentration at 6 and 10 DAFB and declined at later stages. Active cytokinins are known to promote cell division in plants (Kieber and Schaller, 2014). Together, these phytohormones likely comprise the growth-promoting component during the bloom interval and early EFD.

Concentrations of ABA as well as its conjugated form, ABA-GE were very high at 6 DAFB, declined by around 4-fold by 10 DAFB, and further by around 30-fold during EFD. Consistently, several ABA biosynthesis-related genes, such as *ZEP*, *ABA4* and multiple *NCEDs*, also displayed high transcript abundance during early stages of EFD and declined later. Expression of several ABA-inducible genes such as *ABI2* and *HIGHLY ABA-INDUCED PP2C 3,* associated with ABA-signaling was also high during early EFD and declined later. This indicates coordinated regulation leading to ABA accumulation and signaling within the flower/fruit cortex around bloom in apple and a subsequent decline. ABA has been previously implicated in restricting growth in multiple organs such as the leaf petiole, the primary root and lateral roots (Brookbank et al., 2021; Luo et al., 2023). ABA promotes a state of dormancy in the developing flower/fruit at anthesis to prevent growth of the fruit in the absence of pollination and fertilization (Rodrigo and Garcia-Martinez, 1998; Vriezen et al., 2007). The ethylene precursor, ACC displayed highest abundance at 6 DAFB

and declined at later stages of EFD by over 13-fold. Considering that ACC synthesis is typically the rate-limiting step for ethylene biosynthesis, this may reflect changes in ethylene biosynthesis. Consistently, Jing and Malladi (2022) reported high transcript abundance of genes coding for ethylene-inducible negative regulators of ethylene signaling, ARGOS1 and ARGOS2 around bloom. Multiple JA-related metabolites displayed a consistent high level of abundance at 6 and 10 DAFB before declining sharply by up to 50-fold by 18 DAFB. This was further supported by the co-regulated expression of multiple components of the JA biosynthetic pathway and multiple genes putatively coding for JAZ proteins, which function as negative regulators of JA signaling and are inducible by JAs to allow for fine-tuning of JA responses (Chini et al., 2007; Thines et al., 2007; Wasternack and Song, 2017). Greater abundance of JAs during early stages of fruit development and a subsequent decline at mid fruit development have been previously reported in apple and have been interpreted to suggest a role for JAs in promoting cell division during early fruit growth (Fan et al., 1997; Kondo et al., 2000). However, multiple recent studies suggest that JAs often function to limit growth and cell division (Swiatek et al., 2002; Pauwels et al., 2008). JAs restrict leaf growth by repressing cell proliferation (Noir et al., 2013). Further, JAZ proteins are proposed to function in growth-defense balance to allow plants to respond to the level of stress by optimizing allocation of resources (Guo et al., 2018). Hence, it is proposed that ABA, ethylene and JAs together function as the growth-restricting component during bloom and shortly thereafter. At bloom, the relatively greater abundance of the growth-restricting module components and their impact leads to inhibition of growth and a state of quiescence.

High cell division activity at the beginning of the fruit growth and development

Following fruit set and the re-initiation of growth, fruit growth is achieved mostly through extensive cell production at early stages and cell expansion at later stages of development. Previous

studies indicated that cell production is high during the period from around 8 to 30 DAFB (Malladi and Johnson, 2011; Dash and Malladi, 2012; Dash et al., 2013). In this study, we found genes associated with microtubules as well as promoters of cell cycle activity are up-regulated between 6 to 10 DAFB, and are subsequently down-regulated between 18 and 26 DAFB, marking this interval as a period of high cell production activity. Microtubules are components of the plant cell cytoskeleton and perform critical functions during cell division. During mitosis, microtubules are reorganized and condensed to form mitotic spindles that aid in segregating chromosomes equally to daughter cells (Gatlin and Bloom, 2010; Kline-Smith and Walczak, 2004; Sampath et al., 2004). CYCLINS and CDKs together are key regulators of the progression of the cell cycle (Francis, 2007; Inze and De Veylder, 2006). Further, genes grouped in clusters 3 and 4 displayed an increasing pattern of abundance from 6 to 10 DAFB (slight increase in cluster 4) and a decreasing pattern from 18 to 26 DAFB. In particular, the increase expression level between 6 and 10 DAFB is greater in cluster 3 and the expression remains elevated until 18 DAFB. GO enrichment analyses indicated genes associated with microtubule activity, spindle assembly, CDKs activity and cell cycle transition GO terms were enriched in cluster 3. This is supported by the expression patterns of several cell cycle associated genes such as *CYCs*, *CDKs*, *FZR3*. In addition, GO terms associated with DNA replication and chromatin remodeling related genes were enriched in cluster 3. In particular, a gene coding for TOPII, involved in DNA replication and repair, and abundant in proliferating tissues (Xie and Lam, 1994; Garcia et al., 2021) was included in this cluster. Also, several genes coding for microtubule-associated proteins involved in mitosis and cytokinesis such as *AUR3*, *AUR1*, and *TPX2* (Demidov et al., 2005; Kawabe et al., 2005; Van Damme et al., 2011) displayed a pattern of highest expression at 10/18 DAFB. Thus, multiple genes associated with the cell cycle, mitosis and cell division were enriched in cluster 3, and exhibited a pattern of increase

during early EFD with a decline at later stages, clearly marking this period as an intensive cell production phase.

Interestingly, none of the phytohormones displayed a substantial increase at the onset of the period of re-initiation of cell division-mediated growth. However, as indicated earlier, a decline in the concentrations of the growth-restricting module, which included ABA, JAs and ethylene was evident at this stage. These data indicate that exit from quiescence and re-initiation of cell division activity, was mediated primarily by de-repression of growth. As the concentrations of components of the growth-restricting module decline, the balance may shift such that the remaining concentrations of the growth-promoting module may allow for the resumption of cell division and growth. The trigger for the de-repression of growth may either be pollination and fertilization or a developmental signal. Li et al. (2022) indicated that changes in the fruit transcriptome consistent with fruit set occurred slightly prior to the window where fertilization occurred, leading them to suggest that pollination was likely sufficient to serve as the trigger. In pollinated and non-pollinated flowers/fruits many genes associated with the cell cycle and organ growth displayed similar patterns of changes in gene expression until at least 8 DAFB (Malladi and Johnson, 2011). As non-pollinated flowers in that study were generated by clipping the styles, pollination was unlikely to serve as the trigger for the noted changes. Hence, a developmental signal may also contribute to the de-repression of growth during early stages of EFD. In any case, the contributions of the developmental, pollination and fertilization signals to growth de-repression during early EFD therefore need further investigation.

Cell division transition to cell expansion at later stage of fruit growth and development

The transitions from cell production-mediated growth to cell expansion-mediated growth was noted towards the later stages of EFD. This transition was marked by a clear decline in transcript

abundance of multiple cell division and cell cycle genes as indicated above. Many of these genes were grouped in cluster 3. In addition, multiple genes associated with photosynthetic activity were markedly down-regulated between 18 and 26 DAFB. The apple fruit is a major sink organ and is mainly supported by carbon translocated from photosynthetically active leaves. However, the apple fruit possesses photosynthetic ability which is intermediate between C3 and C4/CAM (Blanke and Lenz, 1989). Fruit photosynthetic activity can meet 5-20 % of the C requirements during EFD. The abundance of multiple photosynthesis-related genes was high during early stages of EFD suggesting that fruit photosynthesis supplements C requirements for robust cell division, at least partially, during EFD (Hansen 1967; Oliviera and Priestley 1988; Forshey and Elfving 1989). Multiple genes coding for proteins associated with the light reactions of photosynthesis, several genes coding for the small subunits of rubisco, and a gene coding for rubisco activase displayed the above pattern and declined markedly between 18 and 26 DAFB, suggesting that photosynthetic activity in the fruit cortex is downregulated coincident with a transition from cell division- to cell expansion-mediated growth. Further research is necessary to determine the capacity of the fruit cortex for photosynthesis and to determine its contribution to the C demands of the developing fruit.

Interestingly, the transition from cell division-mediated to cell expansion-mediated growth, and the decline of photosynthesis-related gene expression (between 18-26 DAFB) was not associated with substantial changes in the concentrations of phytohormones. It is possible that a gradual decline in concentrations of the phytohormone components of the growth-promoting module below a threshold level, as noted here, is sufficient to allow for cortex cells to exit cell production. Alternatively, other mechanisms such as developmental regulation which allows for limited plasticity in the extent of cell production may regulate this transition. Alternatively, organ

growth regulating mechanisms may contribute to this transition. Negative organ growth regulators such CNR20a and CNR20b, and positive regulators such as the GRF11/16-GIF3 module may potentially function as part of such organ-level growth regulation that determines this transition during EFD (Jing and Malladi, 2022).

Cell expansion is the irreversible process of cell wall extension driven by increase in turgor pressure. Turgor driven cell expansion is a complicated process that requires multiple steps, including water uptake and accumulation, cell wall loosening, and new cell wall synthesis (Cosgrove, 2005; Farrokhi et al., 2006). Genes associated with cell growth, and cell wall metabolism were enriched in cluster 6 which grouped genes that generally exhibited an increase in transcript abundance during EFD, particularly at the later stages. Multiple genes coding for proteins associated with cell wall modification such as cellulose synthases (MD08G1147200; MD15G1123200), xylosyltransferase 1 (MD16G1169000), expansin A15 (MD001125400), and COBRA-like GPI-anchored protein family (MD14G1214800) were included in this group. Together, these data indicate coordinated increase in transcript abundance of multiple cell expansion-associated genes. It should be noted that many of these genes increased gradually during EFD often showing a larger increase either between 10 and 18 DAFB or between 18 and 26 DAFB. These data suggest that increase in cell expansion activity is likely a continual process that overlaps with the period where cell production occurs, particularly as the cortex tissue is comprised of a population of asynchronous cells.

References

Barbez, E., Dunser, K., Gaidora, A., Lendl, T., and Busch, W. (2017). Auxin steers root cell expansion via apoplastic pH regulation in Arabidopsis thaliana. *Proc Natl Acad Sci U S A* **114**, E4884-E4893.

Beshir, W. F., Mbong, V. B. M., Hertog, M., Geeraerd, A. H., Van den Ende, W., and Nicolai, B. M. (2017). Dynamic Labeling Reveals Temporal Changes in Carbon Re-Allocation within the Central Metabolism of Developing Apple Fruit. *Front Plant Sci* **8**, 1785.

Blanke, M. M., and Lenz, F. (1989). Fruit Photosynthesis. *Plant Cell and Environment* **12**, 31-46.

Bolger, A. M., Lohse, M., and Usadel, B. (2014). Trimmomatic: a flexible trimmer for Illumina sequence data. *Bioinformatics* **30**, 2114-20.

Bu, H., Yu, W., Yuan, H., Yue, P., Wei, Y., and Wang, A. (2020). Endogenous Auxin Content Contributes to Larger Size of Apple Fruit. *Front Plant Sci* **11**, 592540.

Cosgrove, D. J. (2005). Growth of the plant cell wall. *Nat Rev Mol Cell Biol* **6**, 850-61.

Dash, M., Johnson, L. K., and Malladi, A. (2013). Reduction of Fruit Load Affects Early Fruit Growth in Apple by Enhancing Carbohydrate Availability, Altering the Expression of Cell Production-related Genes, and Increasing Cell Production. *Journal of the American Society for Horticultural Science* **138**, 253-262.

Dash, M., and Malladi, A. (2012). The AINTEGUMENTA genes, MdANT1 and MdANT2, are associated with the regulation of cell production during fruit growth in apple (Malus x domestica Borkh.). *BMC Plant Biol* **12**, 98.

Devoghalaere, F., Doucen, T., Guitton, B., Keeling, J., Payne, W., Ling, T. J., Ross, J. J., Hallett, I. C., Gunaseelan, K., Dayatilake, G. A., Diak, R., Breen, K. C., Tustin, D. S., Costes, E., Chagne, D., Schaffer, R. J., and David, K. M. (2012). A genomics approach to

understanding the role of auxin in apple (Malus x domestica) fruit size control. *BMC Plant Biol* **12**, 7.

Elliott, A., and Shaw, S. L. (2018). Update: Plant Cortical Microtubule Arrays. *Plant Physiol* **176**, 94-105.

Fan, X. T., Mattheis, J. P., Fellman, J. K., and Patterson, M. E. (1997). Changes in jasmonic acid concentration during early development of apple fruit. *Physiologia Plantarum* **101**, 328-332.

Farrokhi, N., Burton, R. A., Brownfield, L., Hrmova, M., Wilson, S. M., Bacic, A., and Fincher, G. B. (2006). Plant cell wall biosynthesis: genetic, biochemical and functional genomics approaches to the identification of key genes. *Plant Biotechnol J* **4**, 145-67.

Forshey, C.G. and D.C. Elfving. 1989. The relationship between vegetative growth and fruiting in apple trees. Hortic. Rev. 11:229–287.

Francis, D. (2007). The plant cell cycle--15 years on. *New Phytol* **174**, 261-78.

Garrido-Bigotes, A., Figueroa, N. E., Figueroa, P. M., and Figueroa, C. R. (2018). Jasmonate signalling pathway in strawberry: Genome-wide identification, molecular characterization and expression of JAZs and MYCs during fruit development and ripening. *PLoS One* **13**, e0197118.

Gatlin, J. C., and Bloom, K. (2010). Microtubule motors in eukaryotic spindle assembly and maintenance. *Semin Cell Dev Biol* **21**, 248-54.

Giourieva, V., and Panteris, E. (2021). Inhibition of cell expansion enhances cortical microtubule stability in the root apex of Arabidopsis thaliana. *J Biol Res (Thessalon)* **28**, 13.

Giovannoni, J. J. (2004). Genetic regulation of fruit development and ripening. *Plant Cell* **16 Suppl**, S170-80.

Hansen, P. 1967. ^{14}C-studies on apple trees. I. The effect of the fruit on the translocation and distribution of photosynthates. Physiol. Plant. 20:383–391.

Inze, D., and De Veylder, L. (2006). Cell cycle regulation in plant development. *Annu Rev Genet* **40**, 77-105.

Jing, S., and Malladi, A. (2020). Higher growth of the apple (Malus x domestica Borkh.) fruit cortex is supported by resource intensive metabolism during early development. *BMC Plant Biol* **20**, 75.

Kalve, S., De Vos, D., and Beemster, G. T. (2014). Leaf development: a cellular perspective. *Front Plant Sci* **5**, 362.

Kim, D., Pertea, G., Trapnell, C., Pimentel, H., Kelley, R., and Salzberg, S. L. (2013). TopHat2: accurate alignment of transcriptomes in the presence of insertions, deletions and gene fusions. *Genome Biol* **14**, R36.

Kline-Smith, S. L., and Walczak, C. E. (2004). Mitotic spindle assembly and chromosome segregation: refocusing on microtubule dynamics. *Mol Cell* **15**, 317-27.

Kondo, S., Tomiyama, A., and Seto, H. (2000). Changes of endogenous jasmonic acid and methyl jasmonate in apples and sweet cherries during fruit development. *Journal of the American Society for Horticultural Science* **125**, 282-287.

Lakso, A. N., Grappadelli, L. C., Barnard, J., and Goffinet, M. C. (1995). An Expolinear Model of the Growth-Pattern of the Apple Fruit. *Journal of Horticultural Science* **70**, 389-394.

Liao, Y., Smyth, G. K., and Shi, W. (2014). featureCounts: an efficient general purpose program for assigning sequence reads to genomic features. *Bioinformatics* **30**, 923-30.

Liu, W., Li, T., Yuan, H., Tan, D., and Wang, A. (2018). Enhancement of apple coloration using jasmonate treatment without sacrificing storage potential. *Plant Signal Behav* **13**, e1422467.

MacDaniels, L.H. 1940. The morphology of the apple and other pome fruit. New York (Cornell University) Agr. Expt. Sta. Mem. 230:3–30.

Majda, M., and Robert, S. (2018). The Role of Auxin in Cell Wall Expansion. *Int J Mol Sci* **19**.

Malladi, A., and Hirst, P. M. (2010). Increase in fruit size of a spontaneous mutant of 'Gala' apple (Malus x domestica Borkh.) is facilitated by altered cell production and enhanced cell size. *J Exp Bot* **61**, 3003-13.

Marchant, H. J., and Hines, E. R. (1979). The role of microtubules and cell-wall deposition in elongation of regenerating protoplasts of Mougeotia. *Planta* **146**, 41-8.

Noir, S., Bomer, M., Takahashi, N., Ishida, T., Tsui, T. L., Balbi, V., Shanahan, H., Sugimoto, K., and Devoto, A. (2013). Jasmonate controls leaf growth by repressing cell proliferation and the onset of endoreduplication while maintaining a potential stand-by mode. *Plant Physiol* **161**, 1930-51.

Oliviera, C.M. and C.A. Priestley. 1988. Carbohydrate reserves in deciduous fruit trees. Hortic. Rev. 10:403–430.

Pratt, C. 1988. Apple flower and fruit: morphology and anatomy. Hortic. Rev. 10:273–308.

Rose, J. K., Braam, J., Fry, S. C., and Nishitani, K. (2002). The XTH family of enzymes involved in xyloglucan endotransglucosylation and endohydrolysis: current perspectives and a new unifying nomenclature. *Plant Cell Physiol* **43**, 1421-35.

Sampath, S. C., Ohi, R., Leismann, O., Salic, A., Pozniakovski, A., and Funabiki, H. (2004). The chromosomal passenger complex is required for chromatin-induced microtubule stabilization and spindle assembly. *Cell* **118**, 187-202.

Shinozaki, Y., Beauvoit, B. P., Takahara, M., Hao, S., Ezura, K., Andrieu, M. H., Nishida, K., Mori, K., Suzuki, Y., Kuhara, S., Enomoto, H., Kusano, M., Fukushima, A., Mori, T., Kojima, M., Kobayashi, M., Sakakibara, H., Saito, K., Ohtani, Y., Benard, C., Prodhomme, D., Gibon, Y., Ezura, H., and Ariizumi, T. (2020). Fruit setting rewires central metabolism via gibberellin cascades. Proc Natl Acad Sci U S A 117, 23970-23981.

Smith, L. G., and Oppenheimer, D. G. (2005). Spatial control of cell expansion by the plant cytoskeleton. *Annu Rev Cell Dev Biol* **21**, 271-95.

Srivastava, A. and Handa, A.K. (2005) Hormonal Regulation of Tomato Fruit Development: A Molecular Perspective. Journal of Plant Growth Regulation, 24, 67-82.

Tian, T., Liu, Y., Yan, H., You, Q., Yi, X., Du, Z., Xu, W., and Su, Z. (2017). agriGO v2.0: a GO analysis toolkit for the agricultural community, 2017 update. *Nucleic Acids Res* **45**, W122-W129.

Vashisth, T., Johnson, L. K., and Malladi, A. (2011). An efficient RNA isolation procedure and identification of reference genes for normalization of gene expression in blueberry. *Plant Cell Rep* **30**, 2167-76.

Wolf, S., Hematy, K., and Hofte, H. (2012). Growth control and cell wall signaling in plants. *Annu Rev Plant Biol* **63**, 381-407.

Xu, J., Yan, J., Li, W., Wang, Q., Wang, C., Guo, J., Geng, D., Guan, Q., and Ma, F. (2020). Integrative Analyses of Widely Targeted Metabolic Profiling and Transcriptome Data

Reveals Molecular Insight into Metabolomic Variations during Apple (Malus domestica) Fruit Development and Ripening. *Int J Mol Sci* **21**.

Zhang, S., Xu, M., Qiu, Z., Wang, K., Du, Y., Gu, L., and Cui, X. (2016). Spatiotemporal transcriptome provides insights into early fruit development of tomato (Solanum lycopersicum). *Sci Rep* **6**, 23173.

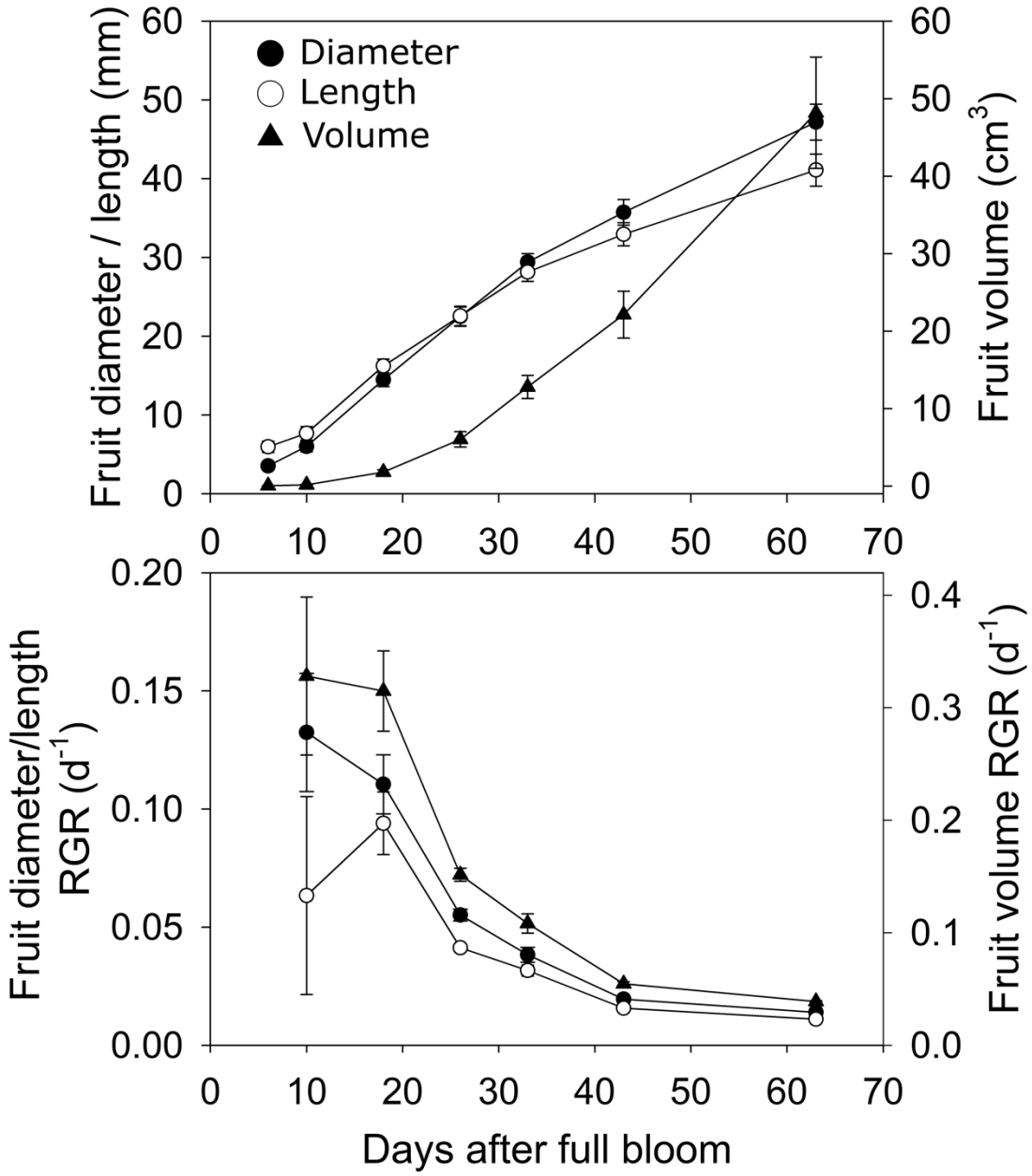

Figure 2.1. Fruit growth in 'Empire'. Fruit diameter, length, and volume were measured from 6 d after full bloom. The relative growth rate (RGR) of fruit diameter, length, and volume were calculated. Error bars represent the standard error of the mean with four replicates (n = 4).

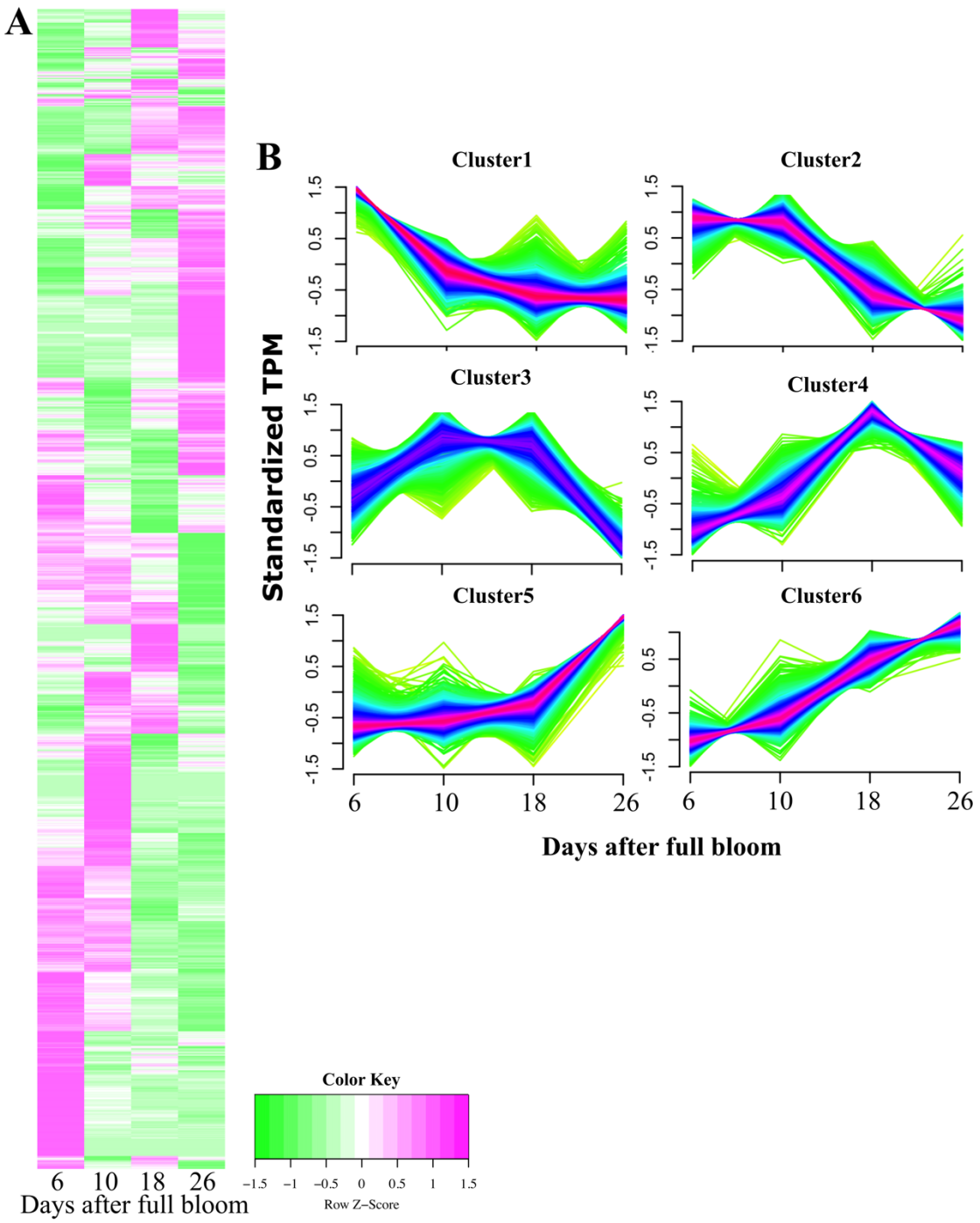

Figure 2.2. Identification of genes involved in early fruit development in 'Empire' apple. (A) a heatmap of genes expressed in the apple cortex at 6 days after full bloom (DAFB), 10 DAFB, 18 DAFB, and 26 DAFB. (B) Grouping of gene expression profiles of differentially expressed genes during early fruit development into six clusters profiles. TPM: transcripts per million.

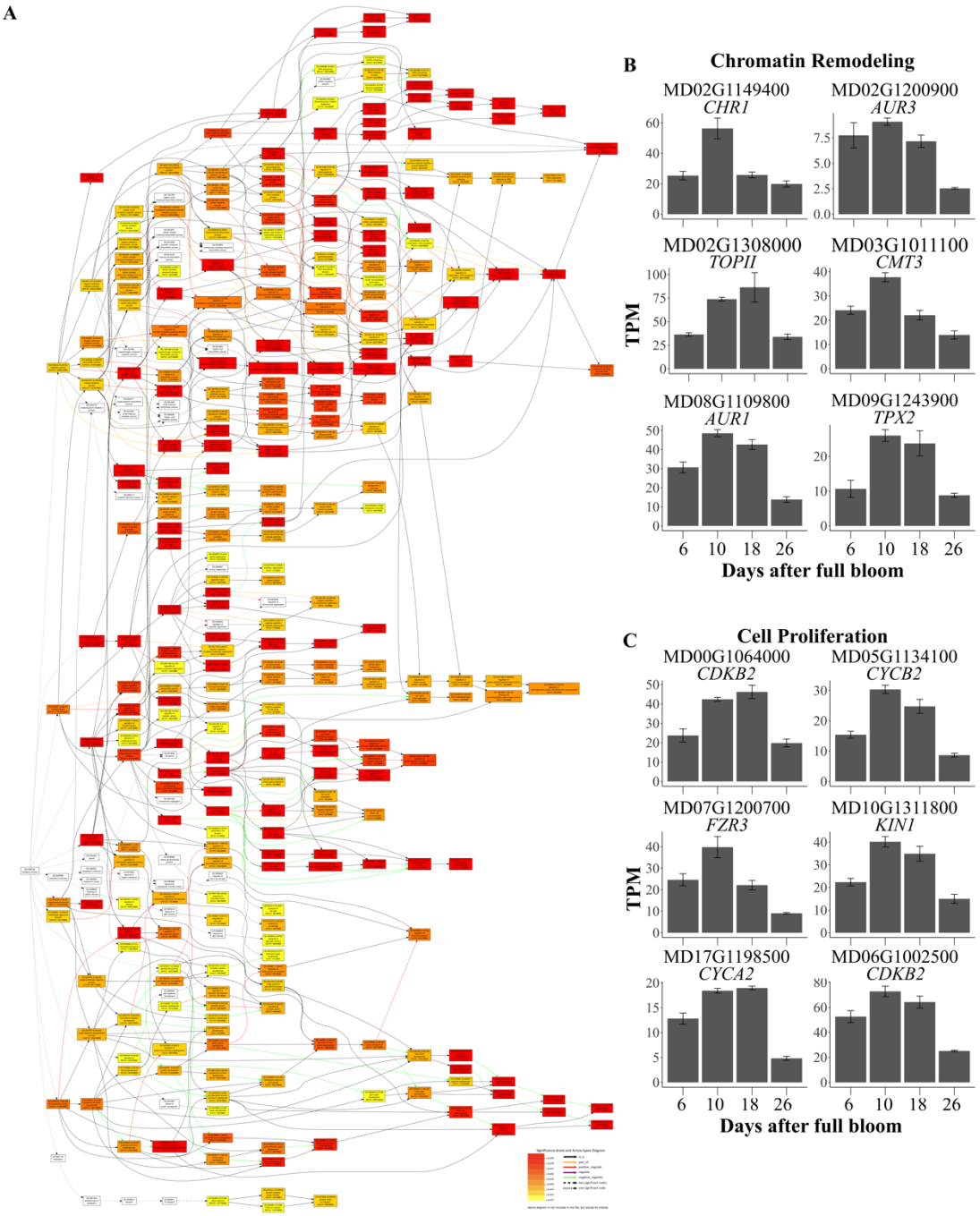

Figure 2.3. Gene ontology (GO) categorization of differentially expressed genes (DEGs) grouped into cluster 3. (A) The functional categorization of DEGs within cluster 3 based on enriched GO terms. (B) The transcript abundance of five selected genes involved in chromatin remodeling: *CHROMATIN REMODELING 1 (CHR1), AURORA 3 (AUR3), TOPOISOMERASE II (TOP II),*

CHROMOMETHYLASE 3 (CMT3), and *AUR1*. (C) The transcript abundance of five selected genes involved in cell proliferation: *B-TYPE CYCLIN-DEPENDENT KINASE (CDKB2), CYCLINB2 (CYCB2), FIZZY-RELATED 3 (FZR3), KINESIN 1 (KIN1),* and *CYCA2*. Error bars represent the standard error of the mean with three replicates (n = 3). TPM: transcripts per million.

A

DAFB	6	10	18	26
6		276	1834	2510
10	314		725	1493
18	2797	1050		919
26	3693	2608	1710	

Down-regulated

Up-regulated

B

C

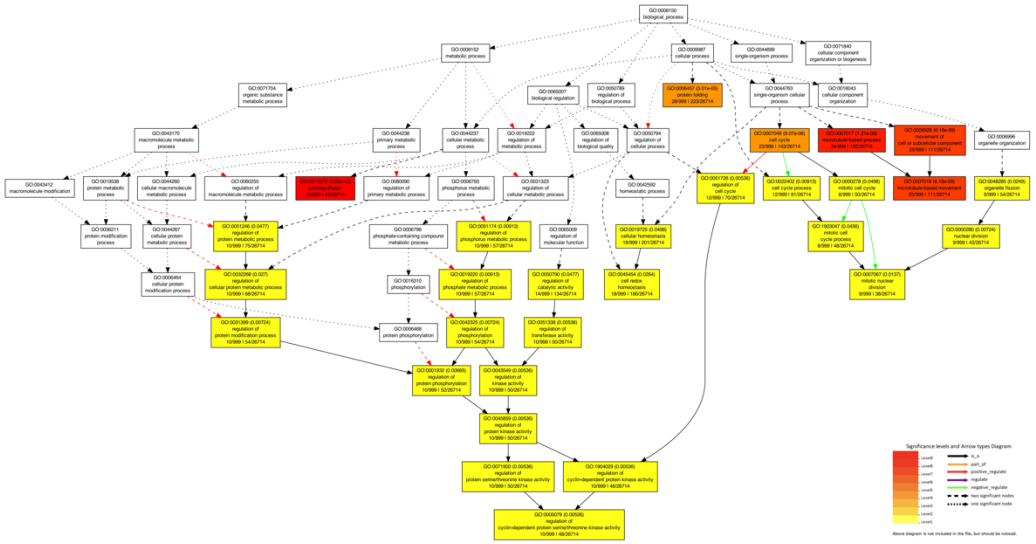

D

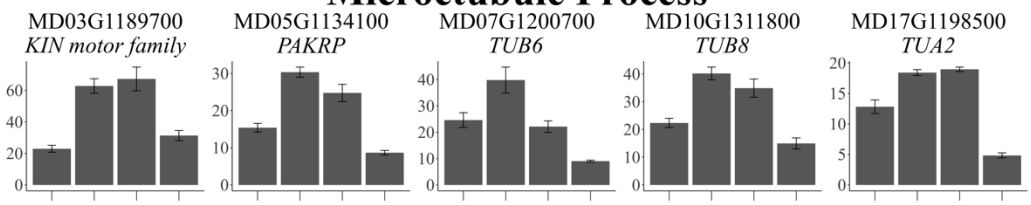

E

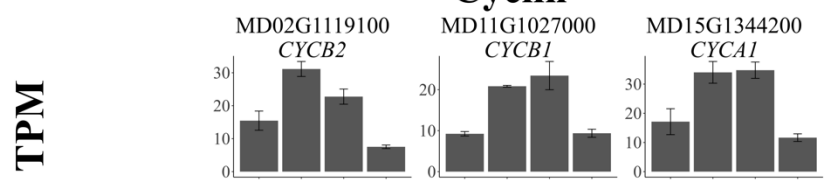

F

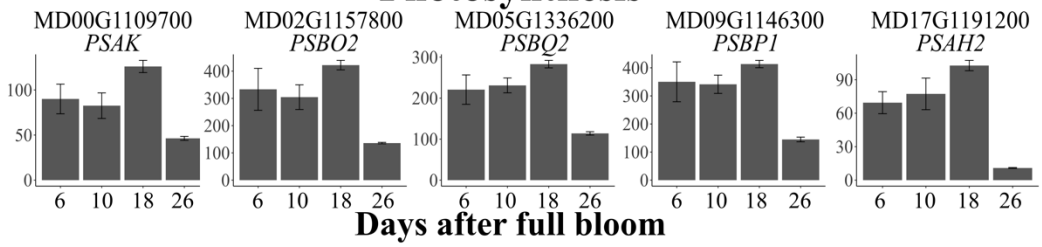

Figure 2.4. Differentially expressed genes (DEGs) in the apple cortex across different stages of early fruit development. (A) Number of DEGs between 6 versus (vs.) 10 days after full bloom (DAFB), 6 vs. 18 DAFB, 6 vs. 26 DAFB, 10 vs. 18 DAFB, 10 vs. 26 DAFB, and 18 vs. 26 DAFB. Magenta represents up-regulated genes, and green represents down-regulated genes. (B) The DEGs within the 6 vs. 10 DAFB comparison that were up-regulated and their GO term enrichment. (C) The DEGs between 18 vs. 26 DAFB comparison and enriched GO term analysis of down-regulated genes. (D) The transcript abundance of five selected genes in microtubule process in the 6 vs. 10 DAFB comparison of up-regulated genes: *KINESIN (KIN) MOTOR FAMILY PROTEIN*, *PHRAGMOPLAST-ASSOCIATED KINESIN-RELATED PROTEIN (PAKRP), TUBULIN BETA 6 (TUB6), TUB8,* and *TUBULIN ALPHA 2 (TUA2)*. (E) The transcript abundance of three selected genes in the 18 vs. 26 DAFB comparison highlighting down-regulated genes: *CYCLIN B2 (CYCB2), CYCB1,* and *CYCA1*. (F) The transcript abundance of five selected genes involved in photosynthesis from the 18 vs. 26 DAFB comparison highlighting down-regulated genes: *PHOTOSYSTEM I SUBUNIT (PSA) K, PHOTOSYSTEM II SUBUNIT (PSB) O2, PSBQ2, PSBP1,* and *PSAH2*. Error bars represent the standard error of the mean with three replicates (n = 3). TPM: transcripts per million.

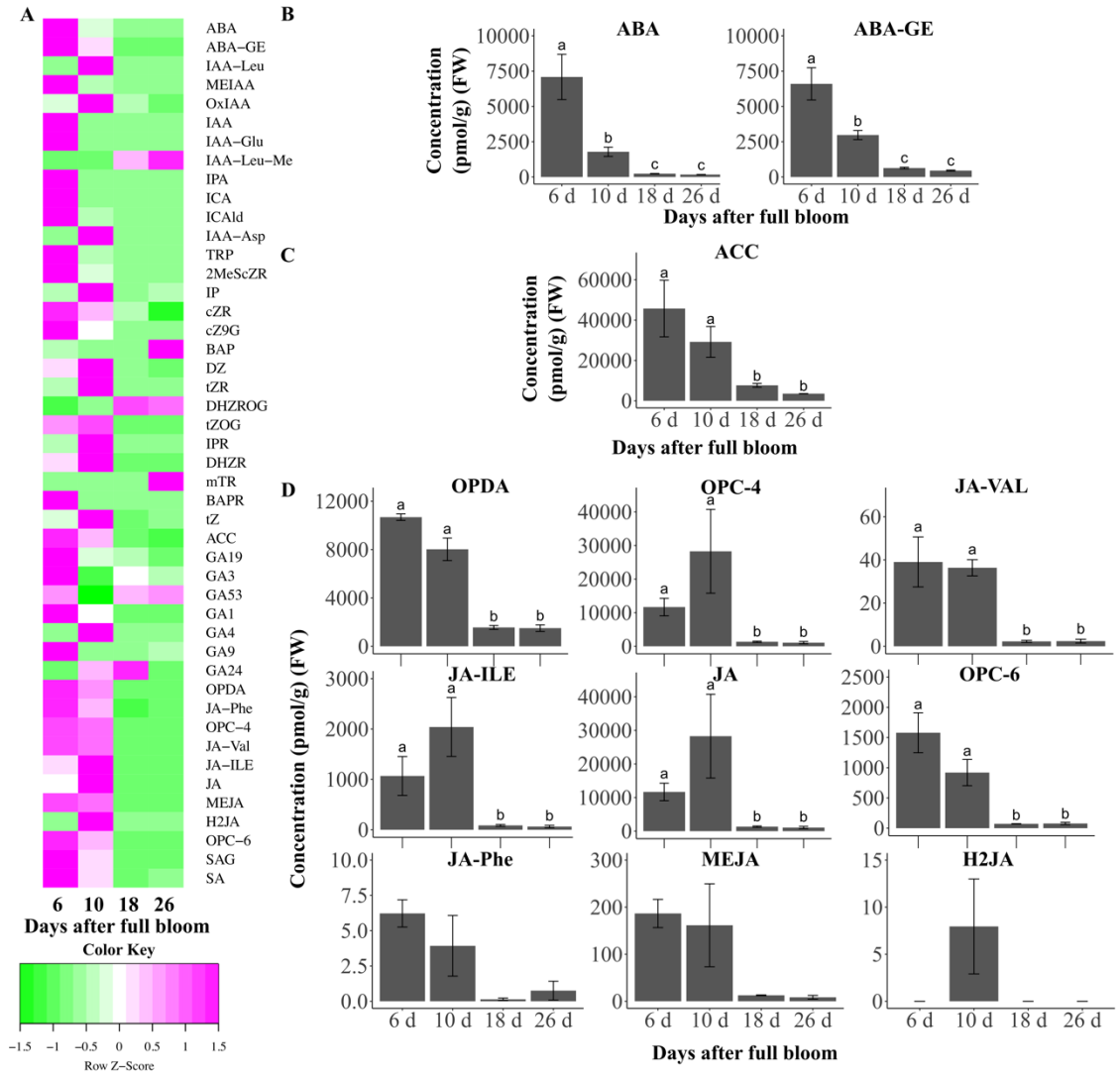

Figure 2.5. The concentration of phytohormones in the 'Empire' apple cortex during early fruit development. (A) A heatmap of phytohormone concentrations in the apple cortex at 6 days after full bloom (DAFB), 10 DAFB, 18 DAFB, and 26 DAFB. The phytohormones that were not detectable at any of the above stages were excluded. (B) The concentration of abscisic acid (ABA) and ABA-glucosyl ester (ABA-GE) during early fruit development. (C) The concentration of cis(+)-12-oxophytodienoic acid (OPDA), 3-oxo-2-(2-(Z)-pentenyl) cyclopentane-1-butyric acid (OPC-4), N-[(-)-jasmonoyl]-(L)-valine (JA-Val), jasmonoyl-L-isoleucine (JA-ILE), jasmonic acid (JA), 3-oxo-2-(2-(Z)-pentenyl) cyclopentane-1-hexanoic acid

(OPC-6), N-[(-)-jasmonoyl]-(l)-phenalanine (JA-Phe), methyl jasmonate (MEJA), and dihydrojasmonic acid (H_2JA) during early fruit development. Means and standard error are displayed with four replicates (n = 4, except n = 3 at 6 DAFB). Tukey's HSD was used for mean separation. Same letter above the bars indicates that the means are not significantly different.

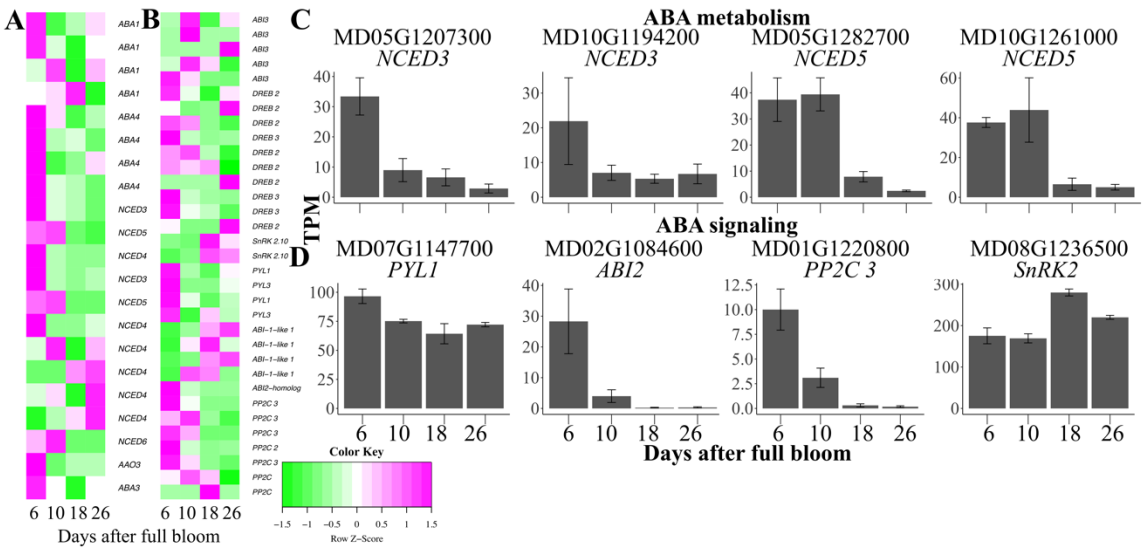

Figure 2.6. Transcript abundance of genes involved in abscisic acid (ABA) metabolism and signaling in the apple cortex during early fruit development. (A) A heatmap of identified genes involved in ABA metabolism in the apple cortex at 6 days after full bloom (DAFB), 10 DAFB, 18 DAFB, and 26 DAFB. (B) A heatmap of genes involved in ABA signaling in the apple cortex at 6 DAFB, 10 DAFB, 18 DAFB, and 26 DAFB. (C) The transcript abundance of four selected genes in ABA metabolism: *NINE-CIS-EPOXYCAROTENOID DIOXYGENASE 3 (NCED3)* and *NCED5*. (D) The transcript abundance of four selected genes in ABA signaling: *REGULATORY COMPONENT OF ABA RECEPTOR 1 (PYL1), ABA INSENSITIVE 2 (ABI2), HIGHLY ABA-INDUCED PP2C GENE 3 (PP2C 3)* and *SNF1-RELATED PROTEIN KINASE (SnRK).* Error bars represent the standard error of the mean with three replicates (n = 3). TPM: transcripts per million.

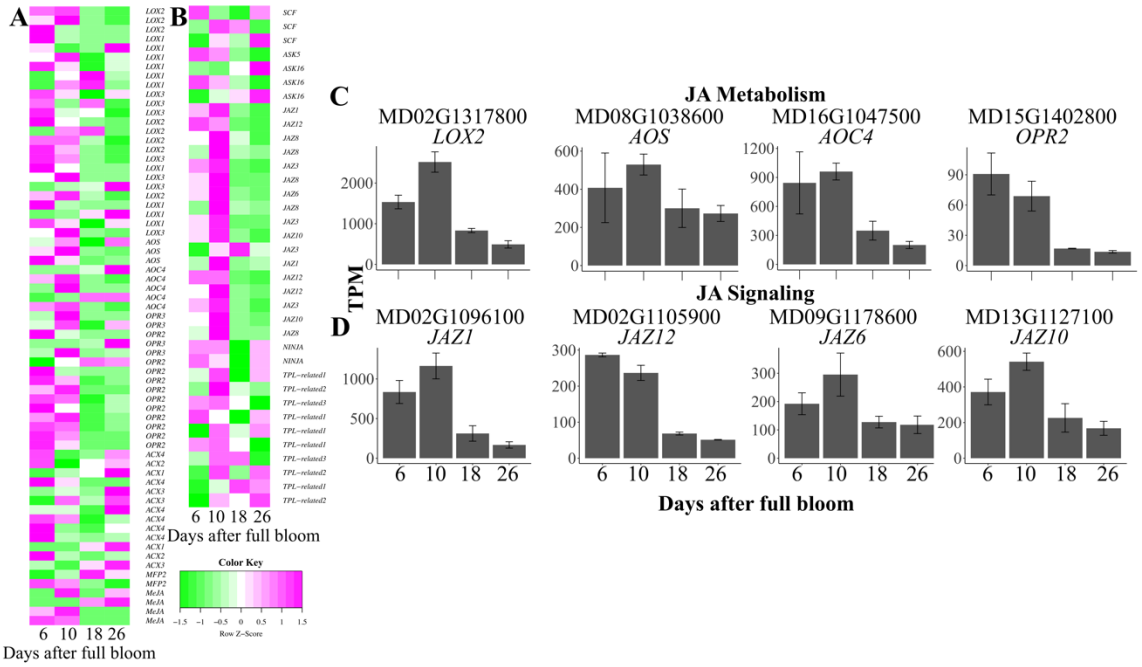

Figure 2.7. Transcript abundance of genes involved in jasmonic acid (JA) metabolism and signaling in the 'Empire' apple cortex during early fruit development. (A) A heatmap of genes involved in JA metabolism in the apple cortex at 6 days after full bloom (DAFB), 10 DAFB, 18 DAFB, and 26 DAFB. (B) A heatmap of genes involved in JA signaling in the apple cortex at 6 DAFB, 10 DAFB, 18 DAFB, and 26 DAFB. (C) The transcript abundance of four selected genes in JA metabolism: *LIPOXYGENASE 2 (LOX2), ALLENE OXIDE SYNTHASE (AOS), ALLENE OXIDE CYCLASE 4 (AOC4)*, and *OXOPHYTODIENOATE-REDUCTASE 2 (OPR2)*. (D) The transcript abundance of four selected genes in JA signaling: *JASMONATE-ZIM-DOMAIN PROTEIN 1 (JAZ1), JAZ12, JAZ6, AND JAZ10*. Error bars represent the standard error of the mean with three replicates (n = 3). TPM: transcripts per million.

CHAPTER 3

THE TCP MODULE AND REGULATION OF EARLY FRUIT GROWTH

Abstract

The TCPs (TEOSINTE BRANCHED – CYCLOIDEA – PROLIFERATING CELL FACTOR) are a family of plant specific transcription factors that regulate organ growth and development. Class I TCPs generally promote cell production, while class II TCPs inhibit it. A previous study identified that *MdTCP2b* is negatively associated with the relative tissue growth rate during early apple fruit development (EFD). Phylogenetic analysis shows that *MdTCP2b* is a member of CIN subclade of class II TCPs that contain a conserved microRNA319 (*miR319*) target site. In this study, *MdTCP2b* transcript abundance was found to be higher in pith tissue compared to the cortex. In the cortex, it increased coincident with the transition from cell production to cell expansion-mediated growth. RLM-RACE analysis indicated MdTCP2b transcripts are cleaved in a manner consistent with miR319-mediated regulation. MdTCP2b binds to a conserved binding motif within the promoters of the apple *KRP4* and *KRP5* genes and potentially enhances their expression. These genes are negative regualtors of the cell cycle and are known to be assocaietd in regulation of cell production. To further understand the role of *MdTCP2b* in plant growth and development, it was ectopically expressed either as the wild-type (*wTCP2b*) or as an *miR319* resistant *MdTCP2b* (*rTCP2b*) form in Arabidopsis. The two *rTCP2b* lines analyzed displayed significant reduction in leaf area in comparison to the wild-type. Transgenic lines expressing the apple *TCP2b* genes displayed leaves with increased positive curvature and an earlier transition from vegetative to reproductive growth. Hence, *MdTCP2b* functions as a negative regulator of organ growth. During EFD in apple, MdTCP2b may restrict growth in the pith region, and determine the timing of exit from cell production to cell expansion in the cortex.

Introduction

The apple fruit is a 'pome' fruit with fleshy tissues of distinct ontogeny. The inner fleshy tissue, referred to here as the pith, is either derived from the ovary, or is mostly an extension of the pith in the pedicel surrounding ovarian tissues (Pratt, 1998; Malladi, 2020). The major fleshy tissue, often contributing to over 80% of the fruit volume, surrounds the pith and is referred to here as the cortex (Malladi et al., 2020). This tissue is of non-ovarian origin, developing either from the fused bases of other floral organs such as the sepals, or an extension of the cortex from the pedicel. Together, these tissues present a spatial context to fruit growth as they display differential growth during early fruit development (EFD). This differential growth is supported by differential metabolic programs across these tissues during EFD (Jing and Malladi, 2020).

Apple fruit development is a complex process including multiple steps from fruit formation to ripening. These include pollination, fruit set, early growth mediated by cell division, subsequent growth mediated largely by cell expansion, and ripening. The growth of the apple fruit has been proposed to fit the expo-linear model by Lakso et al. (1995). Early fruit growth is considered exponential and primarily associated with multiple rounds of cell production (generation of new cells form an existing population). Cell production lasts for 3-4 weeks after full bloom (WAFB) (Dash and Malladi, 2012; Malladi and Hirst, 2010). Then the fruit growth transitions to cell expansion-mediated growth during which increase in fruit size is largely linear, until ripening. This stage occurs until 15-25 WAFB and encompasses mid- and late- fruit development wherein different phases of fruit metabolism are apparent (Li et al., 2012; Jing and Malladi, 2020). For example, mid fruit development (MFD) is marked by increase in starch accumulation, while late fruit development (LFD) involves the initiation of ripening and an associated decline in starch content. Although both cell production and cell expansion contribute

to fruit growth in apple, cell number determined by cell production during EFD is a major factor that determines final fruit size. The rate and duration of cell production are critical components determining the extent of cell production during EFD. Therefore, factors that regulate the rate of cell production and/or the extent of the cell production period by determining the timing of exit from cell production and thereby the transition to cell expansion-mediated growth are important regulators of fruit growth. Together, these parameters provide a temporal context to apple fruit growth.

Identification and characterization of organ growth regulators that regulate apple spatial and temporal patterns of apple fruit growth can contribute greatly to our understanding of the complex control of fruit growth. In a previous study, weighted gene co-expression network analysis (WGCNA) of RNA-seq data generated across the cortex and pith tissues during different stages of fruit development was performed to identify such candidates. Specifically, WGCNA using relative tissue growth rate (RTGR) across the two fleshy tissues at three stages of fruit development and in response to changes in fruit load was performed. These analyses revealed a module that was negatively correlated with RTGR. From within this module, *MdTCP2b* was identified as a gene displaying high module membership and being strongly correlated (negatively) with RTGR. TCP refers to TEOSINTE BRANCHED1 (maize), CYCLOIDEA (snapdragon), and *PCF* (PROLIFERATING CELL FACTOR; rice), which is large plant specific transcription factor family. TCPs are grouped broadly into two classes based on the characteristics of a non-canonical basic helix-loop-helix (bHLH) domain: Class I and Class II TCPs (Danisman et al., 2012; Martin-Trillo and Cubas, 2010). Class II TCPs are further sub-divided into CYC/TB1- and CINCINNATA (CIN)- subclades (Cubas et al., 1999; Das Gupta et al., 2014; Kosugi and Ohashi, 1997). Phylogenetic analyses indicated that MdTCP2b is a member of the CIN subclade and displays

closest homology to the Arabidopsis, *AtTCP2*. In Arabidopsis, the CIN sub-clade of Class II TCPs (CIN-TCPs) is comprised of *AtTCP2, AtTCP3, AtTCP4, AtTCP5, AtTCP10, AtTCP13, AtTCP17* and *AtTCP24*. Their gene products control various aspects of plant growth and development and have particularly well documented roles in the regulation of leaf growth (Sarvepalli and Nath, 2018). Specifically, CIN-TCPs regulate the transition from cell proliferation to cell expansion during leaf development. Further, the spatial and temporal expression patterns of these genes are considered to serve critical functions in such regulation (Sarvepalli and Nath, 2018). Early overexpression of *TCP4* in emerging primordia results in meristem termination or formation of miniature leaves, while expression of *TCP4* at later stages leads to smaller and narrower leaves. Expression specifically at later stages results in largely normal leaves (Efroni et al., 2008). Those examples suggested that CIN-TCPs are heterochronic regulators that regulate leaf morphology and promote differentiation (Efroni *et al.*, 2008). The two classes of TCPs contain different, but partially overlapping consensus binding motifs. The consensus binding site for class I TCPs (GGNCCCAC) was first described by Kosugi and Ohashi (2002) in rice. Schommer et al. (2008) and Aggarwal et al. (2010) identified that the core binding site for class II TCPs, *AtTCP4* and *AtTCP24*, was 'GGNCCA'. CIN-TCPs can therefore bind to these motifs within the promoters of target genes to repress growth. One mode of action of CIN-TCPs in directly repressing the cell cycle is mediated by their interaction with *CYCLIN-DEPENDENT KINASE INHIBITOR 1 (ICK1)/ KIP-RELATED PROTEINS (KRPs)* (Schommer et al., 2014). Alternatively, CIN-TCPs may indirectly regulate cell production by modulating phytohormone synthesis, transport and signaling. Auxin biosynthesis gene (*YUCCA5*) and jasmonic acid (JA) biosynthesis gene (*LOX2*) are both direct targets of CIN-TCPs (Challa *et al.*, 2016; Schommer et al., 2008). Five of these *TCPs*, *AtTCP2-4*, *AtTCP10* and *AtTCP24* contain a conserved microRNA319 (miR319*)* binding site and

are regulated post-transcriptionally (Efroni et al., 2008; Koyama et al., 2007). High levels of miR319 post-transcriptionally down-regulate the transcript abundance of these *TCPs* and result in critical phenotypic changes (Palatnik et al., 2003; Rodriguez et al., 2016; Rubio-Somoza et al., 2014). The functions of miR319-regulated TCPs in other plants have been described, including regulation of leaf morphogenesis, promotion of the transition to cell differentiation, mediation of the biosynthesis and signaling of several phytohormones such as IAA (auxin) and JA, and control of floral organogenesis.

It is hypothesized that MdTCP2b promotes the transition from cell proliferation to cell expansion during EFD in apple. Further, it is hypothesized that MdTCP2b performs its function at least in part by regulating the expression of downstream targets involved in the cell cycle. To test these hypotheses, characterization of the function of MdTCP2b and its regulation were performed. are explored.

Materials and methods

Plant materials

Transcription abundance of *MdTCP2b* and *miR319* was performed using 'Empire' and 'Golden Delicious Smoothee' apple fruit and has been described previously (Jing and Malladi, 2020; Chapter 2). For both cultivars, the cortex and pith tissues were separated manually at each of the sampling stages, frozen in liquid nitrogen, then stored at -80 °C for later use.

Arabidopsis plants used in this study were of the Columbia (Col-0) ecotype. Wild type Arabidopsis plants and transgenic lines were grown in a Conviron growth chamber at 20 to 22 °C under a 16-h-light/8-h-dark cycle. Light intensity in this study was maintained at 170 $mol \cdot m^2 \cdot s^{-1}$ during the light cycle.

RNA extraction and qRT-PCR

Total RNA was extracted using the CTAB method as described in Vashisth et al. (2011) and Jing and Malladi (2020). One μg of total RNA of cortex and pith samples was using to synthsize cDNA with ImProm II reverse transcriptase (Promega, USA) following the DNase I treatment. The cDNA was diluted 5-fold and used for qRT-PCR following the method described previously to quantitate the transcript abundance of *MdTCP2b*, *MdKRP4* and *MdKRP5* (Dash et al., 2013). *MdCACS2* and *MdACTIN* were used as the reference genes.

Stem-loop qRT-PCR was used to quantitate the transcript abundance of miR319 as described previously (Kramer, 2011). One μg of total RNA after DNase I treatment was using to synthesize cDNA with miR319-specific primers. The cDNA was diluted 5-fold and used for qRT-PCR following the method described previously (Dash et al., 2013). *MdCACS2* was used as the reference gene.

RLM-RACE

RNA samples at 19 DAFB and 23 DAFB were selected to purify by Monarch RNA Cleanup Kit (NEB) after DNase I treatment. The poly(A) RNA was isolated by NEBNext Poly(A) mRNA Magnetic Isolation Module (NEB). A 5' RNA adaptor was ligated to the purified mRNA by T4 RNA ligase as described in Llave et al. (2011). After purification of ligated RNA, cDNA was synthesized using a gene-specific primer (GSP). The cDNA was diluted 10 times and was amplified using an adaptor-specific primer (ASP) and GSP. The amplified products were analyed by 1–2% agarose gel electrophoresis, purified by Zymoclean Gel DNA Recovery Kit (ZYMO RESEARCH).The purifiied PCR products were cloned into The pGEM-T Easy Vector (Promega) and transformed to JM109 competent cells. After colonies grew at 37°C for 1 d, 56 white colonies were re-streaked on to new LB-agar medium and incubated at 37°C for 1 day. The plamids were

extracted using ZymoPURE Plasmid Miniprep Kit (ZYMO RESEARCH) and send to Azenta for sequencing. The sequencing results were aligned with against the *MdTCP2b* sequence using Clustal Omega to determine the location of the transcript cleavage site.

Protein Expression and purification

The pGEX-5X-2 vector was used for production of bacterially expressed TCP2b protein. The full-length cDNA of TCP2b was amplified using primers to which EcoRI and XhoI sites were added (5′ and 3′, respectively). (5'-ATGCGAATTCCCATGGAGGTGGAGGAG-3' and 5'-CAGTCTCGAGTCAGTTCTTTGCTTTGCCC-3'). Then the TCP2b expression construct pGEX-5X-2-TCP2b was transformed into Rosetta™ 2(DE3) pLysS Singles™ Competent Cells. The pGEX-5X-2 empty vector was also transformed into Rosetta™ 2(DE3) pLysS Singles™ Competent Cells as a negative control. Single colony of pGEX-5X-2-TCP2b was selected and sequenced for confirmation.

20 ml LB containing 100 µg/ml ampicillin and 34 µg/ml chloramphenicol was inoculated with 500 µL of overnight grown culture and grown at 37 °C to the mid-log phase (OD_{600}=0.6). Recombinant protein expression was induced with 0.5 mM isopropyl β-D-1-thiogalactopyranoside (IPTG) followed by incubation at 30 °C. Glutathione S-transferase (GST) protein from the empty vector was also induced following the same induction procedure. Cells were harvested after 6 h of induction by centrifugation (10000 g for 10 min at 4 °C). Cells were lysed by sonication in 800 µL of lysis buffer (50 mM Tris-HCl pH = 8, 400 mM NaCl, 0.1% Triton X-100, and 5% glycerol) with 10 µL protease inhibitor after freezing thaw. The lysate was centrifuged at 20000 g for 10 min at 4 °C to separate the supernatant and the pellet. The pellet was diluted with 400 µL of lysis buffer for the later sodium dodecyl sulfate polyacrylamide gel electrophoresis (SDS-PAGE) along with the supernatant.

SDS-PAGE gel was prepared using 10% SDS running gel and 5% stacking gel. A 10 well-comb was used. 12 µL of supernatant and diluted pellet samples with 4 µL of 4x protein loading dye were loaded in each lane. The gel was then electrophoresed at 120 V for 1 hour. The gel was stained with Coomassie gel-staining solution for 3 h and de-stained for 3 h.

The supernatant was further processed with the MagneGST™ Pull-Down System (Promega) following manufacturer's protocol with modification to isolate the TCP2b protein with GST tag. 350 µL of cleared cell lysate were added to 300 µL of equilibrated magnetic particles and eluted by 100 µL elution buffer (50 mM Glutathione and 50 mM Tris-HCl pH = 8.1). SDS-PAGE was conducted to identify the purified TCP2b protein described above.

Protein concentration was measured using the Bradford assay. A BSA (bovine serum albumin) standard curve was prepared. 200 µL of diluted Bradford reagent was mixed carefully with 10 µL protein sample and a blank, incubated at room temperature in dark for around 15 min. The absorbance was measured at 595 nm against a blank. The values obtained were used to calculate protein concentration based on the plotted standard curve.

Electrophoretic Mobility Shift Assay

Electrophoretic mobility shift assays (EMSAs) were performed using a LightShift™ Chemiluminescent EMSA Kit (ThermoFisher Scientific) according to the manufactuer's instructions with minor modifications. The binding reaction was carried out in a total volume of 20 µL containing 30 fmol of oligonucleotide probe with 5′ biotin labeling, 1X binding buffer, 1 µg Poly (dI•dC), 2 mM EDTA, 0.05% BSA, 10% glycerol and 50- 500 ng of protein. Four pmol of unlabeled probes were add to the reaction as an unlabeled-probe competition. Two mutant probes were also generated in which the core motif sequence was modified. The probe sequences are listed in Table 3.1. The mixture was incubated at room temperature for 30 min and loaded on

6% native polyacrylamide gel. Electrophoretic transfer of binding reactions to nylon membrane was performed *via* Semi-Dry Trans-blot (Bio-Rad) at constant 300 mA for 20 min. After chemiluminescence reaction, biotin-labeled DNA was detected using the PXI Gel Doc system (Syngene).

Yeast one-hybrid assay

The yeast one-hybrid (Y1H) assay was performed following the Matchmaker® Gold Yeast One-Hybrid Library Screening System (Clontech) with minor modifications. The 308 bp *MdKRP4* promoter fragment containing the binding motif GGACCA (-338 to -31 relative to the translational start site) was inserted into the pAbAi vector to generate the bait vector. Two mutant bait vectors wherein the core binding site was substituted as GGAaCA in Mutant 1 (M1) and GGAaCt in Mutant 2 (M2) were also generated by gene synthesis followed by cloning. These bait vectors were integrated into the genome of Y1HGold yeast strains by digestion with BstBI and transformation into Y1HGold. The bait yeast strains were screened to determine the minimal inhibitory concentration of Aureobasidin A (AbA) as per manufacturer's instructions.

The full-length cDNA TCP2b was ligated into the pGADT7 vector to generate the AD-MdTCP2b prey vector. The AD-MdTCP2b prey vector was co-transformed into Y1HGold yeast strains (containing pAbBi-MdKRP4 or pAbAi-Mutants, M1 or M2) to confirm the interaction of MdTCP2b protein with the *MdKRP4* promoter. From each transformation reaction, the yeast was cultured on SD/–Leu plate and incubated at 30°C for 3 d. Then yeast colonies were resuspended with distilled water to OD_{600}= 0.002 and spotted on SD/–Leu AbA^{1000} for 2-3 d at 30 °C. The pGADT7 empty vector that was co-transformed into Y1HGold yeast strains with pAbBi-MdKRP4 served as a negative control. The pGADT7-p53 vector that was co-transformed into Y1HGold yeast strains with pAbBi-p53 served as a positive control.

MdTCP2b expression in Arabidopsis: Plasmid construction and transformation

The full-length cDNA TCP2b was amplified from 'Golden Delicious' fruit tissue. Following the protocol of the manufacturer, QuikChange II Site-Directed Mutagenesis Kit (Agilent Technologies), mutagenesis was carried out to construct versions of TCP2b resistant to miR319 (rTCP) by introducing modification to the miR319 target site but without altering the amino acids sequence. According to the protocol, primers were designed to cause seven sites mutations. Wild-type MdTCP2b (wTCP) and rTCP were integrated into pCN-S-OX vector with 35S promoter. The wTCP and rTCP constructs were transformed into Agrobacterium GV3101 with empty pCN-S-OX vector (SOX) as a control. Floral dip transformation was conducted to generate transgenic Arabidopsis (Clough and Bent, 1998). Homozygous transgenic lines were confirmed by PCR genotyping.

The sixth and seventh fully expanded leaves were detached from the rosette and scanned as such (without flattening) on a flatbed scanner (Epson V600) when the length of bolts was 2 cm. Subsequently, edges of the leaves were cut to flatten the leaf and re-scanned on the flatbed scanner. Leaf width, length and area before and after flattening were measured by ImageJ software (https://imagej.nih.gov/ij/). The curvature index was calculated by $1-A_0/A_1$, where A_0 and A_1 represent leaf width/length/area before and after cutting, respectively, as per Liu et al. (2010), except that the parameter of leaf area was introduced. The flowering time was determined as the number of rosette leaves when the leaf samples were collected (when bolt was 2 cm in length).

Results

Spatial and temporal patterns of *MdTCP2b* expression during apple fruit development

During fruit development, transcript abundance of *MdTCP2b* in 'Empire' fruit cortex tissue gradually declined 2.5-fold from 6 to 26 DAFB, then increased 4.5-fold by 33 DAFB and remained

at a higher level at 43 DAFB (Figure 3.1). However, it did not vary substantially in the pith tissue, except for 2- and 1.5-fold higher abundance at 10 and 26 DAFB (Figure 3.1). The transcript abundance of *MdTCP2b* in 'Golden Delicious' fruit cortex tissue decreased 2.5-fold between 11 to 30 DAFB and increased 4.5-fold at 37 DAFB. In the pith tissue, *MdTCP2b* transcript abundance sharply increased 2.5-fold between 19 and 30 DAFB, and remained high thereafter (Figure 3.1). Overall, *MdTCP2b* transcript abundance was low during EFD (until 26 DAFB) (Figure 3.1). At later stages, coincident with the onset of cell-expansion mediated growth, its transcript abundance increased by several fold in both cultivars. Further, the pith tissue displayed higher transcript abundance of *MdTCP2b* during EFD by up to 7.4-fold, in both cultivars (Figure 3.1).

Spatial and temporal expression patterns of miR319

Multiple potential miR319 genes were identified in apple using miRbase (miRbase.org). The transcript abundance of one of these, *miR319a*, in the 'Empire' fruit cortex tissue increased almost 3-fold between 6 and 18 DAFB, decreased almost 3-fold between 18 and 26 DAFB, and decreased further to very low levels by 43 DAFB (Figure 3.2A). It did not vary substantially in the pith tissue during the early stages and decreased to very low levels by 43 DAFB (Figure 3.2A). In 'Golden Delicious', the transcript abundance of *miR319a* in cortex and pith tissues declined between 11 and 30 DAFB to undetectable levels and increased by 57 DAFB (Figure 3.2A). *miR319a* transcript abundance was higher in the cortex than in the pith across both genotypes during EFD (Figure 3.2A). The transcript abundance of *miR319b* in 'Empire' gradually declined to almost 0 between 6 and 43 DAFB in both tissues (Figure S3.1). In 'Golden Delicious', *miR319b* transcript abundance increased 7-fold between 19 and 30 DAFB, and then sharply declined 26-fold between 30 and 58 DAFB in the cortex tissue (Figure S3.1). It was not substantially altered in the pith tissue except for a transient 2.6-fold increase at 19 DAFB (Figure S3.1). Together, *miR319* abundance in cortex

tissue was greater than that in the pith during EFD. Further, transcript abundance of at least *miR319a* declined greatly during the later stages of EFD, during the period of transition between cell production- and cell-expansion mediated growth (Figure 3.2A).

miR319-mediated cleavage of *MdTCP2b* transcripts

The expression of *MdTCP2b* may be post-transcriptionally regulated by *miR319* since it contains a potential *miR319* binding site at 3′ of the transcript. Cleavage of the transcript between bases 10 and 11 in relation to the 5' end of the miRNA is considered a hallmark of miRNA-dependent transcript regulation in plants (Llave et al., 2002). Hence, RLM-RACE was used to determine cleavage of the *MdTCP2b* transcripts and the location of such cleavage.

Out of 34 samples that displayed cleavage of the *MdTCP2b* transcripts, 31 displayed a cleavage site between bases 10 and 11 from 5′ end of miR319 binding (Figure 3.2C). The other 3 samples displayed cleavage between the 9 and 10 nucleotides from the 5′ of end miR319 binding (Figure 3.2C). *MdTCP2a* (Md10G1259500) is the closest homolog of *MdTCP2b*, and shares high similarity in sequence especially in proximity to the conserved miRNA binding site. Of 21 sequenced *MdTCP2a* samples, 18 displayed a cleavage site between bases 10 and 11 from the 5′ end of miR319 binding, while the other 3 displayed it between bases 9 and 10.

Binding of MdTCP2b to the *MdKRP4* promoter

Previous research showed that the CIN-TCP*,* TCP4 from Arabidopsis negatively regulates cell production and promotes the transition to cell differentiation during organ growth by directly interacting with *ICK1/KRP1*, a cell-cycle repressor which inhibits CYCD and CDKB complex activity (Schommer et al., 2014). High levels of *ICK1/KRP1* overexpression inhibits cell proliferation and reduces leaf growth in Arabidopsis (De Veylder et al., 2001; Verkest et al., 2005; Wang et al., 2000). In apple, *KRP4* and *KRP5* were previously identified as potential negative

regulators of fruit growth (Malladi and Johnson, 2011; Dash et al., 2013). Analysis of *MdKRP4* expression in 'Empire' indicated that its transcript abundance was largely similar to that of *MdTCP2b* (Figure 3.3A). It decreased during early stages of EFD and subsequently increased coinciding transition to cell expansion, in the cortex (Figure 3.3A). Further, *MdKRP4* abundance was several-fold higher in the pith than in the cortex (Figure 3.3A). A conserved CIN-TCP binding site with the motif, GGACCA (Schommer et al., 2008), was also identified in the *MdKRP4* and *MdKRP5* promoters (Figure 3.3A). Therefore, it was hypothesized that MdTCP2b binds to the promoters of *MdKRP4* and *MdKRP5* and regulates their expression.

To further demonstrate that MdTCP2b binds to the promoter of *MdKRP4* and *MdKRP5*, the MdTCP2b protein tagged to GST was expressed. The 80 kDa TCP2b-GST fusion protein was isolated using the GST pull-down system (Figure S3.2). A probe based on the consensus binding motif (consensus probe) of TCP4 was designed based on Schommer et al. (2008) to serve as a positive control (Table 3.1). At 7 bp upstream of the potential binding site within the *MdKRP4* promoter, a single nucleotide polymorphism (A/G) was identified, with 'Golden Delicious' being heterozygous for the same. Hence, two probes each with one of the alleles was designed and named Probe A and Probe G (Table 3.1). Electrophoretic mobility shift assays (EMSAs) indicated a strong band shift with the MdTCP2b-GST protein upon incubation with Probe A (Figure 3.3B). This shift was similar to that elicited by the consensus probe (Figure 3.3C). Further, competition experiments with excess unlabeled oligonucleotide probes indicated a loss of mobility shift confirming the specificity of the MdTCP2b Probe A interaction (Figure 3.3B). However, mutation of either one or two conserved bases within the core binding sequence (Probes M1 and M2, respectively) eliminated the interaction and the resultant mobility shift, underlining the specificity of the binding (Figure 3.3C). Similarly, MdTCP2b-GST also interacted specifically with Probe G as well as the

probe designed with the *MdKRP5* promoter sequence (Probe 5) indicating that MdTCP2b binds to these promoters as well (Figure 3.3B). Mobility shift did not occur when the GST protein alone was used indicating that MdTCP2b was required for such binding (Figure 3.3B).

Yeast-one-hybrid assays were also performed to determine interaction between MdTCP2b and the *MdKRP4* promoter. Yeast colonies of AD-MdTCP2b / MdKRP4-pAbAi grew normally on SD/–Leu AbA^{1000} plate, indicating that the AbA^r gene reporter was expressed upon interaction of MdTCP2b protein with the *MdKRP4* promoter fragment (Figure 3.3D). Mutations of the *MdKRP4* promoter, M1 and M2 displayed suppressed colony growth under the same conditions (Figure 3.3D). Taken together, the Y1H results strongly support that MdTCP2b protein binds to the *MdKRP4* promoter region.

Transgenic overexpression of *MdTCP2b* in Arabidopsis

Previous studies of the CIN-TCP gene, *AtTCP4*, indicate that it represses cell proliferation and triggers cell differentiation during leaf growth and development (Efroni et al., 2008). To understand further the role of *MdTCP2b* genes in plant and organ growth, the *MdTCP2b* (wTCP2b) gene was ectopically overexpressed in Arabidopsis. The target site of miR319-dependent transcript degradation is highly conserved between the Arabidopsis *CIN-TCPs* and *MdTCP2b*. Hence, rTCP2b transgenic lines were also generated to ectopically overexpress a mutated version of MdTCP2b with an altered miR319 binding site (Figure 3.4B&C). Transgenic plants wTCP2b and rTCP2b overexpressing *MdTCP2b* were generated with the gene driven by the constitutive 35S promoter (Figure 3.4A). An empty vector transgenic line (pSOX) and wild type col-0 (WT) were used as controls.

Four independent (wTCP2b1, wTCP2b4; rTCP2b1 and rTCP2b2), single-copy transgenic homozygous T2 lines and one pSOX line were obtained (Figure 3.4D). Preliminary experiments

indicated that wTCP2b1 and wTCP2b4 displayed the highest transcript abundance of *MdTCP2b* among wTCP2b lines. Similarly, rTCP2b1 and rTCP2b2 displayed the greatest transcript abundance of *MdTCP2b* from among rTCP2b lines.

Flowering time was determined as the number of rosette leaves when the inflorescence bolt attained 2 cm in length (bolting). Both wTCP2b and rTCP2b transgenic lines displayed fewer rosette leaves compared to the WT (Col-0) and pSOX (empty vector) controls indicating earlier flowering in response to MdTCP2b over expression (Figure 3.5A). Under long day conditions, WT and pSOX bolted after producing 10.85 ± 0.18 and 10.65 ± 0.22 rosette leaves, respectively (Figure 3.5A). wTCP2b1 and wTCP2b4 produced transgenic line bolted upon production of 8.85 ± 0.13 and 8.8 ± 0.16 rosette leaves, respectively (Figure 3.5A). The rTCP2b1 and rTCP2b2 transgenic lines produced 8.95 ± 0.14 and 7.8 ± 0.14 rosette leaves at bolting (Figure 3.5A).

Detailed comparison of leaf size was performed on the sixth and seventh rosette leaves. WT and the pSOX lines displayed similar size of the 6th leaf with and area of 2.91 ± 0.11 and 2.96 ± 0.17 cm^2, respectively (Figure 3.5B). wTCP2b1 and wTCP2b4 showed similar leaf size compared with the control pSOX lines at and 3.3 ± 0.12 and 2.5 ± 0.09 cm^2, respectively (Figure 3.5B). However, the wTCP2b4 line displayed smaller leaf area (by 25%) than wTCP2b1 (Figure 3.5B). The rTCP2b1 and rTCP2b2 lines displayed considerably reduced area of the 6th leaf compared to the control (Figure 3.5B). Particularly, rTCP2b2 displayed a leaf area of 1.59 ± 0.07 cm^2 which was around 45% lower than that of the WT (Figure 3.5B). The area of leaf 7 displayed a similar pattern to that observed in leaf 6 (Figure 3.5B).

TCPs have been reported play important roles in leaf organogenesis, thus influencing leaf morphology (Palatnik et al., 2003; Nath et al., 2003). Previous studies showed that hyper-activated *TCP4* in Arabidopsis results in cup-shaped leaf with the central portion extending upward,

resulting in a positive curvature phenotype (Sarvepalli and Nath, 2011). Similar changes in leaf curvature were noted in the wTCP2b and rTCP2b transgenic lines. Thus, the CI was used to quantitatively analyze leaf width, length and area curvature. The WCI (curvature index along leaf medio-lateral axis) in the controls was less than 0.1 (leaf 6), while it was greater than 0.2 in wTCP2b lines and greater than 0.3 in rTCP2b lines, indicating increased leaf curvature along the medio-lateral axis (Figure 3.6). The ACI (curvature index along entire leaf lamina) in the controls was around 0.1 (leaf 6), while it was greater than 0.2 in all transgenic lines, indicating that overall leaf curvature was also enhanced in the transgenic lines (Figure 3.6). The LCI (curvature index along leaf length) of wTCP2b4 and rTCP2b1 was higher (leaf 6) compared to the controls (Figure 3.6). Similar results were obtained through the analysis of leaf 7 (Figure 3.6). Overall, these data indicate that ectopic overexpression of *MdTCP2b* reduces leaf area, increases leaf curvature and promotes flowering in Arabidopsis. Similar results were obtained when the experiment was repeated under similar conditions as well as under conditions of low light intensity (~ 40 $\mu mol \cdot m^2 \cdot s^{-1}$).

Discussion

MdTCP2b may regulate the timing of exit from cell production during EFD

CIN-TCPs expression patterns are highly correlated with spatio-temporal control of cell fate transitions during organ development. In Arabidopsis, the expression of *CIN-TCPs* shows a proximo-distal gradient that overlaps with the arrest front during leaf growth and development (Sarvepalli and Nath, 2018). Further, CIN-TCPs also demonstrate a gradient along the medio-lateral axis with greater abundance towards the margins. The role of CIN-TCPs in leaf morphogenesis through the direct activation of inhibitors of cell division indicated their function in onset of cell differentiation indicating a temporal role for these regulators (Bresso et al., 2018;

Nath et al., 2003; Nicolas and Cubas, 2016). Further, higher abundance of CIN-TCPs along leaf margins results in growth restriction thereby affecting leaf curvature and promoting leaf flatness (Nath et al., 2003). Together, CIN-TCPs are proposed to regulate the overall extent of cell production, and spatial growth in organs such as the leaf (Sarvepalli and Nath, 2018). In apple, the cortex and pith tissues display differential growth during EFD. While their size is comparable at bloom, the cortex displays preferential growth during EFD with 5-fold higher growth rate than that in pith, and cortex tissue accounts for more than 80% of the fruit volume at maturity (Jing and Malladi, 2020; Malladi et al., 2020). As growth during EFD is largely mediated by cell production, these data indicate spatial differences in cell production capacities during this period (Jing and Malladi, 2020). In the cortex, the transitions from cell production to cell expansion mediated growth typically occurs around 3-5 WAFB. The transcript abundance patterns of *MdTCP2b* across two genotypes clearly indicated two aspects: 1. Spatial differences such that it was multiple-fold higher in the pith than in the cortex during EFD; and 2: Increase in abundance during the transition from cell production to cell expansion in the cortex (Figure 3.1). Together, these expression patterns across cultivars are highly consistent with a role for MdTCP2b in spatio-temporal regulation of EFD in apple by determining the transition to cell differentiation in the cortex and by potentially restricting the extent of cell production in the pith.

***MdTCP2b* transcript abundance is regulated by miR319**

miRNAs are a class of 19-24 nucleotide-long non-coding RNAs that control plant growth and development, and stress responses (Eulalio et al., 2008; Voinnet, 2009). In plants, most miRNAs are perfectly complementarity to their targets and post-transcriptionally regulate target gene expression by slicing the mRNA. A sub-group of *CIN-TCPs* carry the miR319 binding site. miR319-dependent regulation of *CIN-TCP* expression domains is a key aspect of organ growth

and developmental regulation. In Arabidopsis, the dominant *jaw-D* (*JAGGED AND WAVY*) mutant results in the simultaneous down-regulation of five *CIN-TCPs* carrying the miR319 binding site (Palatnik et al., 2003; Schommer et al., 2012). Overexpression of versions of CIN-TCPs resistant to miR319-mediated cleavage largely rescue the jaw-D phenotype (Palatnik et al., 2003; Schommer et al., 2008). In apple, *MdTCP2b* and its closest paralog, *MdTCP2a*, carried the conserved miR319 binding site suggesting that they are regulated by miR319. The transcript abundance of at least one of miR319s was higher during early stages of EFD and declined during the period of transition from cell production to cell expansion mediated growth (Figure 3.2A). Further, the abundance of this miR319 was greater in the cortex than in the pith during EFD (Figure 3.2A). Together, these expression patterns are complimentary to that of MdTCP2b and further support its regulation by miR319. Ultimately, RLM-RACE clearly indicated that *MdTCP2b* as well as *MdTCP2a* transcripts were cleaved predominantly between positions 10 and 11 with respect to the 5′ end of the miR319 binding site, a hallmark of miRNA-dependent transcript cleavage in plants (Llave et al., 2002). Together, these data clearly demonstarte that *MdTCP2b* is regulated post-transcriptionally by miR319 during EFD. However, it also appears likely that other mechanisms are involved in the regulation of *MdTCP2b* abundance as it increases during later stages of fruit development, a period during which miR319 abundance was also greater in one of the two genotypes analyzed. Fine spatial resolution of miR319 and MdTCP2b expression patterns may provide further insights. Mechanisms that are involved in the regulation of miR319 and changes in its abundance are not clear. In future studies, it would be important to determine the regualtion of miR319 by phytohormones or developmental signals.

MdTCP2b negatively regulates cell proliferation by binding to *MdKRP4* and *MdKRP5* promoters

As transcription factors, TCP proteins are able to bind the *cis*-element of target genes and regulate their expression levels. Several studies have identified the different consensus binding motifs of different classes of TCPs (Aggarwal et al., 2010; Kosugi and Ohashi, 2002; Schommer et al., 2008). The consensus binding site for class I TCPs is GGNCCCAC, and the core elements [(T)TGGGCC, GCCCR, GG(A/T)CCC] were identified in Arabidopsis. Meanwhile, the sequence of the binding motif of class II TCPs is 'GTGGNCCC' with the core element TGGNCC, which partially overlaps with that of class I sites. Thus, the sequences containing G (T/C) GGNCCCAC can be recognized by both subclades TCPs.

CIN-TCPs may regulate cell production potentially through direct and indirect mechanisms (Sarvepalli and Nath, 2018). One of the downstream targets by which CIN-TCPs can directly regulate the cell cycle and thereby cell production is by altering the expression of *KRPs* in Arabidopsis (Schommer et al., 2014). *KRP1* expression is increased several-fold in plants expressing the miR319-resistant version of *TCP4* in Arabidopsis. Further, chromatin immunoprecipitation experiments indicate that TCP4 binds directly to the *KRP1* promoter region harboring the binding site (Schommer et al., 2014). In Arabidopsis, *KRP1* and *KRP2* decrease the kinase activity of CDKs to inhibit progression of the cell cycle (Wang et al., 2000; De Verkest eta l., 2005). Bioinformatic analysis of *MdKRP4* and *MdKRP5* indicated the presence of a *cis*-element with the core binding sequence, GGACCA (Figure 3.3A). EMSA results clearly indicated that MdTCP2b protein binds to the conserved GGACCA motif as present within the apple *KRP4* and *KRP5* promoters (Figure 3.3B). Mutation of the core sequence by altering 1 (Probe M1) or 2 (Probe M2) bases results in loss of MdTCP2b binding, underlining the specificity of this interaction

(Figure 3.3C). These data were further supported by Y1H experiments wherein a 300 bp region of the promoter containing the putative binding site was used (Figure 3.3D). Together, these data indicate that MdTCP2b interacts with the GGACCA motif present within the promoter regions of the two apple *KRP* genes. Transcript abundance patterns of *MdKRP4* and *MdKRP5* were correlated with that of *MdTCP2b*. Both the *KRPs* have been previously implicated in the negative regulation of cell production during fruit growth in apple (Malladi and Johnson, 2011; Dash et al., 2012; 2013). Hence, MdTCP2b is likely to regulate cell production during EFD in part *via* binding to the promoters of the *KRP* genes and increasing their abundance. Such regulation appears to occur both in a spatial context as well as a temporal context. *MdKRP4* expression is several-fold higher in the pith than in the cortex and its expression in the cortex increases during the transition from cell production to cell expansion mediated growth.

CIN-TCPs negatively regulate cell production through various mechanisms beyond that mediated by KRPs such as their interaction with *miR396* and *LOX2* (Sarvepalli and Nath, 2018). In the current study, MdTCP2b interacted with the 'GGACCA' motif in different sequence contexts such as that of *MdKRP4* and *MdKRP5*. Further, a SNP upstream of this motif did not alter binding capacity substantially. Together, these data suggest that MdTCP2b is likely to have additional targets that carry the 'GGACCA' motif in their promoter regions. Identification and characterization of such targets may allow for more insights into the mechanisms by which MdTCP2b regulates EFD.

MdTCP2b restricts growth and promotes maturation

CIN-TCPs limit cell proliferation in the lamina by restricting the duration of proliferation phase and by initiating cell differentiation. Further, they are involved in restricting growth along the leaf margin, thereby allowing for maintenance of leaf flatness (Nath et al., 2003). As indicated earlier,

jaw-D mutants display larger and crinkly leaves, due to excess growth at the margins that folds the lamina (Palatnik et al., 2003). Reduced growth at the margins under conditions of CIN-TCPs overexpression lead to cup-shaped leaves (Sarvepalli and Nath, 2011; Schommer et al., 2008). In addition, CIN-TCPs regulate flowering time since loss of function *tcp4* mutants display a delayed flowering phenotype. Overexpressed *TCP4* transgenic lines underwent shorter adult vegetative period than wild-type and resulted in precocious flowering transition (Li et al., 2017). In fact, the *jaw-D* mutant was also initially identified as displaying a delayed flowering phenotype (Weigel et al., 2000; Palatnik et al., 2003).

Three key aspects of plant growth and development were altered upon the ectopic overexpression of *MdTCP2b* in Arabidopsis, either as wTCP2b or in a miR319-resistant form (rTCP2b): (1.) Acceleration of bolting: Both forms of *MdTCP2b* overexpression resulted in accelerated flowering in Arabidopsis with the rTCP2b2 line displaying a stronger phenotype (Figure 3.5A). miR319-regulated CIN-TCPs promote photoperiodic flowering in Arabidopsis by promoting the expression of *CONSTANS*, directly and indirectly (Kubota et al., 2017; Liu et al., 2017). In apple, MdTCP2a and MdTCP2b interacted with MdFT1 (FLOWERING LOCUS T), although such interaction was interpreted as an indication of a role for FTs in regulating fruit growth (Mimida et al., 2011). (2.) Reduction in leaf area: While expression of wTCP2b did not reduce leaf area in Arabidopsis, expression of rTCP2b resulted in a consistent decline in leaf area by up to 45% (Figure 3.5B). These data clearly indicate a role for MdTCP2b in restricting organ growth, consistent with previous reports of CIN-TCPs in regulating leaf growth and development (Sarvepalli and Nath, 2018). Further evaluation is necessary to determine if MdTCP2b expression reduced Arabidopsis leaf size by restricting cell production. (3.) Increase in leaf curvature: Both forms of MdTCP2b expression in Arabidopsis increased positive curvature of the leaf (Figure 3.6).

This was particularly evident along the width of the leaf lamina. miR319-regulated CIN-TCPs display a medio-lateral gradient in expression, and their greater abundance along the margins restricts margin growth (Nath et al., 2003). Consistently, *MdTCP2b* expression may restrict growth along the leaf margin, thereby resulting in enhanced leaf curvature. However, in the current study, *MdTCP2b* expression was driven by a constitutive promoter which may not allow for the formation of a gradient in its expression. Two possible explanations may be presented to explain increased leaf curvature under these conditions. 1. TCP-mediated restriction of growth along the leaf margins may require additional interacting proteins which may display such a gradient/localization along the leaf margin. 2. Downstream targets of TCP associated may be post-transcriptionally restricted to the leaf margins thereby mediating growth restriction. In any case, increase in leaf curvature upon *MdTCP2b* expression is consistent with a growth restricting function of its gene product.

Conclusion

Data from this study demonstrate that MdTCP2b functions as a negative regulator of organ growth. The spatial and temporal expression profiles of *MdTCP2b* during apple fruit growth indicate a role for it in repressing growth by decreasing the extent of cell production and determining the timing of exit from cell production to cell expansion mediated growth. MdTCP2b functions in promoting the exit from cell production at least in part by binding to the promoters of *MdKRP* genes and promoting their expression. Such an increase in the expression of negative regulators of the cell cycle may trigger the exit from cell production. Together, MdTCP2b is likely to serve as a key negative regulator of growth during EFD in apple.

Reference

Aggarwal, P., Das Gupta, M., Joseph, A. P., Chatterjee, N., Srinivasan, N., and Nath, U. (2010). Identification of specific DNA binding residues in the TCP family of transcription factors in Arabidopsis. *Plant Cell* **22**, 1174-89.

Bresso, E. G., Chorostecki, U., Rodriguez, R. E., Palatnik, J. F., and Schommer, C. (2018). Spatial Control of Gene Expression by miR319-Regulated TCP Transcription Factors in Leaf Development. *Plant Physiol* **176**, 1694-1708.

Cheng, Y., Cao, L., Wang, S., Li, Y., Shi, X., Liu, H., Li, L., Zhang, Z., Fowke, L. C., Wang, H., and Zhou, Y. (2013). Downregulation of multiple CDK inhibitor ICK/KRP genes upregulates the E2F pathway and increases cell proliferation, and organ and seed sizes in Arabidopsis. *Plant J* **75**, 642-55.

Cubas, P., Lauter, N., Doebley, J., and Coen, E. (1999). The TCP domain: a motif found in proteins regulating plant growth and development. *Plant J* **18**, 215-22.

Danisman, S., van der Wal, F., Dhondt, S., Waites, R., de Folter, S., Bimbo, A., van Dijk, A. D., Muino, J. M., Cutri, L., Dornelas, M. C., Angenent, G. C., and Immink, R. G. (2012). Arabidopsis class I and class II TCP transcription factors regulate jasmonic acid metabolism and leaf development antagonistically. *Plant Physiol* **159**, 1511-23.

Das Gupta, M., Aggarwal, P., and Nath, U. (2014). CINCINNATA in Antirrhinum majus directly modulates genes involved in cytokinin and auxin signaling. *New Phytol* **204**, 901-12.

Dash, M., and Malladi, A. (2012). The AINTEGUMENTA genes, MdANT1 and MdANT2, are associated with the regulation of cell production during fruit growth in apple (Malus x domestica Borkh.). *BMC Plant Biol* **12**, 98.

Dash M, Johnson LK, Malladi A. (2013) Reduction of fruit load affects early fruit growth in apple by enhancing carbohydrate availability, altering the expression of cell production-related genes, and increasing cell production. J Amer Soc Hort Sci **138**, 253–62.

De Veylder, L., Beeckman, T., Beemster, G. T., Krols, L., Terras, F., Landrieu, I., van der Schueren, E., Maes, S., Naudts, M., and Inze, D. (2001). Functional analysis of cyclin-dependent kinase inhibitors of Arabidopsis. *Plant Cell* **13**, 1653-68.

Efroni, I., Blum, E., Goldshmidt, A., and Eshed, Y. (2008). A protracted and dynamic maturation schedule underlies Arabidopsis leaf development. *Plant Cell* **20**, 2293-306.

Eulalio, A., Huntzinger, E., and Izaurralde, E. (2008). Getting to the root of miRNA-mediated gene silencing. *Cell* **132**, 9-14.

Francis, D. (2007). The plant cell cycle--15 years on. *New Phytol* **174**, 261-78.

Inze, D., and De Veylder, L. (2006). Cell cycle regulation in plant development. *Annu Rev Genet* **40**, 77-105.

Jing, S., and Malladi, A. (2020). Higher growth of the apple (Malus x domestica Borkh.) fruit cortex is supported by resource intensive metabolism during early development. *BMC Plant Biol* **20**, 75.

Kalve, S., De Vos, D., and Beemster, G. T. (2014). Leaf development: a cellular perspective. *Front Plant Sci* **5**, 362.

Kim, H. J., Oh, S. A., Brownfield, L., Hong, S. H., Ryu, H., Hwang, I., Twell, D., and Nam, H. G. (2008). Control of plant germline proliferation by SCF(FBL17) degradation of cell cycle inhibitors. *Nature* **455**, 1134-7.

Kosugi, S., and Ohashi, Y. (1997). PCF1 and PCF2 specifically bind to cis elements in the rice proliferating cell nuclear antigen gene. *Plant Cell* **9**, 1607-19.

Kosugi, S., and Ohashi, Y. (2002). DNA binding and dimerization specificity and potential targets for the TCP protein family. *Plant J* **30**, 337-48.

Koyama, T., Furutani, M., Tasaka, M., and Ohme-Takagi, M. (2007). TCP transcription factors control the morphology of shoot lateral organs via negative regulation of the expression of boundary-specific genes in Arabidopsis. *Plant Cell* **19**, 473-84.

Kramer, M. F. (2011). Stem-loop RT-qPCR for miRNAs. *Curr Protoc Mol Biol* **Chapter 15**, Unit 15 10.

Lakso AN, Corelli Grappadelli L, Barnard J, Goffinet MC. (1995) An expolinear model of the growth pattern of the apple fruit. J Hort Sci **70**, 389–94.

Li, M., Feng, F., and Cheng, L. (2012). Expression patterns of genes involved in sugar metabolism and accumulation during apple fruit development. *PLoS One* **7**, e33055.

Llave, C., Franco-Zorrilla, J. M., Solano, R., and Barajas, D. (2011). Target validation of plant microRNAs. *Methods Mol Biol* **732**, 187-208.

Llave, C., Xie, Z., Kasschau, K. D., and Carrington, J. C. (2002). Cleavage of Scarecrow-like mRNA targets directed by a class of Arabidopsis miRNA. *Science* **297**, 2053-6.

Magyar, Z., Horvath, B., Khan, S., Mohammed, B., Henriques, R., De Veylder, L., Bako, L., Scheres, B., and Bogre, L. (2012). Arabidopsis E2FA stimulates proliferation and endocycle separately through RBR-bound and RBR-free complexes. *EMBO J* **31**, 1480-93.

Malladi, A., and Hirst, P. M. (2010). Increase in fruit size of a spontaneous mutant of 'Gala' apple (Malus x domestica Borkh.) is facilitated by altered cell production and enhanced cell size. *J Exp Bot* **61**, 3003-13.

Malladi, A., and Johnson, L. K. (2011). Expression profiling of cell cycle genes reveals key facilitators of cell production during carpel development, fruit set, and fruit growth in apple (Malusxdomestica Borkh.). *J Exp Bot* **62**, 205-19.

Martin-Trillo, M., and Cubas, P. (2010). TCP genes: a family snapshot ten years later. *Trends Plant Sci* **15**, 31-9.

Mendez-Vigo, B., de Andres, M. T., Ramiro, M., Martinez-Zapater, J. M., and Alonso-Blanco, C. (2010). Temporal analysis of natural variation for the rate of leaf production and its relationship with flowering initiation in Arabidopsis thaliana. *J Exp Bot* **61**, 1611-23.

Nath, U., Crawford, B. C., Carpenter, R., and Coen, E. (2003). Genetic control of surface curvature. *Science* **299**, 1404-7.

Nicolas, M., and Cubas, P. (2016). TCP factors: new kids on the signaling block. *Curr Opin Plant Biol* **33**, 33-41.

Palatnik, J. F., Allen, E., Wu, X., Schommer, C., Schwab, R., Carrington, J. C., and Weigel, D. (2003). Control of leaf morphogenesis by microRNAs. *Nature* **425**, 257-63.

Rodriguez, R. E., Schommer, C., and Palatnik, J. F. (2016). Control of cell proliferation by microRNAs in plants. *Curr Opin Plant Biol* **34**, 68-76.

Rubio-Somoza, I., Zhou, C. M., Confraria, A., Martinho, C., von Born, P., Baena-Gonzalez, E., Wang, J. W., and Weigel, D. (2014). Temporal control of leaf complexity by miRNA-regulated licensing of protein complexes. *Curr Biol* **24**, 2714-9.

Sarvepalli, K., and Nath, U. (2011). Hyper-activation of the TCP4 transcription factor in Arabidopsis thaliana accelerates multiple aspects of plant maturation. *Plant J* **67**, 595-607.

Sarvepalli, K., and Nath, U. (2018). CIN-TCP transcription factors: Transiting cell proliferation in plants. *IUBMB Life* **70**, 718-731.

Schommer, C., Debernardi, J. M., Bresso, E. G., Rodriguez, R. E., and Palatnik, J. F. (2014). Repression of cell proliferation by miR319-regulated TCP4. *Mol Plant* **7**, 1533-44.

Schommer, C., Palatnik, J. F., Aggarwal, P., Chetelat, A., Cubas, P., Farmer, E. E., Nath, U., and Weigel, D. (2008). Control of jasmonate biosynthesis and senescence by miR319 targets. *PLoS Biol* **6**, e230.

Shen, W. H. (2002). The plant E2F-Rb pathway and epigenetic control. *Trends Plant Sci* **7**, 505-11.

Vashisth, T., Johnson, L. K., and Malladi, A. (2011). An efficient RNA isolation procedure and identification of reference genes for normalization of gene expression in blueberry. *Plant Cell Rep* **30**, 2167-76.

Verkest, A., Weinl, C., Inze, D., De Veylder, L., and Schnittger, A. (2005). Switching the cell cycle. Kip-related proteins in plant cell cycle control. *Plant Physiol* **139**, 1099-106.

Voinnet, O. (2009). Origin, biogenesis, and activity of plant microRNAs. *Cell* **136**, 669-87.

Wang, H., Zhou, Y., Gilmer, S., Whitwill, S., and Fowke, L. C. (2000). Expression of the plant cyclin-dependent kinase inhibitor ICK1 affects cell division, plant growth and morphology. *Plant J* **24**, 613-23.

White, D. W. (2006). PEAPOD regulates lamina size and curvature in Arabidopsis. *Proc Natl Acad Sci U S A* **103**, 13238-43.

Table 3.1. Probe sequence for electrophoretic mobility shift assay.

Probe	Target	Sequence (from 5' to 3')
Cons	*Consensus*[x]	AGATGAGGGGGACCACATAGATGT
Probe A	*MdKRP4*	TAACAGAGTCTGGACCACCTTTTGCC
Probe G	*MdKRP4*	TAACGGAGTCTGGACCACCTTTTGCC
Probe 5	*MdKRP5*	TAACGGAGTCTGGACCACCTTGGCCA
Probe m1[y]	*MdKRP4*	TAACAGAGTCTGGAaCACCTTTTGCC
Probe m2[z]	*MdKRP4*	TAACAGAGTCTGGAaCtCCTTTTGCC

[x]Consensus probe based on previous studies in Arabidopsis (Schommer et al., 2008)

[y]Mutated probe with alteration of one base within the core binding motif

[z]Mutated probe with alteration of two bases within the core binding motif

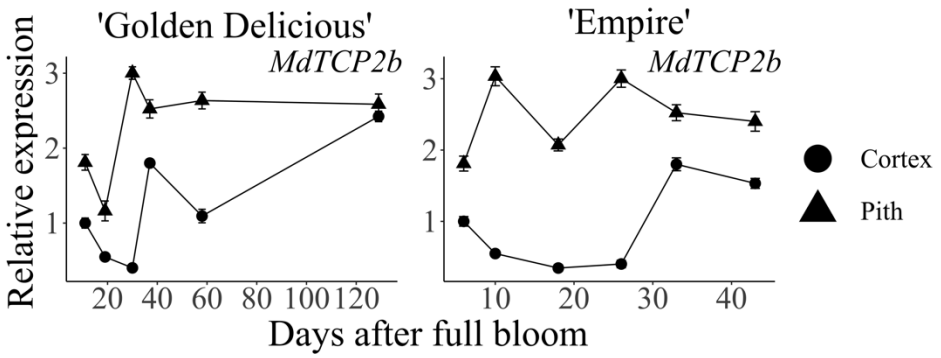

Figure 3.1. Transcript abundance of *MdTCP2b* in ‘Golden Delicious Smoothee’ and ‘Empire’ fruit cortex and pith. Data (mean ± SE; n = 4) are presented in relation to abundance in the cortex at 11 d after full bloom for ‘Golden Delicious’, and in the cortex at 6 d after full bloom for ‘Empire’.

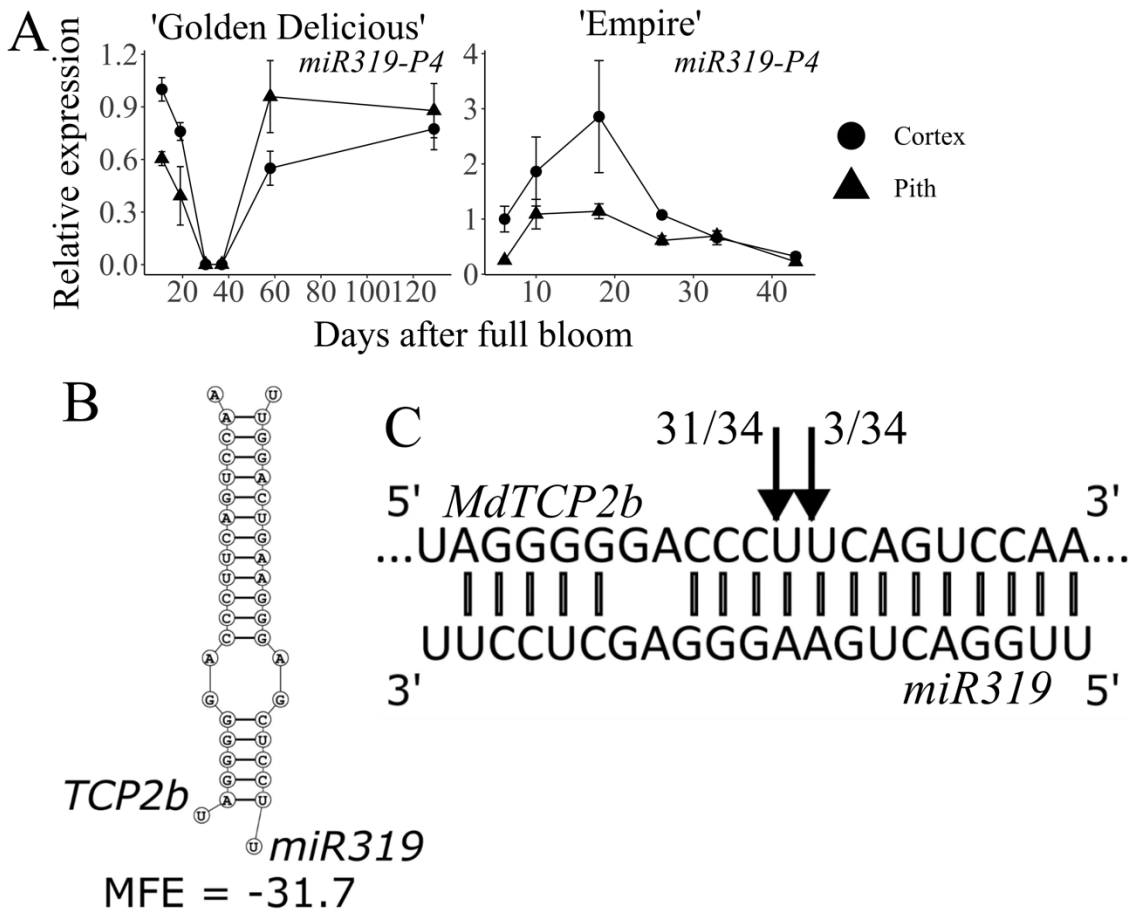

Figure 3.2. Post-transcriptional regulation of *MdTCP2b* transcript by miR319. A. Transcript abundance of *miR319* in 'Golden Delicious Smoothee' and 'Empire' fruit cortex and pith. Data (mean ± SE; n = 4) are presented in relation to abundance in the cortex at 11 d after full bloom for 'Golden Delicious', and in the cortex at 6 d after full bloom for 'Empire'. B. RNAstructure plot shows potential binding of miR319 with *MdTCP2b* (MFE: minimum free energy). C. Cleavage positions identified by 5′ RNA ligase mediated RACE (RLM-RACE) are indicated with arrows. The number of clones identified at each specific position relative to the total number of clones analyzed is indicated at each location.

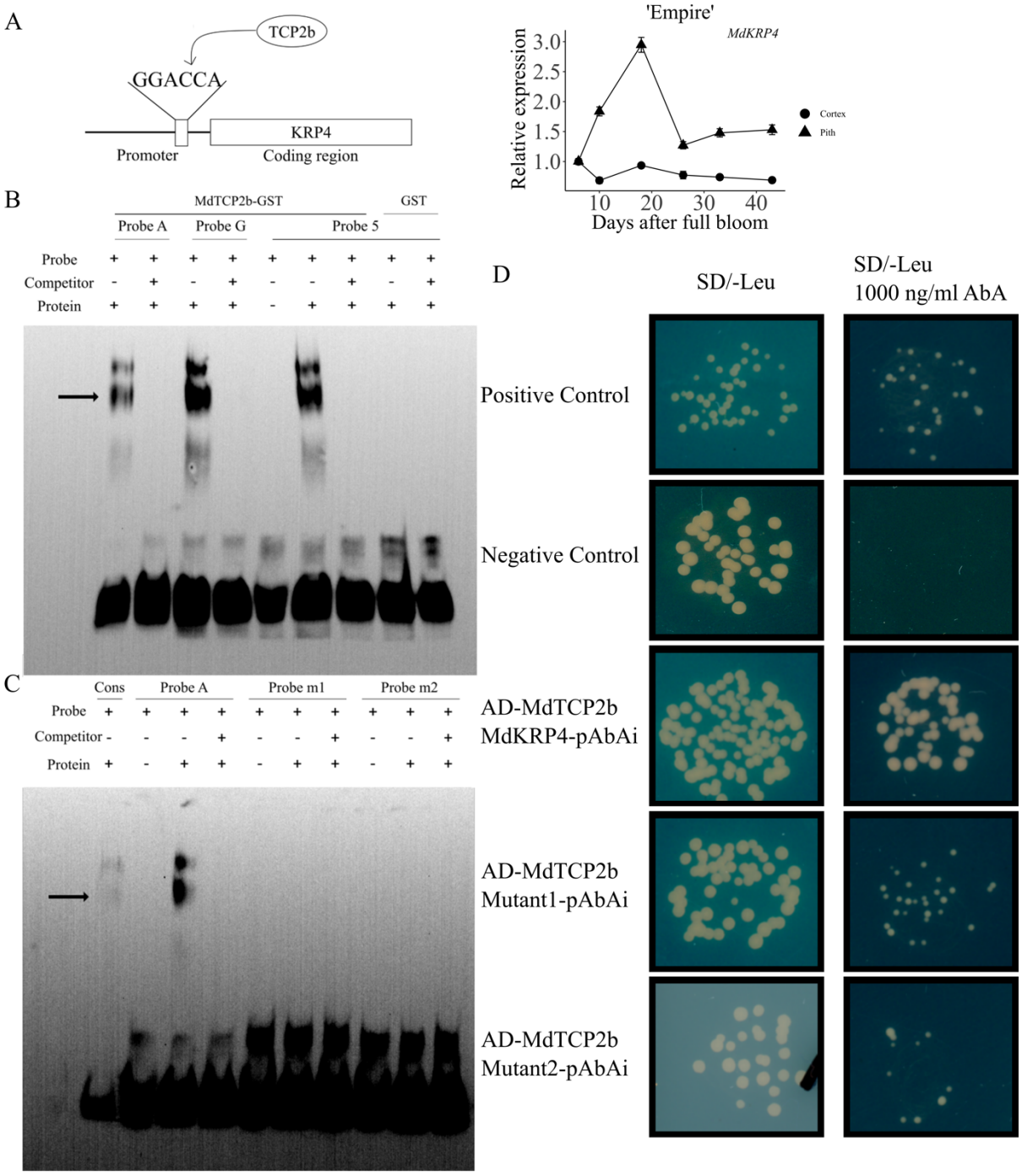

Figure 3.3. Interaction of MdTCP2b with *MdKRP4* and *MdKRP5* promoters. A. The potential binding motif within the *MdKRP4* promoter is indicated. Transcript abundance of *MdKRP4* during 'Empire' fruit development. B-C. Electrophoretic mobility shift assays (EMSAs) were performed to determine the interaction between MdTCP2b-GST protein and specific probes

[Cons: consensus probe (based on Schommer et al., 2008); Probe A: *MdKRP4* promoter probe with 'A' allele; Probe G: *MdKRP4* promoter probe with the 'G' allele; Probe 5: *MdKRP5* promoter probe; Probe m1: mutation 1 of *MdKRP4* promoter probe, Probe m2: mutation 2 of *MdKRP4* promoter probe]. "+" represents the presence of the component in the binding reaction. "-" represents the absence of the component in binding reaction. D. The interaction of MdTCP2b protein with the *MdKRP4* promoter (-338 to -31), and with mutations within the binding motif identical to those described above. Positive control and negative controls were performed as per the manufacturer's instructions. AbA: aureobasidin A.

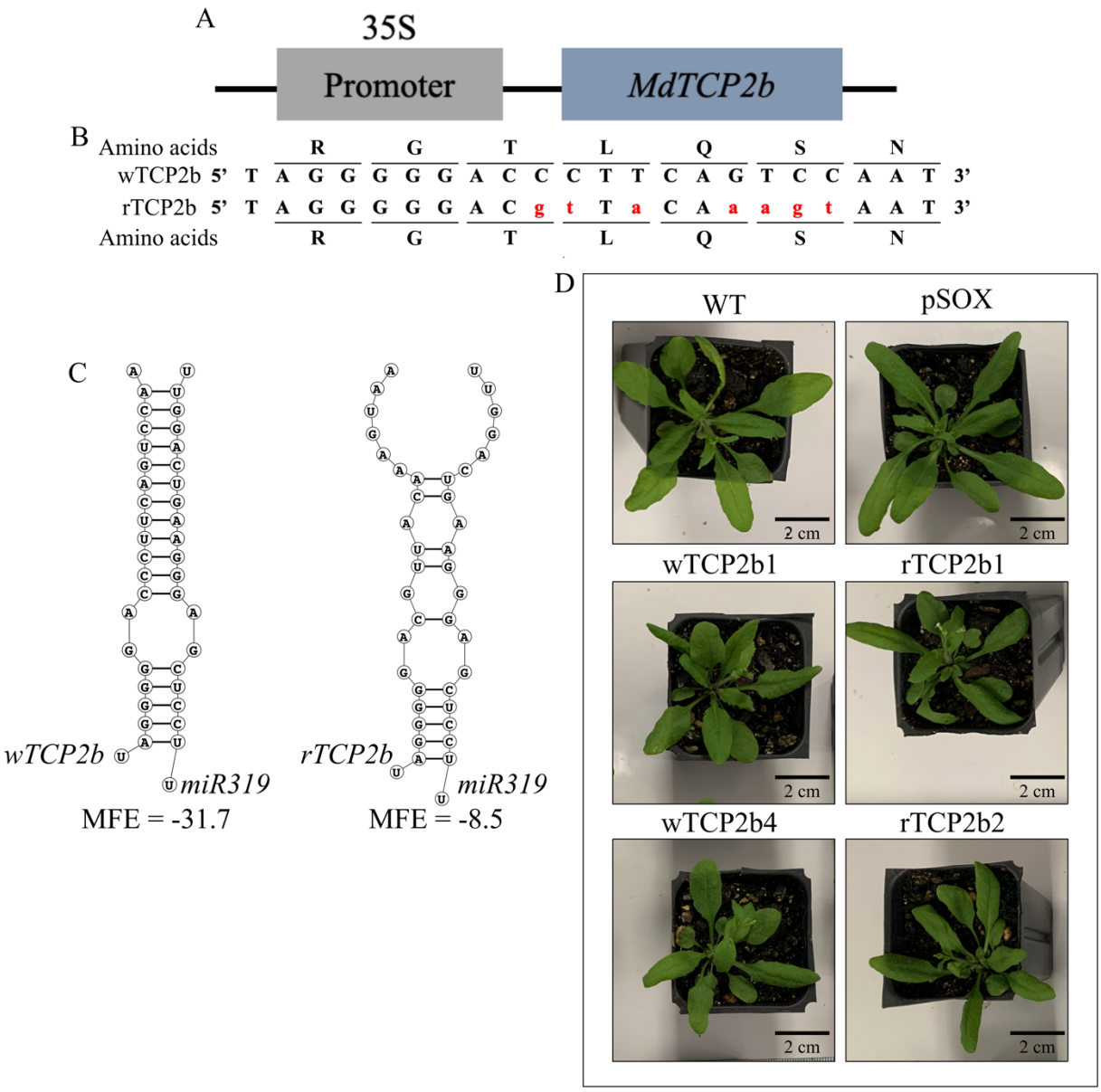

Figure 3.4. Heterologous overexpression of *MdTCP2b* in Arabidopsis. A. Scheme of overexpression of *MdTCP2b* driven by the 35S promoter. B. Amino acid sequence and nucleotide sequence of wTCP2b and rTCP2b versions. Red and lowercase letter represents the mutation within the miR319 binding site. C. RNAstructure plot shows minimum free energy (MFE) of wTCP2b and rTCP2b binding to miR319. D. Rossette of WT (wild type Col-0), pSOX

(empty vector with 35S promoter), two wTCP2b lines and two rTCP2b lines when inflorescence was 2 cm long. Bar = 2 cm.

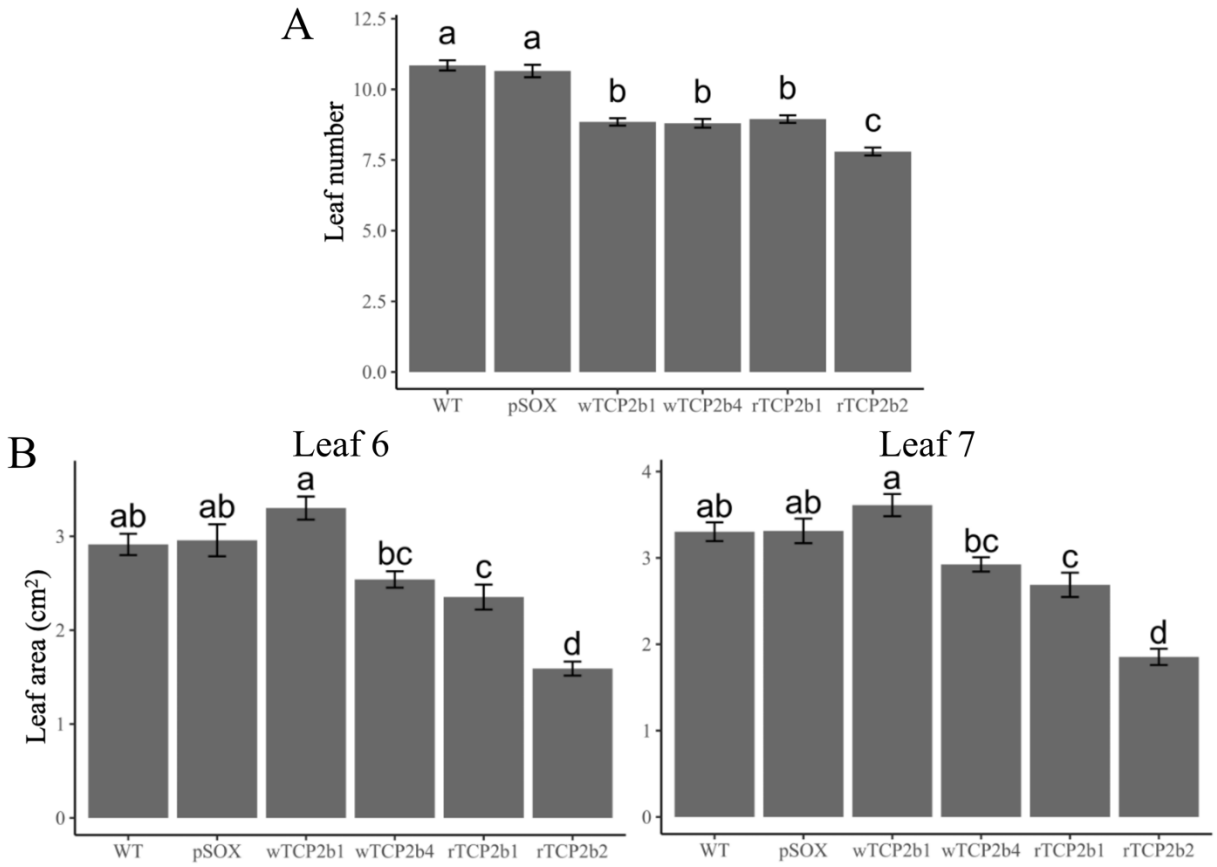

Figure 3.5 Heterologous expression of *MdTCP2b* promotes flowering time and reduced leaf size in Arabidopsis. A. Time to bolting was determined as the number of rosette leaves when bolt was 2 cm in length. B. Leaf area of 6th and 7th leaves when inflorescence was 2 cm long. Leaf area was determined after leaves were scanned and processed using ImageJ. Different letters indicate significant differences between means within different genotypes as determined by ANOVA ($P < 0.05$), followed by Tukey's Honestly Significant Difference (HSD). Error bars indicate SE (n = 20).

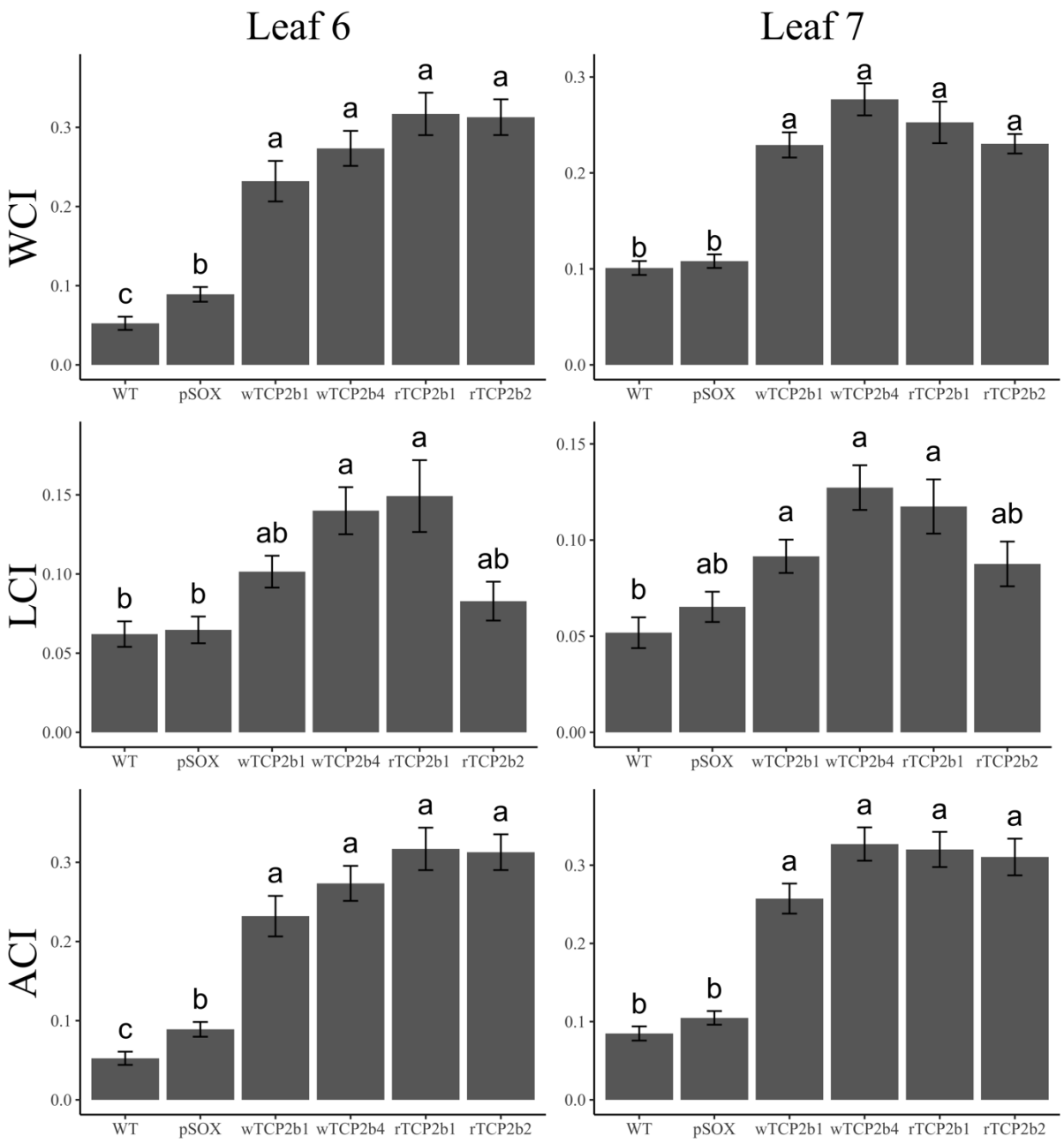

Figure 3.6. Heterologous expression of *MdTCP2b* promotes positive leaf curvature in Arabidopsis. Curvature index (CI) was used to determine the change in leaf curvature. Leaves were excised and scanned. Incisions were made along eh leaf margin to flatten the leaf, followed by scanning. Image processing was performed in ImageJ. The width, length, and area curvature index of the 6th and 7th leaves was measured when inflorescence was 2 cm long. Different letters indicate significant differences between means within different genotypes as determined by

ANOVA ($P < 0.05$), followed by Tukey's Honestly Significant Difference (HSD) Error bars indicate SE (n=20).

CHAPTER 4

THE GRF/GIF MODULE AND REGULATION OF EARLY FRUIT GROWTH

Abstract

GROWTH REGULATING FACTORs (GRFs) transcription factor family plays important roles in regulating plant growth and development. A previous study identified that *MdGRF11* and *MdGIF3* are potentially involved in spatio-temporal regulation of cell production during early fruit development (EFD) in apple. Here, these roles were further validated, and their regulation was characterized. *MdGRF11* and *MdGIF3* displayed higher expression during EFD and very low transcript abundance at later stages. RLM-RACE analyses indicated that *MdGRF11* is targeted by microRNA396 (miR396) as transcripts of *MdGRF11* were predominatly cleaved between the 10th and 11th bases of the miR396 binding region. These data indicate that *MdGRF11* is post-transcriptionally regulated by miR396-mediated degradation. A single nucleotide polymorphism (SNP) in the miR396 binding site of *MdGRF11* was identified in 'Golden Delicious', a genotype heterozygous for this SNP. A greater proportion of *MdGRF11* transcripts during EFD in 'Golden Delicious' carried the 'C' allele indicating that this allele is likely to be targeted with lower efficiency for miR396-mediated degradation. Genotyping analyses for this SNP indicated that only four out of 56 genotypes tested were homozygous for the 'TT' allele suggesting selection against this allele. Yeast-two-hybrid analyses indicated that MdGRF11 and MdGIF3 display protein-protein interaction. Deletion of the N-terminal region of MdGRF11 abolished this interaction indicating that the interaction is specific and requires a potential QLQ motif within the N-terminal region of this protein. Together, this study demonstrates that the miR396-GRF11-GIF3 module is functional and associated with regulation of cell production during EFD in apple.

Introduction

Fruit growth is a cooperative process involving cell proliferation and cell expansion. After dormancy and bud break, growth of the accessory tissue surrounding the ovary is mediated by cell production and expansion. Subsequently, growth, cell proliferation and expansion are paused until fruit set from around 7 d before full bloom (DBFB) to around 8-11 d after full bloom (DAFB) (Malladi and Johnson, 2011). After pollination and fertilization result in fruit set, the fruit undergoes a period of vigorous growth mediated by cell proliferation, while cell size increases slightly in the fruit cortex (Bain and Robertson, 1951; Dash and Malladi, 2012). Cell number increases over 8-fold between 7 DAFB and 28 DAFB, which generates a large cell population that undergoes post-mitotic cell expansion to mediate fruit growth (Dash and Malladi, 2012; Jing and Malladi, 2020). The cell expansion phase lasts until around 120-180 DAFB and results in over a 1500-fold increase in cell area (Janssen et al., 2008; Malladi and Johnson, 2011; Jing and Malladi, 2020).

Some molecular mechanisms that regulate apple fruit growth have been illustrated, including that mediated by the GROWTH REGULATING FACTORs (GRFs) transcription factor family. GRFs regulate plant growth and development in many plant species (Kim et al., 2003; van der Knaap et al., 2000; Kim and Tsukaya, 2015). GRF proteins contain the highly conserved QLQ (Gln, Leu, Gln) and WRC (Trp, Arg, Cys) domains at the N-terminal and the variable C-terminal, respectively. Previous studies revealed that the QLQ domain contains the QX3LX2Q motif, which is highly similar to that in the SWITCH2/SUCROSE NONFERMENTING2 (SWI/SNF) chromatin remodeling ATPase that possess the protein-protein interaction function (de Bruijn et al., 2001; Horiguchi et al., 2005; Kato et al., 2002; Kim et al., 2003). The WRC domain is the DNA-protein interaction domain that also carries a nuclear localization signal (NLS) (Kuijt et al.,

2014; Osnato et al., 2010). The C-terminal of GRF plays a role in transactivation, as some GRFs with extremely short C terminals do not display transactivation capacity (Wu et al., 2014; Zhang et al., 2021).

GRF transcription factors greatly impact plant growth and development. Triple mutants in Arabidopsis, *grf1/2/3,* display smaller and narrower leaves than the wild type, while single mutants and double mutants display relatively minor changes in leaf size, owing to redundancy in function (Kim et al., 2003). GRFs may also play important roles in apple fruit growth and development. More than 17 genes coding for GRFs have been identified in the apple genome (Jing and Malladi, 2022; Zheng et al., 2018). Jing and Malladi (2022) determined that the transcript abundance of *MdGRF11* and *MdGRF16* was high during initial stages of EFD and decreased towards the end of the cell proliferation period, indicating that their gene products may regulate cell production during fruit growth. Multiple members of the *GRF* family genes contain a conserved target site for *microRNA396 (miR396)* and are post-transcriptionally regulated. Seven out of nine *AtGRFs*, 11 out of 12 *OsGRFs* (*Oryza sativa*), and 12 out of 14 *ZmGRFs* (*Zea mays*) can complimentarily bind to *miR396* (Choi et al., 2004; Das Gupta and Nath, 2015; Rodriguez et al., 2010). All *MdGRFs*, except *MdGRF7* and *MdGRF9*, contain a potential miR396 binding site (Allen et al., 2005; Jing and Malladi, 2022).

GRF-INTERACTING FACTORs (GIFs) were identified as partner proteins of GRFs that regulate the rate and duration of cell division thereby regulating growth. GIFs do not contain DNA-binding domains and likely interact with other proteins such as the GRFs to serve as transcriptional co-regulators. The SYT (synovial translocation) N-terminal homology (SNH) domain at the N-terminal of GIFs is critical for protein-protein interactions (de Bruijn and Geurts van Kessel, 2006; Horiguchi et al., 2005; Kim and Kende, 2004). Several studies have confirmed the partnership of

GRFs and GIFs in Arabidopsis, rice, and maize, but, this has not yet been established in apple (Horiguchi et al., 2005; Lu et al., 2020; Zhang et al., 2018). The *gif* mutants in Arabidopsis cease cell division several days earlier than in the wild type (Kim and Kende, 2004). The mutation of *gif1*, also named *angustifolia 3* (*an3*) results in narrower leaves and petals (Kim and Kende, 2004). The triple *gif* mutants (*gif1gif2gif3*) exhibit severely reduced plant size and malformation of floral organs (Kim and Tsukaya, 2015; Lee et al., 2009). There are four members of the *GIF* family in apple. Among these, *MdGIF3* shares greatest sequence similarity with the *AtGIF1/AN3* (74% identity; Jing and Malladi, 2022). The transcript abundance of *MdGIF3* was high during early fruit development (EFD), subsequently declined and remained low at later stages of development (Jing and Malladi, 2022). Furthermore, *MdGIF3* transcript abundance was positively correlated with the relative cell production rate (RCPR) during EFD, and the transcript abundance of *MdGRF11* and *MdGRF16*, supporting a potential role of the GRF-GIF module in the spatio-temporal regulation of early fruit growth (Jing and Malladi, 2022). Several aspects regarding this potential module remain to be investigated. These include the potential for direct interaction between MdGRF11 and MdGIF3, and the regulation of *MdGRF11* transcript abundance by miR396. The main objective of this study was to address these questions in apple.

Materials and methods

Plant materials

Samples of 'Golden Delicious Smoothee' apple fruit used in this study were obtained from a previous study (Jing and Malladi, 2020). In that study, fruit load was reduced by manually removing all fruitlets in clusters, except king fruit, at 11 days after full bloom (DAFB). 'Empire' fruit tissue from the study described previously in Chapter 2 were also used. Fruit load reduction of 'Empire' was performed at 6 DAFB. Samples collected at 6, 10, 18, 26, 33 and 43 DAFB in

‘Empire’, and at 11, 19, 30, 37, 58, and 129 DAFB in ‘Golden Delicious’ were further used in this study. In this study, the cortex and pith tissues were separated and frozen in liquid nitrogen, and stored at -80 °C for later use, to allow for analysis of spatial expression patterns during apple fruit growth.

RNA extraction and qRT-PCR

Total RNA of cultivar ‘Golden Delicious Smoothee’ and ‘Empire’ were extracted by the CTAB method as described in Vashisth et al. (2011) and Jing and Malladi (2020). One µg of total RNA of cortex and pith samples in ‘Empire’ were using for cDNA synthesis using ImProm II reverse transcriptase (Promega, USA) after the DNaseI treatment. The cDNA was diluted 5-foldand used for qRT-PCR following the method described previously to quantitate the transcript abundance of *MdGRF11* and *MdGIF3* (Jing and Malladi, 2022).

Stem-loop qRT-PCR was used to quantitatively analyze miR396 transcript abundance following Varkonyi-Gasic et al. (2007) with a few modifications. One µg of total RNA of cortex and pith samples in ‘Golden Delicious Smoothee’ were used to synthesize cDNA with a miR396 RT primer after DNase I treatment. The cDNA was diluted 5-fold and used for qRT-PCR. *MdCACS2* was used for normalization.

RNA Ligase Mediated – Rapid Amplification of cDNA Ends (RLM-RACE)

5′ RLM-RACE was used to identify the cleavage site of *MdGRF11* based on the method described in Llave et al. (2002) with minor modification. Total RNA after DNaseI treatment and purification was utilized for ligation with a 5′ RNA adaptor. The ligated product was ioslated and then synthesis of cDNA was performed. Samples of RNA used here were from the ‘Golden Delicious Smoothee’ fruit cortex tissue at 19 and 23 DAFB.

MdGRF11 SNP identification

cDNA of cortex and pith samples in 'Golden Delicious' at 23 and 30 DAFB were synthesized as described earlier. Gene specific primers amplifying products across the miR396 target site in *MdGRF11* were designed and used for PCR amplification. The PCR products were analyzed by agarose gel electrophoresis and purified using the Zymoclean Gel DNA Recovery Kit (ZYMO RESEARCH). The purifiied PCR products were cloned into the pGEM-T Easy Vector (Promega) and transformed into JM109 competent cells. After colonies were grown at 37°C for 1 day, 24 independent colonies from each stage were used for plasmid isolation and sequenced. The sequences were aligned against the *MdGRF11* sequence using Clustal Omega to determine the presence of 'T' and 'C' variants (SNPs) within the miR396 target site of the transcript.

Double-mismatch allele-specific qPCR (DMAS-qPCR) was performed to identify the 'T' and 'C' variants across apple genotypes based on the description in Lefever et al. (2019). Genomic DNA was isolated from 56 apple genotypes. Leaf sample for the genotypes used in this study were obtained from the USDA apple germplasm collection (Geneva, NY, USA), or collected from the Mountain Research and Education Center, UGA, Blairsville, GA and the Mountain Horticultural Crops Research and Education Center, North Carolina State University (Mills River, NC). Two specific reverse primers were designed to conduct the qPCR along with a common forward primer as per Lefever et al. (2019).

Yeast two-hybrid assay

The yeast two-hybrid (Y2H) system from Matchmaker Yeast Two-Hybrid System (Takara) was used to verify protein-protein interactions between MdGRF11 and MdGIF3. The full-length cDNA of *MdGRF11* and *MdGIF3* were cloned from total RNA isolated from 'Golden Delicious Smoothee' fruit cortex using the primers (5'-ATCGCATATGATGGACTTCTACCTTAAG-3'

and 5’-CGATGAATTCTCAAGTGCTGATAAAGC-3’ for MdGRF11, and 5’-ATCGGAATTCATGCAGCAGCACCTGA-3’ and 5’-AGCTGGATCCTTAATTTCCATCATCGGTCG-3’ for MdGIF3). The open-reading frame (ORF) of *MdGRF11* with NdeI and EcoRI ends and *MdGIF3* with EcoRI and BamHI ends were introduced into bait (pGBKT7) and prey (pGADT7) vectors separately. Additionally, a cDNA fragment of *MdGRF11* lacking the N terminal region required for protein-protein interaction (QLQ-domain) was amplified with primers (5’-AGTCCATATGGGTTCTGCTCCTTATTTT-3’ and 5’-CGATGAATTCTCAAGTGCTGATAAAGC-3’). This was cloned into the bait vector and interactions with the MdGIF3 prey were evaluated to test the specificity of interaction between MdGRF11 and MdGIF3.

The bait recombinants were transformed into Y2HGold yeast strains and evaluated for autoactivation and toxicity; and the prey recombinants were transformed into Y187 yeast strains. The two-hybrid mating experiments were conducted by placing the bait-MdGIF3 and prey-MdGRF11 colonies in 500 µL 2X YPDA overnight at 30 °C with shaking, as well as bait-MdGRF11 and prey- MdGIF3 colonies. Then the mated cultures were spread on SD/–Leu/–Trp (DDO: double drop out media) and DDO/X-alpha-Gal/AbA (DDO/X/A; AbA:aureobasidin) agar media and incubated at 30 °C for 3 d. The putative transformants were transferred to SD/–Ade/–His/–Leu/–Trp/X-alpha- Gal/AbA (QDO [quadruple drop out) /X/A] agar media for further verification after the yeast cells had grown from DDO and DDO/X/A plates. To distinguish genuine positive interactions from false positives, the bait and prey recombinants were co-transformed into Y2HGold yeast strains with empty pGBKT7 and prey vectors. The cells were transferred to DDO/X and QDO/X/A agar plates incubated at 30 °C for 4 d to analyze the results.

pGBKT7-53 with pGADT7-T was used as a positive control, and pGBKT7-Lam with pGADT7 was used as a negative control, following manufacturer's instructions.

Results

Transcript abundance of *MdGRF11*, *MdGIF3* during fruit development

There are over 17 genes encoding GRF transcription factors in apple and among them *MdGRF11* is most closely related to *AtGRF3* and *AtGRF4*, genes that positively regulate cell production and are involved in multiple aspects of plant growth and development (Zheng et al., 2018; Jing and Malladi, 2022). There are four GIF family members in apple, and *MdGIF3* displays 74% identity with *AtGIF1* (Jing and Malladi, 2022). In 'Golden Delicious Smoothee', the transcript abundance of *MdGIF3* and *MdGRF11* displayed a strong positive correlation. The transcript abundance of *MdGRF11* and *MdGIF3* in cortex and pith tissue was determined during 'Empire' fruit development.

Transcript abundance of *MdGRF11* was high in both cortex and the pith during early fruit development. It gradually declined in the cortex during EFD. In the pith, it increased slightly between 6 and 10 DAFB and declined to undetectable levels at later stages (Figure 4.1). Transcript abundance of *MdGIF3* in cortex was highest at 6 DAFB and declined to gradually to undetectable levels by 43 DAFB, while it increased slightly in the pith between 6 and 10 DAFB and declined at later stages (Figure 4.1). Overall, the transcript abundance patterns of these genes were similar to that in 'Golden Delicious Smoothee' (Jing and Malladi, 2022).

Transcript abundance of miR396 during fruit development

Transcript abundance of *miR396* in the cortex of 'Golden Delicious Smoothee' was high at 11 DAFB and sharply decreased to nearly undetectable levels by 58 DAFB (Figure 4.2). While transcript abundance of *miR396* was low in pith during EFD, it declined 2-fold between 11 and 30

DAFB and continually decreased to undetectable levels at later stages (Figure 4.2). The abundance of *miR396* was higher in cortex than that in pith during EFD by up to 4-fold.

Cleavage site in the *MdGRF11* transcript for miR396-dependent regulation

The expression of *MdGRF11* may be negatively regulated by *miR396*, since it contains a potential *miR396* binding site towards the 3′ end of the gene. This was confirmed with *in silico* analysis of the potential binding using RNAstructure (rna.urmc.rochester.edu/RNAstructure.html) (Figure 4.3A). There is an unmatched site between 7 and 8 of miR396 complementarity region with *AtGRFs*, which can alter the strength of interaction (Allen et al., 2005; Debernardi et al., 2012). RNAstructure predicted a similar unmatched site between bases 7 and 8 in the complementarity region of miR396 with *MdGRF11* (Figure 4.3A). RLM-RACE analysis was performed to determine if miR396 binding can result in *MdGRF11* cleavage. There were thirty six independent clones displayed the cleavage site between 10^{th} and 11^{th} nucleotides in relation to the 5′ end of *miR396*, which is a hallmark of plant transcript cleavage upon miRNA binding (Llave et al., 2002) (Figure 4.3B). Hence, these data indicate that *MdGRF11* transcripts are cleaved in a miR396-dependent manner in the developing apple fruit.

SNP within the miR396 binding site of MdGRF11

During sequencing of *MdGRF11* transcripts, a single base polymorphism from 'T' to 'C' within the miR396 binding site which modified it from 5'-GTTCAAGAAAGCCTGTGGAA-3' to 5'-GTTCAAGAAAGCCTGCGGAA-3' was noted in 'Golden Delicious' which was heterozygous and carried both alleles (Figure 4.3C). RNAstructure analyses predicted that such a SNP (T to C) can potentially affect the efficiency of miR396 binding and thereby degradation of *MdGRF11* transcripts, ultimately allowing for greater transcript accumulation and promotion of cell production (Figure 4.3C). Therefore, the proportion of transcripts containing the 'T' and 'C' alleles

in the fruit cortex and pith tissues were determined at 23 and 30 DAFB by sequencing multiple independent colonies from a pool of cloned *MdGRF11* transcripts at each stage. At 23 DAFB, four colonies with a 'T' allele and 17 with the 'C' allele were sequenced in the cortex ($P = 0.0036$). In the pith, 0 'T' allele and 23 'C' allele containing clones were sequenced ($P < 0.001$) (Table 4.1). At 30 DAFB, two 'T' allele and 18 'C' allele containing colonies were sequenced from the cortex ($P < 0.001$), and four 'T' allele and 17 'C' allele containing colonies were identified in the pith ($P = 0.0036$) (Table 4.1). The χ^2 analysis clearly showed a greater proportion of 'C' allele containing transcripts. This suggested that miR396 mediates the cleavage of 'T' variants with higher efficiency and that the 'C' variants are potentially more stable during apple fruit growth.

Subsequently, double-mismatch allele-specific quantitative PCR (DMAS-qPCR) was performed to genotype the SNP in 56 apple genotypes. These analyses showed that 22 genotypes were heterozygous for the SNP (T/C), and 30 were homozygous for the 'C' allele (C/C). Only the genotypes, Ellis Bitter, Frequin Tardive de la Sarthe, Tale Sweet, and Redfree were homozygous for the 'T' allele (T/T) (Figure 4.4).

MdGRF11 interacts with MdGIF3

The interaction of GRF and GIF proteins mediated by QLQ and SNH domains has been reported in Arabidopsis, but it has not been demonstrated in apple (Horiguchi et al., 2005; Kato et al., 2002; Kim et al., 2003). Jing and Malladi (2022) indicated co-regulation of *MdGRF11* and *MdGIF3* during fruit development in apple. Hence, the ability of MdGRF11 to physically interact with MdGIF3 was tested using the Yeast two-hybrid assay.

The full-length cDNA of *MdGRF11* and *MdGIF3* were cloned into the bait (pGBKT7) and prey (pGADT7) vectors (Figure 4.5A). The bait vectors were transformed into Y2HGold yeast strains, and the prey vectors were transformed into Y187 yeast strains. Autoactivation tests

indicated that pGBKT7-MdGRF11 and pGBKT7-MdGIF3 baits do not autonomously activate the reporter genes in Y2HGold yeast strains. Further, toxicity tests demonstrated that both bait proteins are not toxic when expressed in yeast.

Initial detection of potential interaction between MdGRF11 and MdGIF3 was conducted by mating yeast colonies of Y2HGold with bait and Y187 with prey. The pGBKT7-MdGRF11 + pGADT7-MdGIF3 and pGBKT7-MdGIF3 + pGADT7-MdGRF11 could grow normally on SD/-Trp-Leu (DDO: Double Drop Out media) and SD/–Ade/–His/–Leu/–Trp/X-alpha-Gal/AbA (QDO/X/A: quadruple drop out supplemented with X-Gal and aureobasidin) media and turned blue on QDO/X/A media (Figure 4.5B). The negative control (pGBKT7-Lam + pGADT7-T) grew normally only on the DDO plate (Figure 4.5B). To further confirm the positive interaction between MdGRF11 and MdGIF3, the bait and prey vectors were co-transformed into Y2HGold yeast strains (Figure 4.5B). The pGBKT7-MdGRF11 + pGADT7-MdGIF3 and pGBKT7-MdGIF3 + pGADT7-MdGRF11 could grow blue colonies on DDO/X and QDO/X/A media, while empty pGBKT7 + pGADT7-MdGIF3 and empty pGBKT7 + pGADT7-MdGRF11 grew only white colonies on DDO/X media, indicating that the interactions required presence of both proteins (Figure 4.5B).

To further test if the interactions between MdGRF11 and MdGIF3 were specific, a truncated *MdGRF11* version lacking the QLQ domain required for protein-protein interactions (*Nqlq-GRF11*) was cloned into the bait vector (Figure 4.5A). The cDNA of *Nqlq-GRF11* encoded amino acids 118 to 397 of MdGRF11. After autoactivation and toxicity tests, the pGBKT7-Nqlq-GRF11 and pGADT7-MdGIF3 vectors were co-transformed into Y2HGold yeast strains. Removal of the N-terminal region containing the QLQ domain from MdGRF11 abolished its interaction

with MdGIF3, indicating that MdGRF11 interacts specifically with MdGIF3 and that the N terminal region is essential for this interaction (Figure 4.5B).

Discussion

MdGRF11-MdGIF3 module regulates fruit growth

GRFs are plant specific transcription factors important for regulating plant growth and development. There are nine *GRF* genes in Arabidopsis; AtGRF1-5 are positive regulators of leaf growth by promoting cell proliferation, but AtGRF9 negativity affects leaf growth (Liebsch and Palatnik, 2020; Liu et al., 2009; Omidbakhshfard et al., 2018). *AtGRF1/2/3* are involved in the complex regulation of root growth, and *AtGRF1-3* and *AtGRF5* are involved in floral organ development (Ercoli et al., 2018; Lee et al., 2018; Rodriguez et al., 2015). The *GRF* gene family in rice contains 12 members. Some of these have positive effects on leaf and floral organ growth. In rice, *OsGRF4/6* defective in *miR396*-mediated transcript-cleavage displays increased grain size, panicle length and grain weight (Gao et al., 2015; Duan et al., 2015; Li et al., 2016).

There are more than 17 GRF members in apple, most *MdGRFs* exhibit high expression in shoot tips and low abundance in fruits (Zheng et al., 2018). Many *MdGRFs* displayed a sharp decline in expression after bloom (Jing and Malladi, 2022). The transcript abundance of *MdGRF11* in this study showed similar expression pattern to that in 'Golden Delicious Smoothee', which was high during the cell proliferation period and declined prior to the transition from cell proliferation to cell expansion (Jing and Malladi, 2022). Further, *MdGIF3* expression pattern was also consistent with that reported in the previous study and largely similar to that of *MdGRF11*. Both genes displayed greater abundance in the cortex tissue during early stages of fruit development in comparison to the pith. Together, these data suggest that the MdGRF11-MdGIF3 module is positively associated with cell proliferation in the cortex during EFD.

MdGRF11 is post-transcriptionally regulated by miR396

Multiple *GRF* transcripts are post-transcriptionally regulated by *miR396*. Overexpression of *miR396* results in smaller plants with declined expression of *GRF* genes (Rodriguez et al., 2010; Wang et al., 2011). Seven out of nine *AtGRFs*, 11 out of 12 *OsGRFs*, and 12 out of 14 *ZmGRFs* can complimentarily bind to the *miR396* (Choi, et al., 2004; Das Gupta and Nath, 2015; Rodriguez, et al., 2010). Majority of the *MdGRFs*, including *MdGRF11*, contain a target site for miR396. However, the transcript abundance of *miR396* is not complimentary to that of *MdGRF11* unlike that reported that in Arabidopsis (Rodriguez et al., 2010) (Figure 4.2). Its abundance was higher in the cortex and substantially lower in the pith during EFD. These data suggest that miR396 was likely more abundant spatially and temporally in tissues and during phases where *MdGRF11* (and other related GRFs such as *MdGRF16* (Jing and Malladi, 2022), were also abundant. RLM-RACE analyses clearly indicated that the *MdGRF11* transcripts were cleaved between positions 10 and 11 within the binding region and from the 5′ end of the *miR396*. Hence, *MdGRF11* transcripts appear to be post-transcriptionally regulated by *miR396*. The similar patterns of expression of *MdGRF11* and *miR396* suggest that fine-regulation of *MdGRF11* occurs in a spatio-temporal manner during EFD in apple.

SNP in *MdGRF11* potentially affects its miR396-directed post-transcriptional regulation

The single base substitution located in the putative *miR396* binding sequence of *MdGRF11* likely perturbs the cleavage by *miR396*, resulting in increased expression of *MdGRF11*. Less free energy within *MdGRF11* and miR396 binding in the allele ‘C’ compared to the allele ‘T’ was noted through RNAstructure analyses, indicating lower stability of the type ‘C’ *GRF11-miR396* duplex (Figure 4.3C). Further, differences in the proportion of the two types of *MdGRF11* transcripts during EFD supported that type ‘T’ *MdGRF11* is likely degraded more while the type ‘C’

MdGRF11 is more stable during EFD (Table 4.1). In rice, a naturally occurring polymorphism within the *miR396*-recognition site of *OsGRF4* perturbs its repression by *miR396* and increases the expression of *OsGRF4* thereby affecting grain length, width and size (GS2 QTL) (Che et al., 2015; Duan et al., 2015). A two bp substitution mutation in *OsGRF4* (1187TC to AA) results in larger and heavier grains by interfering with *miR396*-directed regulation. The mutation with 'AA' increases epidermal cell size and cell number in spikelet hulls, suggesting that GS2 promotes both cell expansion and cell proliferation to produce larger grains, which greatly supports the positive role of *OsGRF4* in regulating cell size and number (Hu et al., 2015). The SNP in *MdGRF11* which appears to disrupt its cleavage mediated by *miR396*, could similarly increase the extent of growth in apple fruit. As *MdGRF11* is primarily expressed within the cell production period of EFD, it may be likely that this disruption promotes cell production. It should be noted that *MdGRF11* expression still declined at later stages. Hence, other mechanisms are operational in its transcriptional down-regulation during later stages of EFD.

Interestingly, among the 56 genotypes evaluated, only four genotypes displayed the 'TT' allele of *MdGRF11*. Either the heterozygous condition ('TC') or the homozygous 'CC' allele were the predominantly observed alleles across this panel of genotypes. These data suggest that the homozygous 'TT' allele may have been selected against owing to its potential effect on reducing the extent of fruit growth. Such a possibility will need to be evaluated using a larger panel of genotypes and through their phenotypic characterization.

Interaction between MdGRF11 and MdGIF3

Previously, Y2H screening studies indicated the interaction of AtGRF1 and AtGIF1/2 in Arabidopsis. Subsequently bimolecular fluorescence complementation (BiFC) and co-immunoprecipitation (co-IP) assays demonstrated that such interactions occur in Arabidopsis, rice

and maize (Debernardi et al., 2014; Kim and Kende, 2004; Liang et al., 2014). Bioinformatics analysis revealed the presence of a QLQ domain in MdGRF11 (78- 114 aa), and an SNH domain in MdGIF3 (19-74 aa). The Y2H assays performed here revealed a specific interaction between MdGRF11 and MdGIF3, consistent with the correlation between the abundance of their transcripts (Jing and Malladi, 2022). Furthermore, such interaction requires the N terminal of MdGRF11 (Figure 4.5B). Together, these data indicate that the miR396-GRF11-GIF3 module is operational during EFD and likely regulates cell production and growth. MdGIF3 may also interact with other GRFs such as MdGRF16 during this period. These interactions will need to be validated in future studies.

The QLQ domain at the N-terminal of GRFs displays homology with the N-terminal of human BRAHMA (hBRM) protein, which is a subunit of the SWI/SNF chromatin remodeling complex that interacts with the human transcriptional coactivator SYT (Horiguchi et al., 2005; Vercruyssen et al., 2014). GIF encodes a homolog of the SYT coactivator and contains a conserved SNH domain at the N-terminal. SYT interacts with hBRM to mediate the loosening of associations between histone octamers and DNA (de Bruijn et al., 2001; Kato et al., 2002). Subsequently, the DNA is exposed to the RNA polymerase II or transcription factors, thereby altering the expression of the downstream genes (Debernardi, et al., 2014; Nelissen, et al., 2015; Vercruyssen, et al., 2014).

In plants, AtGIF1/AN3 interacts with the plant homologs of SWI/SNF subunits, including BRM, SYD, ACTIN RELATED PROTEINS (ARP4 and ARP7), SWI3C, SWI3D, and SWI/SNF ASSOCIATED PROTEINS 73 (SWP73A and SWP73B) (Vercruyssen, et al., 2014). AtGIF3/AN3 recruits the SWI/SNF chromatin remodeling complexes to the genomic region of downstream genes, such as *GRF5, GRF6, GIF1, HOMEOBOX PROTEIN 33 (HB33), HEC1, CYTOKININ RESPONSE FACTOR 2 (CRF2), COL5*, and *ARABIDOPSIS RESPONSE REGULATOR 4 (ARR4)*

(Vercruyssen, et al., 2014). Similarly, it is possible that MdGIF3 interacts with proteins other than GRFs to regulate downstream target genes. Y2H screening of MdGIF3 interacting proteins using libraries developed from EFD-related tissues can provide further insights into such interacting partners.

The transcript abundance patterns of many positive regulators of the cell cycle, such as *A-* and *B-type CYCLINS (CYCs)* and *B-type CYCLIN DEPENDENT KINASES (CDKBs)*, partially overlap with that of *MdGRF11* and *MdGIF3* during apple EFD (Malladi and Johnson, 2011). Similarly, the expression of *CYCB* and *KNOLLE* decreased in a similar way to the *GRFs* in Arabidopsis during early leaf development, and overexpression of *AtGIF1* results in higher expression of *CYCB, CDC2b* and *CYCD* (Lee et al., 2009; Rodriguez et al., 2010). Therefore, it is possible that the miR396-GRF11-GIF3 module serves as a regulator of cell proliferation by regulating the cell cycle machinery during EFD. However, a direct relationship between GRF-GIFs and cell cycle gene expression has not yet been established. Therefore, future work should focus on potential downstream target genes of the miR396-GRF11-GIF3 module.

References

Allen, E., Xie, Z., Gustafson, A. M., and Carrington, J. C. (2005). microRNA-directed phasing during trans-acting siRNA biogenesis in plants. *Cell* **121**, 207-21.

Bain, J. M., and Robertson, R. N. (1951). The physiology of growth in apple fruits. I. Cell size, cell number, and fruit development. *Aust J Sci Res B* **4**, 75-107.

Che, R., Tong, H., Shi, B., Liu, Y., Fang, S., Liu, D., Xiao, Y., Hu, B., Liu, L., Wang, H., Zhao, M., and Chu, C. (2015). Control of grain size and rice yield by GL2-mediated brassinosteroid responses. *Nat Plants* **2**, 15195.

Choi, D., Kim, J. H., and Kende, H. (2004). Whole genome analysis of the OsGRF gene family encoding plant-specific putative transcription activators in rice (Oryza sativa L.). *Plant Cell Physiol* **45**, 897-904.

Das Gupta, M., and Nath, U. (2015). Divergence in Patterns of Leaf Growth Polarity Is Associated with the Expression Divergence of miR396. *Plant Cell* **27**, 2785-99.

Dash, M., and Malladi, A. (2012). The AINTEGUMENTA genes, MdANT1 and MdANT2, are associated with the regulation of cell production during fruit growth in apple (Malus x domestica Borkh.). *BMC Plant Biol* **12**, 98.

de Bruijn, D. R., dos Santos, N. R., Thijssen, J., Balemans, M., Debernardi, S., Linder, B., Young, B. D., and Geurts van Kessel, A. (2001). The synovial sarcoma associated protein SYT interacts with the acute leukemia associated protein AF10. *Oncogene* **20**, 3281-9.

de Bruijn, D. R., and Geurts van Kessel, A. (2006). Common origin of the human synovial sarcoma associated SS18 and SS18L1 gene loci. *Cytogenet Genome Res* **112**, 222-6.

Debernardi, J. M., Mecchia, M. A., Vercruyssen, L., Smaczniak, C., Kaufmann, K., Inze, D., Rodriguez, R. E., and Palatnik, J. F. (2014). Post-transcriptional control of GRF

transcription factors by microRNA miR396 and GIF co-activator affects leaf size and longevity. *Plant J* **79**, 413-26.

Debernardi, J. M., Rodriguez, R. E., Mecchia, M. A., and Palatnik, J. F. (2012). Functional specialization of the plant miR396 regulatory network through distinct microRNA-target interactions. *PLoS Genet* **8**, e1002419.

Duan, P., Ni, S., Wang, J., Zhang, B., Xu, R., Wang, Y., Chen, H., Zhu, X., and Li, Y. (2015). Regulation of OsGRF4 by OsmiR396 controls grain size and yield in rice. *Nat Plants* **2**, 15203.

Ercoli, M. F., Ferela, A., Debernardi, J. M., Perrone, A. P., Rodriguez, R. E., and Palatnik, J. F. (2018). GIF Transcriptional Coregulators Control Root Meristem Homeostasis. *Plant Cell* **30**, 347-359.

Gao, F., Wang, K., Liu, Y., Chen, Y., Chen, P., Shi, Z., Luo, J., Jiang, D., Fan, F., Zhu, Y., and Li, S. (2015). Blocking miR396 increases rice yield by shaping inflorescence architecture. *Nat Plants* **2**, 15196.

Horiguchi, G., Kim, G. T., and Tsukaya, H. (2005). The transcription factor AtGRF5 and the transcription coactivator AN3 regulate cell proliferation in leaf primordia of Arabidopsis thaliana. *Plant J* **43**, 68-78.

Hu, J., Wang, Y., Fang, Y., Zeng, L., Xu, J., Yu, H., Shi, Z., Pan, J., Zhang, D., Kang, S., Zhu, L., Dong, G., Guo, L., Zeng, D., Zhang, G., Xie, L., Xiong, G., Li, J., and Qian, Q. (2015). A Rare Allele of GS2 Enhances Grain Size and Grain Yield in Rice. *Mol Plant* **8**, 1455-65.

Janssen, B. J., Thodey, K., Schaffer, R. J., Alba, R., Balakrishnan, L., Bishop, R., Bowen, J. H., Crowhurst, R. N., Gleave, A. P., Ledger, S., McArtney, S., Pichler, F. B., Snowden, K. C.,

and Ward, S. (2008). Global gene expression analysis of apple fruit development from the floral bud to ripe fruit. *BMC Plant Biol* **8**, 16.

Jing, S., and Malladi, A. (2020). Higher growth of the apple (Malus x domestica Borkh.) fruit cortex is supported by resource intensive metabolism during early development. *BMC Plant Biol* **20**, 75.

Jing, S., and Malladi, A. (2022). Identification of potential regulators of cell production and early fruit growth in apple (Malus × domestica Borkh.). *Scientia Horticulturae* **297**, 110939.

Kato, H., Tjernberg, A., Zhang, W., Krutchinsky, A. N., An, W., Takeuchi, T., Ohtsuki, Y., Sugano, S., de Bruijn, D. R., Chait, B. T., and Roeder, R. G. (2002). SYT associates with human SNF/SWI complexes and the C-terminal region of its fusion partner SSX1 targets histones. *J Biol Chem* **277**, 5498-505.

Kim, J. H., Choi, D., and Kende, H. (2003). The AtGRF family of putative transcription factors is involved in leaf and cotyledon growth in Arabidopsis. *Plant J* **36**, 94-104.

Kim, J. H., and Kende, H. (2004). A transcriptional coactivator, AtGIF1, is involved in regulating leaf growth and morphology in Arabidopsis. *Proc Natl Acad Sci U S A* **101**, 13374-9.

Kim, J. H., and Tsukaya, H. (2015). Regulation of plant growth and development by the GROWTH-REGULATING FACTOR and GRF-INTERACTING FACTOR duo. *J Exp Bot* **66**, 6093-107.

Kuijt, S. J. H., Greco, R., Agalou, A., Shao, J. X., 't Hoen, C. C. J., Overnas, E., Osnato, M., Curiale, S., Meynard, D., van Gulik, R., Maraschin, S. D., Atallah, M., de Kam, R. J., Lamers, G. E. M., Guiderdoni, E., Rossini, L., Meijer, A. H., and Ouwerkerk, P. B. F. (2014). Interaction between the GROWTH-REGULATING FACTOR and KNOTTED1-LIKE HOMEOBOX Families of Transcription Factors1[W]. *Plant Physiology* **164**, 1952-1966.

Lee, B. H., Ko, J. H., Lee, S., Lee, Y., Pak, J. H., and Kim, J. H. (2009). The Arabidopsis GRF-INTERACTING FACTOR gene family performs an overlapping function in determining organ size as well as multiple developmental properties. *Plant Physiol* **151**, 655-68.

Lee, S. J., Lee, B. H., Jung, J. H., Park, S. K., Song, J. T., and Kim, J. H. (2018). GROWTH-REGULATING FACTOR and GRF-INTERACTING FACTOR Specify Meristematic Cells of Gynoecia and Anthers. *Plant Physiol* **176**, 717-729.

Li, S., Gao, F., Xie, K., Zeng, X., Cao, Y., Zeng, J., He, Z., Ren, Y., Li, W., Deng, Q., Wang, S., Zheng, A., Zhu, J., Liu, H., Wang, L., and Li, P. (2016). The OsmiR396c-OsGRF4-OsGIF1 regulatory module determines grain size and yield in rice. *Plant Biotechnol J* **14**, 2134-2146.

Liang, G., He, H., Li, Y., Wang, F., and Yu, D. (2014). Molecular mechanism of microRNA396 mediating pistil development in Arabidopsis. *Plant Physiol* **164**, 249-58.

Liebsch, D., and Palatnik, J. F. (2020). MicroRNA miR396, GRF transcription factors and GIF co-regulators: a conserved plant growth regulatory module with potential for breeding and biotechnology. *Curr Opin Plant Biol* **53**, 31-42.

Liu, D., Song, Y., Chen, Z., and Yu, D. (2009). Ectopic expression of miR396 suppresses GRF target gene expression and alters leaf growth in Arabidopsis. *Physiol Plant* **136**, 223-36.

Lu, Y., Meng, Y., Zeng, J., Luo, Y., Feng, Z., Bian, L., and Gao, S. (2020). Coordination between GROWTH-REGULATING FACTOR1 and GRF-INTERACTING FACTOR1 plays a key role in regulating leaf growth in rice. *BMC Plant Biol* **20**, 200.

Malladi, A., and Johnson, L. K. (2011). Expression profiling of cell cycle genes reveals key facilitators of cell production during carpel development, fruit set, and fruit growth in apple (Malusxdomestica Borkh.). *J Exp Bot* **62**, 205-19.

Omidbakhshfard, M. A., Fujikura, U., Olas, J. J., Xue, G. P., Balazadeh, S., and Mueller-Roeber, B. (2018). GROWTH-REGULATING FACTOR 9 negatively regulates arabidopsis leaf growth by controlling ORG3 and restricting cell proliferation in leaf primordia. *PLoS Genet* **14**, e1007484.

Osnato, M., Stile, M. R., Wang, Y. M., Meynard, D., Curiale, S., Guiderdoni, E., Liu, Y. X., Horner, D. S., Ouwerkerk, P. B. F., Pozzi, C., Muller, K. J., Salamini, F., and Rossini, L. (2010). Cross Talk between the KNOX and Ethylene Pathways Is Mediated by Intron-Binding Transcription Factors in Barley. *Plant Physiology* **154**, 1616-1632.

Rodriguez, R. E., Ercoli, M. F., Debernardi, J. M., Breakfield, N. W., Mecchia, M. A., Sabatini, M., Cools, T., De Veylder, L., Benfey, P. N., and Palatnik, J. F. (2015). MicroRNA miR396 Regulates the Switch between Stem Cells and Transit-Amplifying Cells in Arabidopsis Roots. *Plant Cell* **27**, 3354-66.

Rodriguez, R. E., Mecchia, M. A., Debernardi, J. M., Schommer, C., Weigel, D., and Palatnik, J. F. (2010). Control of cell proliferation in Arabidopsis thaliana by microRNA miR396. *Development* **137**, 103-12.

van der Knaap, E., Kim, J. H., and Kende, H. (2000). A novel gibberellin-induced gene from rice and its potential regulatory role in stem growth. *Plant Physiol* **122**, 695-704.

Vercruyssen, L., Verkest, A., Gonzalez, N., Heyndrickx, K. S., Eeckhout, D., Han, S. K., Jegu, T., Archacki, R., Van Leene, J., Andriankaja, M., De Bodt, S., Abeel, T., Coppens, F., Dhondt, S., De Milde, L., Vermeersch, M., Maleux, K., Gevaert, K., Jerzmanowski, A., Benhamed, M., Wagner, D., Vandepoele, K., De Jaeger, G., and Inze, D. (2014). ANGUSTIFOLIA3 binds to SWI/SNF chromatin remodeling complexes to regulate transcription during Arabidopsis leaf development. *Plant Cell* **26**, 210-29.

Wang, L., Gu, X., Xu, D., Wang, W., Wang, H., Zeng, M., Chang, Z., Huang, H., and Cui, X. (2011). miR396-targeted AtGRF transcription factors are required for coordination of cell division and differentiation during leaf development in Arabidopsis. *J Exp Bot* **62**, 761-73.

Wu, L., Zhang, D., Xue, M., Qian, J., He, Y., and Wang, S. (2014). Overexpression of the maize GRF10, an endogenous truncated growth-regulating factor protein, leads to reduction in leaf size and plant height. *J Integr Plant Biol* **56**, 1053-63.

Zhang, B., Tong, Y., Luo, K., Zhai, Z., Liu, X., Shi, Z., Zhang, D., and Li, D. (2021). Identification of GROWTH-REGULATING FACTOR transcription factors in lettuce (Lactuca sativa) genome and functional analysis of LsaGRF5 in leaf size regulation. *BMC Plant Biol* **21**, 485.

Zhang, D., Sun, W., Singh, R., Zheng, Y., Cao, Z., Li, M., Lunde, C., Hake, S., and Zhang, Z. (2018). GRF-interacting factor1 Regulates Shoot Architecture and Meristem Determinacy in Maize. *Plant Cell* **30**, 360-374.

Zheng, L., Ma, J., Song, C., Zhang, L., Gao, C., Zhang, D., An, N., Mao, J., and Han, M. (2018). Genome-wide identification and expression analysis of GRF genes regulating apple tree architecture. *Tree Genetics & Genomes* **14**, 54.

Table 4.1. Number of cloned *MdGRF11* transcripts displaying the 'T and 'C' alleles during apple early fruit development.

Tissue	Stage	T	C	p-value[x]
Cortex	23 DAFB[y]	4	17	0.0036
Pith	23 DAFB	0	23	<0.001
Cortex	30 DAFB	2	18	<0.001
Pith	30 DAFB	4	17	0.0036
Total		10	75	<0.001

[x]chi-square analyses; [y]DAFB: days after full bloom

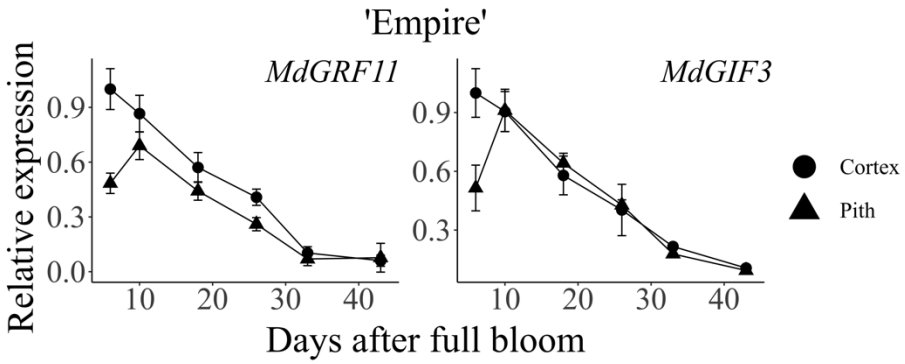

Figure 4.1. Transcript abundance of *MdGRF11* and *MdGIF3* in 'Empire' fruit cortex and pith. Data (mean ± SE; n = 4) are presented in relation to abundance in the cortex at 6 d after full bloom.

Figure 4.2. Transcript abundance of *miR396* in ‘Golden Delicious Smoothee’ fruit cortex and pith. Data (mean ± SE; n = 4) are presented in relation to abundance in the cortex at 11 d after full bloom.

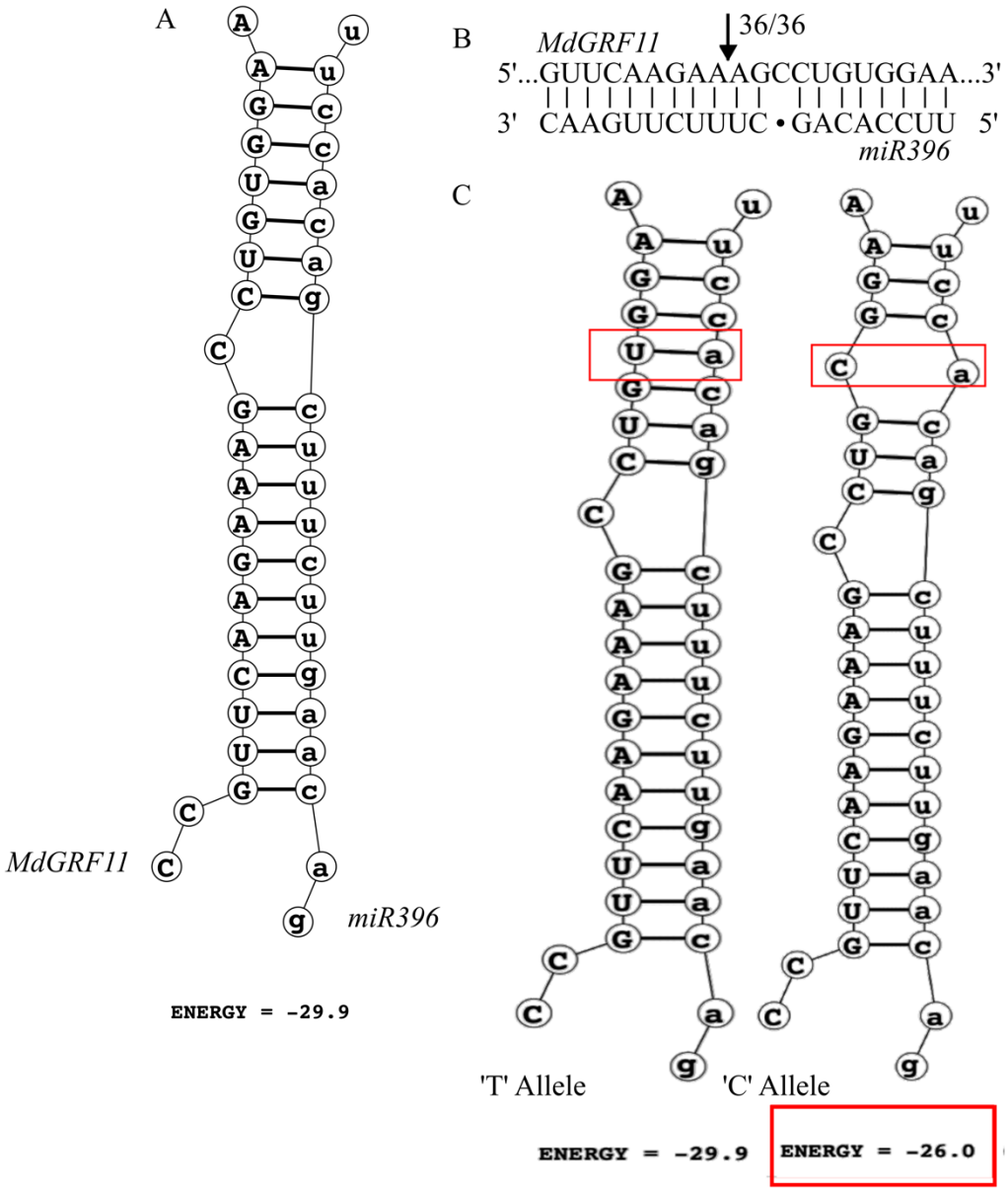

Figure 4.3. Post-transcriptional regulation of *MdGRF11* transcript by *miR396*. A. RNAstructure plot shows potential binding of *miR396* with *MdGRF11* (MFE: minimum free energy). B. Cleavage position identified by 5′ RLM-RACE is indicated with an arrow. The number of clones identified at a specific position relative to the total number of clones analyzed is indicated above the arrow. C. RNAstructure plot shows potential binding of *miR396* with two variants of *MdGRF11* shown in the red box. Less minimum free energy in type ‘C’ suggests lower stability.

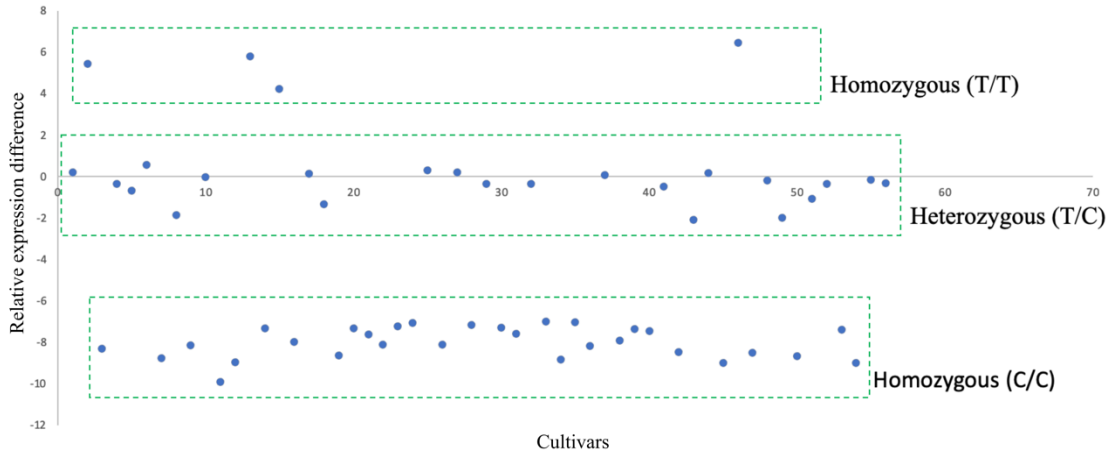

Figure 4.4. Genotyping of the MdGRF11 single nucleotide polymorphisms across 56 apple genotypes. Double-mismatch allele-specific (DMAS) quantitative PCR was used for genotyping. Blue dots represent each specific genotype. Green dashed boxes separate 56 genotypes into homozygous (T/T), heterozygous (T/C), and homozygous (C/C) groups.

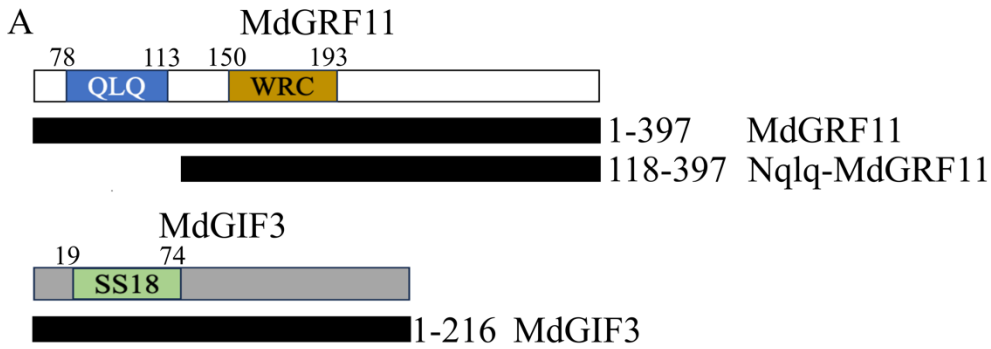
A
MdGRF11
78
113
150
193
QLQ
WRC
1-397 MdGRF11
118-397 Nqlq-MdGRF11
MdGIF3
19
74
SS18
1-216 MdGIF3

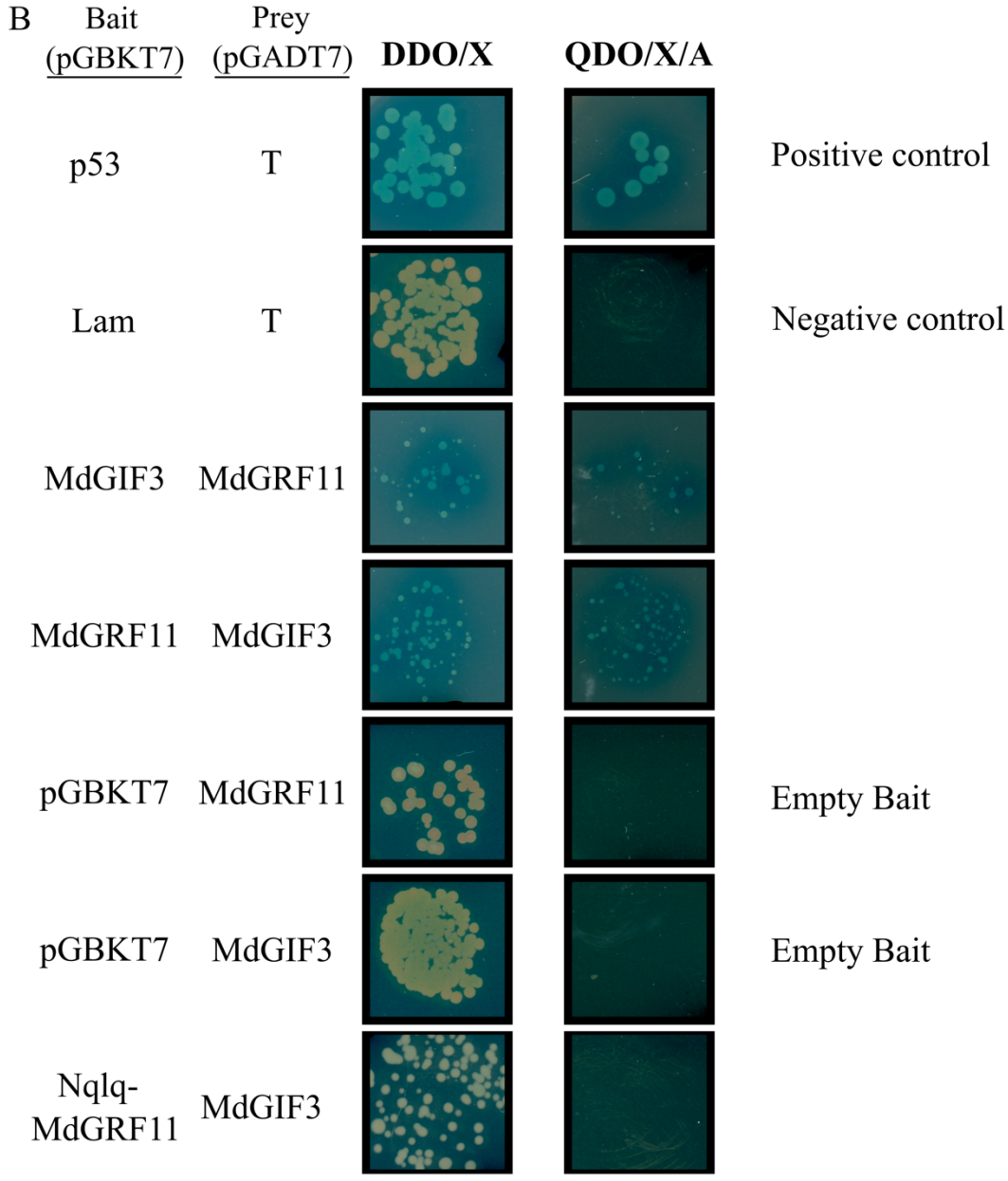
B
Bait (pGBKT7)
Prey (pGADT7)
DDO/X
QDO/X/A
p53
T
Positive control
Lam
T
Negative control
MdGIF3
MdGRF11
MdGRF11
MdGIF3
pGBKT7
MdGRF11
Empty Bait
pGBKT7
MdGIF3
Empty Bait
Nqlq-MdGRF11
MdGIF3

Figure 4.5. Protein-protein interaction between MdGRF11 and MdGIF3. Yeast two-hybrid analysis was used for determining the interaction between MdGRF11 and MdGIF3. A. The conserved QLQ and WRC domains in MdGRF11, and conserved SNH domain in MdGIF3 is indicated. Numbers represents the amino acids position. B. The interaction of MdGIF3 with MdGRF11, and with N-terminally truncated MdGRF11. Empty bait interactions were used as controls. Positive control and negative controls were performed as per the manufacturer's instructions. DDO: SD/-Trp-Leu Double Drop Out. QDO: SD/–Ade/–His/–Leu/–Trp Quadruple Drop Out. X: X-alpha-Gal. A: aureobasidin A (AbA).

APPENDICES

Table S2.1. Mapping statistics of the RNA-seq dataset.

sample	6d-1	6d-3	6d-4	10d-1	10d-3	10d-4	18d-1	18d-3	18d-4	26d-1	26d-3	26d-4
Input reads	13470999	13181929	12676273	19761358	13376952	12309100	11473293	20664355	1276395	9484443	9771401	8423712
Map rate	89.70%	89.10%	89.60%	90.70%	90.60%	90.50%	91.30%	91%	91.10%	91.90%	92.10%	91.30%
Aligned paires	11628908	11212622	10930831	17224666	11617069	10695546	10033792	18012513	11149770	8404472	8663726	7377634
Concordant rate	84.80%	83.60%	85%	85.60%	85.30%	85.50%	86%	85.70%	86.10%	87.10%	86.90%	86%
assigned	10696103	11063498	10559419	16391257	11189886	10330794	9973636	18095084	11139769	7695344	7829766	7202552

Table S2.2. The concentration of phytohormones in the 'Empire' apple fruit cortex at 6 days after full bloom (DAFB), 10 DAFB, 18 DAFB, and 26 DAFB. Phytohormones that were not detectable at any stage were excluded. The mean ± standard error is displayed (pmol/g fresh weight).

Index	Compounds	6 DAFB	10 DAFB	18 DAFB	26 DAFB
ABA	Abscisic acid	7087.40541	1785.34015	236.23389	171.812419
ABA-GE	ABA-glucosyl ester	6598.58796	2973.1479	637.446202	454.033819
IAA-Leu	N-(3-Indolylacetyl)-L-leucine	0	2.80887497	0	0
MEIAA	Methyl indole-3-acetate	137.144348	4.25310367	1.3554521	0.63243413
OxIAA	2-oxindole-3-acetic acid	94.3749384	368.91109	52.626923	0
IAA	Indole-3-acetic acid	217.262291	0	0	0
IAA-Glu	Indole-3-acetyl glutamic acid	5.29928295	0	0	0
IAA-Leu-Me	Indole-3-acetyl-L-leucine methyl ester	0	0	0.04408216	0.07261808
IPA	3-Indolepropionic acid	642.822895	0	0	0
ICA	Indole-3-carboxylic acid	235.502162	0	0	0
ICAld	Indole-3-carboxaldehyde	25728.7727	3208.7952	160.959204	85.6354071
IAA-Asp	Indole-3-acetyl-L-aspartic acid	0	10.6253907	0	0
TRP	L-tryptophan	288271.875	22847.8571	4220.12273	3089.36944
2MeScZR	2-Methylthio-cis-zeatin riboside	17.2163026	4.1534704	0.52202362	0.15195447
IP	N6-isopentenyladenine	0.2928196	2.47724102	0.06423635	0.46745204
cZR	cis-Zeatin riboside	3.37975861	2.23665228	1.06167013	0.12037444
cZ9G	cis-Zeatin-9-glucoside	4.13462415	1.21845579	0.02928523	0
BAP	6-Benzyladenine	1.35190899	0	0	11.8311768
DZ	Dihydrozeatin	1.32917188	2.64456966	0.38475512	0.20731237
tZR	trans-Zeatin riboside	21.2818524	205.18244	5.88118293	6.75726512
DHZROG	Dihydrozeatin-O-glucoside riboside	0	0.06683517	0.39483894	0.3425169
tZOG	trans-Zeatin-O-glucoside	12.9717283	17.1561537	1.07011446	0.9488677
IPR	N6-isopentenyladenosine	4.35941882	32.2515688	1.09692597	1.08875075
DHZR	Dihydrozeatin ribonucleoside	6.69923041	10.9685304	2.27065629	2.50843843
mTR	meta-Topolin riboside	0	0	0	0.0345448
BAPR	6-Benzyladenosine	0.09183045	0	0	0
tZ	trans-Zeatin	23.8550441	70.9646404	5.56119676	11.1168256
ACC	1-Aminocyclopropanecarboxylic acid	45745.6056	29216.6289	7684.46359	3553.04316
GA19	Gibberellin A19	238.967412	85.999792	71.4309095	37.2735122
GA3	Gibberellin A3	18.662601	0	8.66432886	5.39838258
GA53	Gibberellin A53	5.57359349	1.66992551	5.33724514	5.52246533
GA1	Gibberellin A1	259.434254	99.7078504	3.60980521	0

GA4	Gibberellin A4	0	1.27167473	0	0
GA9	Gibberellin A9	26.1075781	0	0	0.42124828
GA24	Gibberellin A24	0	1.64183587	2.61416796	0
OPDA	cis(+)-12-Oxophytodienoic acid	10680.8891	8019.77304	1555.62069	1497.46347
JA-Phe	N-[(-)-Jasmonoyl]-(l)-phenalanine	6.22298604	3.92705355	0.13997995	0.75232925
OPC-4	3-oxo-2-(2-(Z)-Pentenyl) cyclopentane-1-butyric acid	2067.69949	1765.43025	162.088515	196.170575
JA-Val	N-[(-)-Jasmonoyl]-(L)-valine	39.0563411	36.3550705	2.24897631	2.38004288
JA-ILE	Jasmonoyl-L-isoleucine	1067.34823	2039.79997	84.8486013	63.3629888
JA	Jasmonic acid	11670.4651	28284.305	1330.19247	1065.94593
MEJA	Methyl jasmonate	186.54697	161.479919	12.6998826	8.45479153
H2JA	Dihydrojasmonic acid	0	7.95006883	0	0
OPC-6	3-oxo-2-(2-(Z)-Pentenyl)cyclopentane-1-hexanoic acid	1578.77199	919.901745	72.2863762	77.9169226
SAG	Salicylic acid 2-O-β-glucoside	3963.09154	1656.07415	88.6628207	74.7418011
SA	Salicylic acid	893.92708	446.430202	125.870294	165.265213

Table S4.1. List of 56 genotypes used for double-mismatch allele-specific (DMAS) qPCR.

GRIN number	Cultivar
PI 589647	Northwood
PI 589650	Ellis Bitter
PI 589653	Harry Masters Jersey
PI 589656	Cheddar Cross
PI 589662	Brow Appl
PI 589666	Dunkerton Late Sweet
PI 589667	Doux Normandie
PI 589674	Pethyre
PI 589679	Fillbarrel
PI 589682	Improved Lambrook Pippin
PI 589683	George Cave
PI 589688	Sweet Coppin
PI 589689	Frequin Tardive de la Sarthe
PI 589690	Le Bret
PI 589691	Tale Sweet
PI 589692	Stembridge Cluster
PI 589693	Stembridge Jersey
PI 589708	Red Dougherty
PI 589711	Carnifex
PI 589721	Reta
PI 589725	Jubilee
PI 589847	Holland
PI 589852	Ohio Nonpareil
PI 589855	Murasaki
PI 589892	Gold Russ
PI 589893	Holly
PI 589895	Macoun
PI 589925	Zoete Ermgaard
PI 590119	Blan Dur
PI 590121	Cornish Aromatic (Wakeley)
PI 590125	Edelroter
PI 590126	Fenouillet de Ribours
PI 590128	Golden Harvey
PI 590129	Golden Pippin
PI 590130	Hubbards Pearmain
PI 590133	Old Pearmain
PI 590136	Reinette de Cuzy

PI 590137	Reinette Franche
PI 590141	Ross Nonpareil
PI 590143	Weidners Goldreinette
PI 590144	Weisser Winter Taffetapfel
PI 590177	Pewaukee
PI 590179	E.8
PI 590209	Sund
PI 594108	Medaille d'Or
PI 594111	Redfree
PI 613949	Shtreifling
PI 613950	Mal't Bagaevskii
PI 613818	Wick
PI 632625	Paulista
	Golden Delicious
	Fuji
	Red Delicious
	Goldrush
	Gala
	Pink Lady

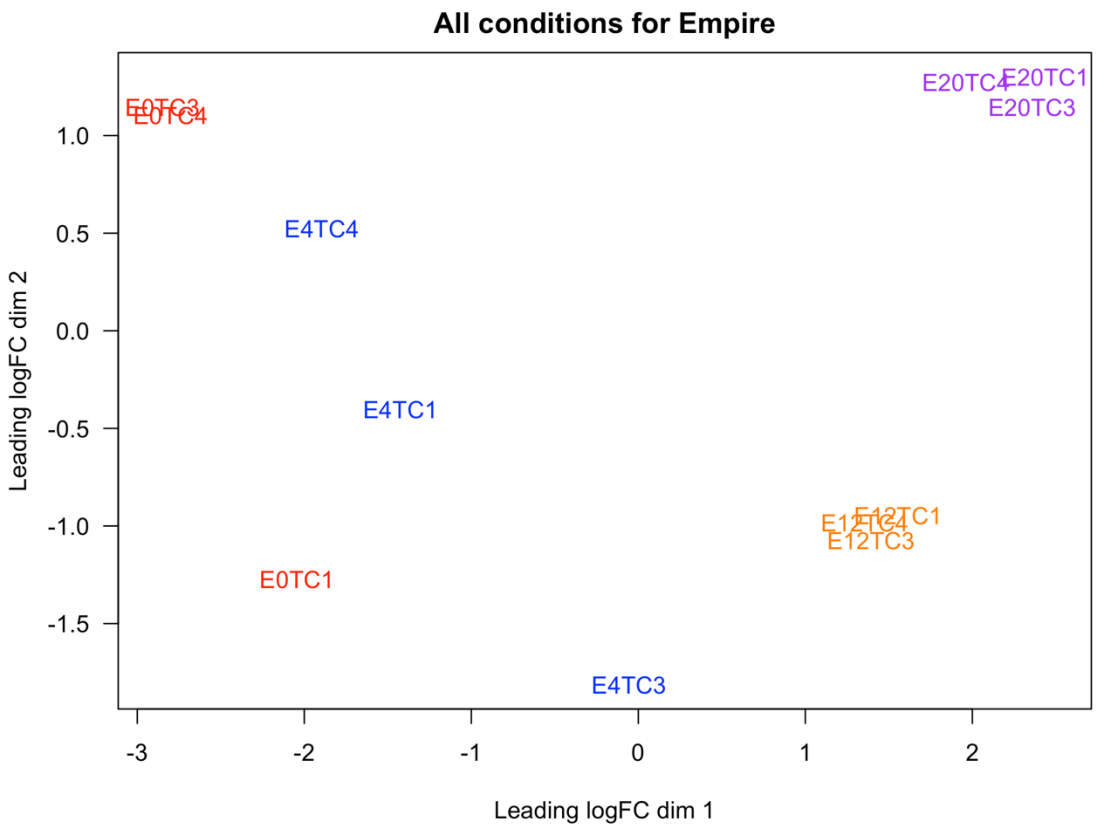

Figure S2.1. Multidimensional scaling (MDS) plot of the RNA-seq data. The E0TC, E4TC, E12TC, and E20TC represent the samples from 6 days after full bloom (DAFB), 10 DAFB, 18 DAFB, and 26 DAFB respectively.

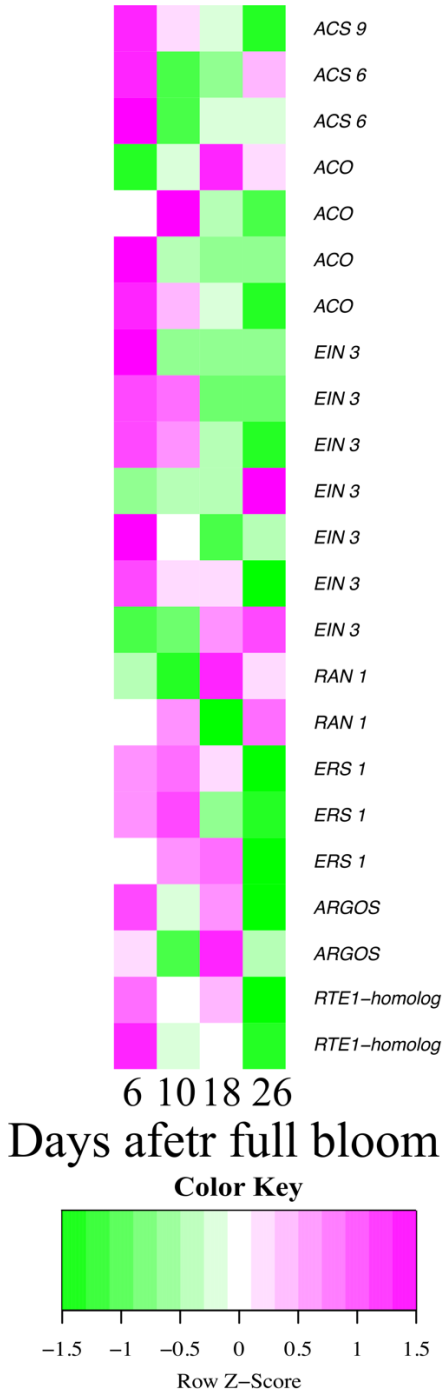

Figure S2.2. A heatmap of transcript abundance of identified genes involved in ethylene metabolism and signaling.

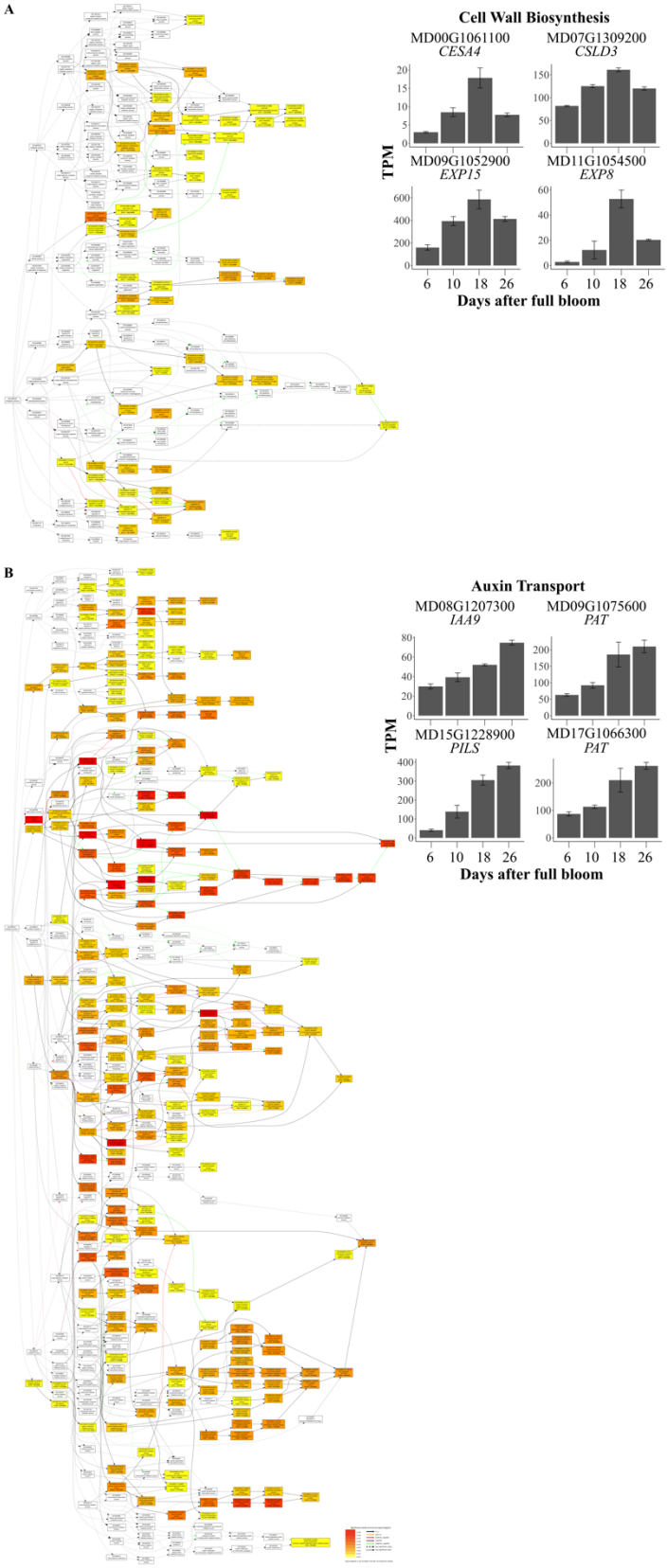
A
Cell Wall Biosynthesis
MD00G1061100
CESA4
MD07G1309200
CSLD3
MD09G1052900
EXP15
MD11G1054500
EXP8
TPM
Days after full bloom
B
Auxin Transport
MD08G1207300
IAA9
MD09G1075600
PAT
MD15G1228900
PILS
MD17G1066300
PAT
TPM
Days after full bloom

Figure S2.3. Gene ontology (GO) enrichment analysis of differentially expressed genes (DEGs) in clusters 4 and 6. (A) The GO enrichment of DEGs in cluster 4 and transcript abundance of four selected genes in cell wall biosynthesis: *CELLULOSE SYNTHASE A4 (CESA4), CELLULOSE SYNTHASE LIKE D3 (CSLD3), EXPANSIN 15 (EXP15),* and *EXP8*. (B) The GO enrichment of DEGs from cluster 6 and transcript abundance of four selected genes involved in auxin signaling and transport: *INDOLE-3-ACETIC ACID INDUCIBLE 9 (IAA9), POLAR AUXIN TRANSPORT (PAT),* and *AUXIN EFFLUX CARRIER GENE (PILS).*

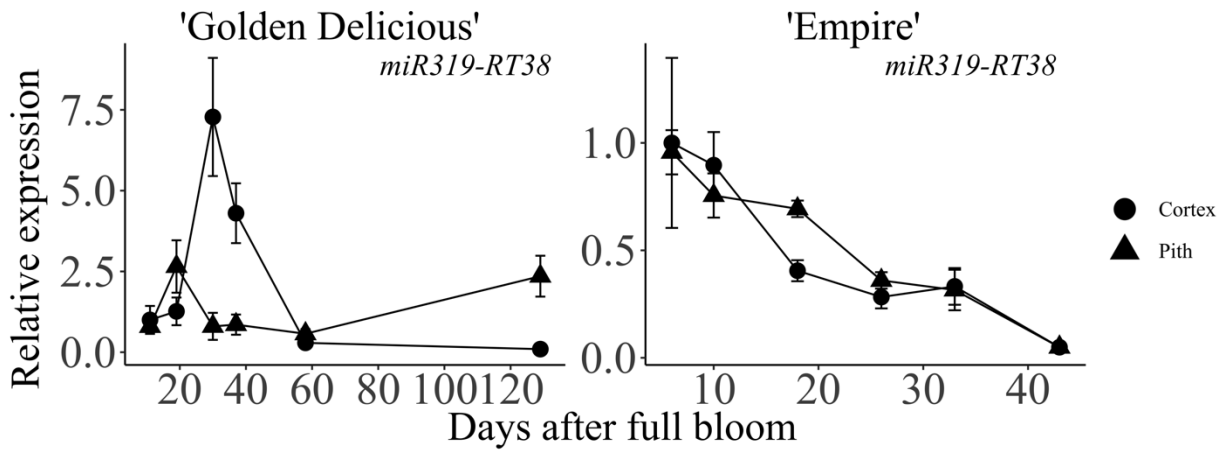

Figure S3.1. Transcript abundance of *miR319b* in 'Golden Delicious Smoothee' and 'Empire' fruit cortex and pith. Data (mean ± SE; n = 4) are presented in relation to abundance in the cortex at 11 d after full bloom for 'Golden Delicious', and in the cortex at 6 d after full bloom for 'Empire'.

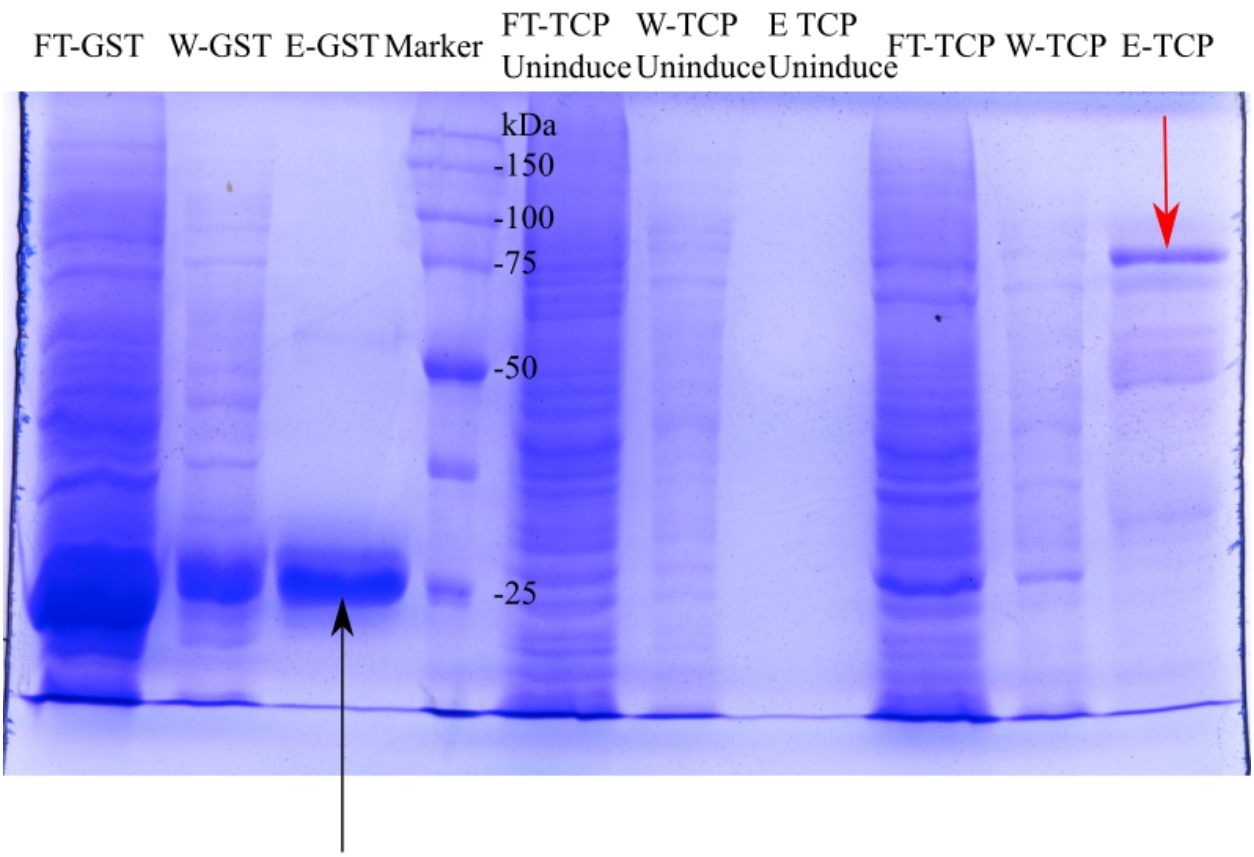

Figure S3.2. SDS-PAGE gel for TCP-GST fusion protein and GST protein. Uninduced cells as negative control. Red arrow indicates TCP-GST protein. Black arrow indicates GST protein. FT: flow through, W: wash, E: elution.

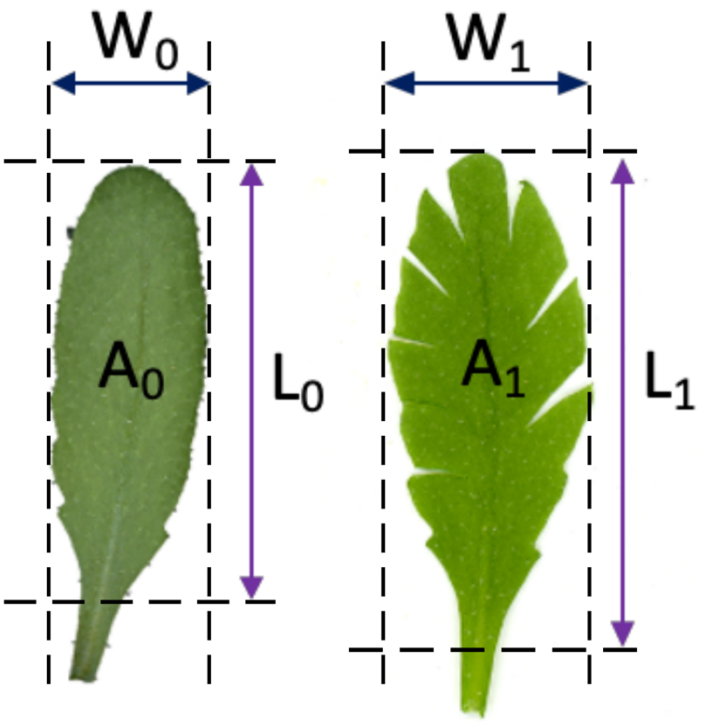

Figure S3.3. Calculation of curvature index (CI). Sixth and seventh leaves were detached from the rosette when inflorescence was 2 cm long and scanned. The margins of the leaves were cut to flatten the leaf, and the leaves were scanned again. Leaf area, leaf width, and length were measured using images from leaves prior to and after scanning. WCI = $1-W_0/W_1$, LCI = $1-L_0/L_1$, and ACI = $1-A_0/A_1$. (W: width, L: length, A: area).